

**AN ULTRA-WIDEBAND TRANSMIT/RECEIVE MODULE USING
10 TO 35 GHZ SIX-CHANNEL MICROSTRIP MULTIPLEXERS
AND ITS APPLICATIONS TO
PHASED-ARRAY ANTENNA TRANSCEIVER SYSTEMS**

A Dissertation

by

SEUNG PYO HONG

Submitted to the Office of Graduate Studies of
Texas A&M University
in partial fulfillment of the requirements for the degree of

DOCTOR OF PHILOSOPHY

August 2006

Major Subject: Electrical Engineering

**AN ULTRA-WIDEBAND TRANSMIT/RECEIVE MODULE USING
10 TO 35 GHZ SIX-CHANNEL MICROSTRIP MULTIPLEXERS
AND ITS APPLICATIONS TO
PHASED-ARRAY ANTENNA TRANSCEIVER SYSTEMS**

A Dissertation

by

SEUNG PYO HONG

Submitted to the Office of Graduate Studies of
Texas A&M University
in partial fulfillment of the requirements for the degree of

DOCTOR OF PHILOSOPHY

Approved by:

Chair of Committee,
Committee Members,

Head of Department,

Kai Chang
Robert D. Nevels
Chin B. Su
Lihong Wang
Costas N. Georghiades

August 2006

Major Subject: Electrical Engineering

ABSTRACT

An Ultra-wideband Transmit/Receive Module Using 10 to 35 GHz Six-channel Microstrip Multiplexers and Its Applications to Phased-array Antenna Transceiver Systems.

(August 2006)

Seung Pyo Hong, B.S.; M.S., Yonsei University

Chair of Advisory Committee: Dr. Kai Chang

This dissertation introduces new and simple techniques for suppression of multi-spurious passbands, which are inherent to the conventional microstrip parallel couple-line bandpass filters. In addition, the operation of harmonic suppression is analyzed using a simple model.

Special emphasis is placed on the applications of several new filter designs for microstrip diplexers and multiplexers. Compact, full-duplex beam scanning antenna transceiver systems with extremely broad bandwidth have also been developed.

Recent advances in broadband monolithic microwave integrated circuit (MMIC) amplifiers make the realization of extremely broadband phased-array transceiver systems possible. The ultra-wideband phased-array transceiver systems can be used in multi-band mobile satellite communication systems and wideband radars. This dissertation presents a multi-band, compact, full-duplex, beam scanning antenna transceiver system for satellite communications and two designs of ultra-wideband, low-cost radar systems as applications of the MMIC amplifiers.

In addition, a multi-frequency antenna has been developed. A single-feed triple frequency microstrip patch antenna is presented as an answer to the recent demand for multi-function systems in the wireless communications.

In summary, the research presented in this dissertation covers every component required to build an ultra-wideband, full-duplex beam scanning phased-array antenna transceiver. The work done in this dissertation should have many applications in the wireless communication systems and wideband radar technologies.

DEDICATION

To my father,
my mother,
my wife, Sejeong,
and
my son, Seong-yoon

ACKNOWLEDGMENTS

I would like to express my sincere gratitude to Dr. Kai Chang for his support and guidance with regards to my Ph.D. studies and research at Texas A&M University. I also appreciate Dr. Robert D. Nevels, Dr. Chin B. Su, Dr. Lihong Wang, and the late Dr. Henry F. Taylor for serving as members on my dissertation committee and for their helpful comments. I would like to thank the U.S. Army, the Texas Telecommunications and Informatics Task Force (TITF), and the National Science Foundation for their financial support as a research assistantship. My work on an ultra-wideband T/R module and radars could hardly been successful without generous donation from Raytheon and TriQuint Semiconductor. I gratefully acknowledge Mr. Ming-yi Li, Matthew. R. Coutant, and other members of the Electromagnetics and Microwaves Laboratory at Texas A&M University for their technical assistance and invaluable discussions.

I would like to thank all my dear friends for their support. I would also like to thank my parents, sister's family, brother's family and mother-in-law for their constant love, encouragement, and support. Finally, I would like to express my deep appreciation to my lovely wife, Sejeong, and my son, Beau Seong-yoon, for their patience, love, and support during my graduate studies. This work would not have been possible without their support and patience.

TABLE OF CONTENTS

	Page
ABSTRACT	iii
DEDICATION	v
ACKNOWLEDGMENTS.....	vi
TABLE OF CONTENTS	vii
LIST OF FIGURES.....	x
LIST OF TABLES	xv
 CHAPTER	
I INTRODUCTION	1
1.1. Introduction	1
1.2. Dissertation organization.....	4
II MODIFIED MICROSTRIP PARALLEL COUPLED-LINE BANDPASS FILTER STRUCTURES FOR SUPPRESSION OF MULTI-SPURIOUS PASSBANDS	6
2.1. Introduction	6
2.2. Harmonic suppression with spur-lines	7
2.3. Harmonic suppression with small resonators.....	14
2.4. Conclusions	22
III STUB-TUNED MICROSTRIP BANDPASS FILTERS FOR MILLIMETER- WAVE DIPLEXER DESIGN	23
3.1. Introduction	23
3.2. Filter and diplexer design.....	25
3.3. Conclusions	31

CHAPTER	Page
IV A 10—35-GHZ SIX-CHANNEL MICROSTRIP MULTIPLEXER FOR WIDEBAND COMMUNICATION SYSTEMS.....	32
4.1. Introduction	32
4.2. Channel filter design	35
4.3. Harmonic suppression of the channel filters	38
4.4. Multiplexer design and measurement	47
4.5. Conclusions	62
V A MULTI-BAND, COMPACT, AND FULL-DUPLEX BEAM SCANNING ANTENNA TRANSCEIVER SYSTEM OPERATING FROM 10 TO 35 GHz.....	64
5.1. Introduction	64
5.2. Wideband T/R module	66
5.3. Antenna and array	72
5.4. System integration and test	82
5.5. Conclusions	89
VI ULTRA-WIDEBAND LOW-COST PHASED-ARRAY RADARS	91
6.1. Introduction	91
6.2. Antenna, array, and phase shifters	93
6.3. 2—20-GHz MMIC-based amplifiers	98
6.4. System tests	101
6.5. Conclusions	108
VII SINGLE-FEED TRIPLE-FREQUENCY RECTANGULAR MICROSTRIP PATCH ANTENNA WITH PAIRS OF SPUR-LINES	110
7.1. Introduction	110
7.2. Antenna design.....	111
7.3. Experiment results.....	118
7.4. Conclusions	121

CHAPTER	Page
VIII SUMMARY AND RECOMMENDATIONS	122
8.1. Summary	122
8.2. Recommendations for future research.....	125
REFERENCES.....	126
VITA	133

LIST OF FIGURES

FIGURE	Page
1. Six-section conventional parallel-coupled microstrip bandpass filter centered at 2.45 GHz.	9
2. Microstrip parallel coupled-line bandpass filter for suppression of the first spurious passband. (a) Layout of the filter incorporated with spur-lines. (b) Detailed view of the coupling section with spur-lines.	10
3. Simulated frequency responses of the conventional parallel coupled-line bandpass filter and the modified bandpass filter shown in Fig. 2 (a).	11
4. Transformation of the filter shown in Fig. 2 (a) to obtain enough suppression of the second spurious passband. (a) Flipping vertically. (b) 90-degree bending and shifting down of sections 2 and 5. (c) Photos of the proposed new filter and the conventional filter. The top photo is for the new filter and the bottom photo is for the conventional filter.	12
5. Simulated and measured frequency responses of the conventional filter and the proposed filter. (a) Simulated results. (b) Measured performances.	13
6. Five-section conventional parallel-coupled microstrip bandpass filter centered at 12 GHz.	16
7. Layout of the new filter with suppression of the first spurious passband.	17
8. Simulated and measured frequency responses of the conventional filter and the new filter with suppression of the second harmonic passband. (a) Simulated responses. (b) Measured responses.	18
9. Layout of the new filter with suppression of both the first and the second spurious passbands.	19
10. (a) Layout of the new parallel-coupled microstrip bandpass filter. (b) Photo of the fabricated filter inside a test fixture.	20
11. Measured results of conventional and new filter. (a) Insertion loss. (b) Return loss.	21
12. Simulated frequency responses of parallel-coupled lines. (w 1 = 0.91 mm, w 2 = 0.43mm, gap = 0.2 mm)	26

FIGURE	Page
13. Layouts of the designed bandpass filters and their simulated responses (a) Tx filter centered at 32 GHz. (gap = 0.2 mm) (b) Rx filter centered at 35 GHz. (gap = 0.15 mm) (c) Simulated responses of the two filters.	27
14. Layout of the designed diplexer.....	29
15. Simulated and measured frequency responses of the diplexer.	30
16. Photo of the fabricated diplexer inside a test fixture	31
17. Block diagram of the multiplexer.	34
18. Layout of the designed filters. ($W_0 = 0.84$ mm).....	36
19. Simulated frequency responses of the designed filters to be placed in the transmit path of the multiplexer. The designed frequencies are 10, 19, and 32 GHz, respectively.....	37
20. Simulated frequency responses of the designed filters to be placed in the receive path of the multiplexer. The designed frequencies are 12, 21, and 35 GHz, respectively.....	38
21. Half wavelength resonators; (a) Single microstrip line. (b) Parallel-coupled microstrip line. (λ_g is the guided wavelength)	41
22. Variations of X_{in} and $X_{in,c}$ with frequency.....	42
23. S11 responses of the single microstrip resonator and the coupled resonator.	43
24. Proposed parallel-coupled microstrip bandpass filter designed at 12 GHz with suppression of both the second and the third harmonic responses.	45
25. Simulated and measured performances of the conventional and proposed filters. (a) Simulated results. (b) Measured results.	46
26. Relative sizes of filters in the transmit path.....	49
27. Layouts of bent filters designed at (a) 10 GHz and (b) 12 GHz.....	51
28. Performance comparisons between the unbent and bent proposed filters (a) Designed at 10 GHz. (b) Designed at 12 GHz.	52

FIGURE	Page
29. Variation of the frequency response of the channel filter with the length between the filters. (a) Filter centered at 10 GHz. (b) Simulated insertion loss of the filter centered at 10 GHz. (c) Filter centered at 35 GHz. (d) Simulated insertion loss of the filter centered at 35 GHz.	53
30. Flow chart of multiplexer design.	56
31. Physical layout of the designed six-channel microstrip multiplexer.	58
32. Physical dimensions of the distances for the interconnecting lines between the channel filters. (Unit: mm).....	59
33. Simulated and measured frequency responses of the six-channel multiplexer. (a) Simulated responses for S21 and S31, (b) Measured responses for S21 and S31, and (c) Simulated and measured responses for S11.	60
34. Assembly diagram of the MMICs. (Unit: mm)	67
35. Small-signal S-parameters of TGA4832 assembly.....	70
36. Small-signal S-parameters of TGA4830 assembly.....	70
37. Layout of the T/R module composed of two multiplexers, two TGA4832s and three TGA4830s. (Unit: cm).	71
38. Configuration of a 1 x 4 <i>H</i> -plane phased-array operated by a PET-controlled phase shifter. From left to right are 1 x 4 power divider, PET controlled phase shifter, space adapter, and 1 x 4 <i>H</i> -plane antenna array.	73
39. Schematic illustrating an antipodal tapered-slot antenna (ATSA).	74
40. Simulated and measured return loss of the ATSA.....	75
41. Measured performance of the phase shifter. (a) S-parameters. (b) Differential phase shift.	76
42. Mirrored ATSA array architecture.	78
43. Measured beam steering patterns at (a) 10 GHz. (b) 12 GHz. (c) 19 GHz. (d) 21 GHz. (e) 32 GHz. (f) 35 GHz.....	79
44. Photograph of the phased-array antenna transceiver system composed of phased-array antenna and T/R module.	83

FIGURE	Page
45. Measured frequency responses of the T/R module.....	84
46. Measured receive patterns of the phased-array antenna transceiver system for the receiving frequencies. (a) 12 GHz. (b) 21 GHz. (c) 35 GHz.	86
47. Measured transmit patterns of the phased-array antenna transceiver system for the transmitting frequencies. (a) 10 GHz. (b) 19 GHz. (c) 32 GHz.....	88
48. Configuration of a 1 x 4 <i>H</i> -plane array operated by a PET-controlled phase shifter. The 8—20-GHz design is shown.....	94
49. Measured return loss of the ATSAs.....	96
50. Measured performance of the phase shifter operating from 8 to 20 GHz. (a) S-parameters. (b) Differential phase shift	96
51. Measured differential phase shift of the phase shifter operating from 3 to 12 GHz.	97
52. A photograph of the assembled PA module including the TGA2509 MMIC, the 50-Ω lines at the input and output, and the bias networks.....	99
53. Gain and output power of the PA MMIC versus frequency.	100
54. System block diagram illustrating the test setup for the beam-steerable pulse radar.	101
55. Experimental setup for the target range test.	102
56. Detected waveform of the received signal can be compared with the waveform of the timing signal in order to measure target range.	103
57. Comparison between measured and ideal time delays for varying target ranges.....	104
58. Measured beam steering patterns at (a) 8 GHz. (b) 16 GHz. (c) 20 GHz.....	105
59. Measured beam steering patterns at (a) 3 GHz. (b) 7 GHz. (c) 12 GHz.....	107
60. (a) Inset-feed rectangular microstrip patch antenna operating at 5.8 GHz (L = 17 mm, W = 18 mm). (b) Spur-line to be embedded in the patch.	112

FIGURE	Page
61. Possible configurations of embedding two-pairs of spur-lines in the non-radiating edges of the rectangular patch.	113
62. Photo of the designed triple-frequency patch antenna.....	116
63. Tuning of the extra resonant frequencies by varying the length of spur-lines. (a) Change of the second extra resonant frequency with the variation of shorter spur-lines (L_1), (b) Change of the first extra resonant frequency with the variation of longer spur-line length (L_2). (Unit of lengths: mm)	117
64. Simulated and measured return losses of the designed antenna with spur-line dimensions shown in Table 10.....	119
65. Measured radiation patterns for the E-plane at three resonant frequencies (f_0, f_1, f_2). (a) $f_0 = 5.19$ GHz, (b) $f_1 = 6.90$ GHz, and (c) $f_2 = 7.89$ GHz	120

LIST OF TABLES

TABLE		Page
1.	Physical parameters for the filter shown in Fig.1. W_i , S_i , and L_i are the width, the separation between coupled-lines, and the length of the i th section, respectively. The input and output port strip width are $W_0 = 1.18$ mm, corresponding to 50Ω . (Unit: mm)	9
2.	Physical parameters for the parallel-coupled microstrip bandpass filter centered at 12 GHz. The strip width of input/output ports (W_0) is 0.84 mm.	16
3.	Physical parameters for the designed filter. (Unit: mm).....	28
4.	Dimension of designed microstrip parallel coupled-line bandpass filters. (Unit: mm)	37
5.	Simulated insertion loss (IL) of the designed bandpass filters.	38
6.	MMIC selections for the T/R module. All parts are manufactured by TriQuint Semiconductor. Performance for the LNA is listed at 12, 21, and 35 GHz; performance for the PAs is listed at 10, 19, and 32 GHz.	68
7.	Measured gain of the antenna array with and without T/R module and the measured gain of T/R module at each operating frequency. (T and R denote transmit and receive frequencies, respectively).....	86
8.	Dimensions of the designed ATSAs.....	95
9.	Dimensions of the designed phase shifters.....	95
10.	Physical dimensions of the spur-line shown in Fig. 60 (c). The shorter spur-lines are the pair of spur-lines located closer to the edge. The location of the spur-lines from the edge with the feed line is $L_3 = 4.5$ mm. (Unit: mm).....	115

CHAPTER I

INTRODUCTION

1.1. Introduction

The fast growth of the wireless communication and radar technologies is demanding many new technological challenges in communication system designs. These challenges include devices with low fabrication cost, compact size, high operating frequency, and multiple operation bands. Filters, diplexers, and multiplexers are the essential parts in the front end of wireless communication systems. But these parts are normally made of metal waveguide when the operating frequencies become higher [1-5]. The waveguide components are normally expensive and bulky. Recently, other technologies such as micromachining techniques have been emerged for filter and diplexer designs in millimeter-wave range [6-8].

Microstrip line is a good candidate for filter and other component designs due to its advantages of low fabrication cost, compact-size, easy fabrication, light weight, planar structure and easy integration with other components on a single circuit board. In millimeter-wave range, however, much attention has not been given to microstrip lines for filter, diplexer and multiplexer designs, because of their relatively high loss in this frequency range. Only a few literatures are reported so far [9]. Despite their relatively high loss in millimeter-wave range, microstrip filters and their applications to diplexer

and multiplexer designs still remain as an attractive research topic due to their aforementioned merits.

Today, it is also required that satellite, mobile, and other communication systems operate in full-duplex mode for seamless communications and wider bandwidth. To meet these requirements, the system should be able to transmit and receive signals simultaneously over its operating frequency range and must have a way to provide high degree of isolation between transmit and receive paths to prevent the receiver from being degraded by the leakage from the transmitter and to maintain good signal to noise ratio. Generally, a circulator or multiplexer is used to provide a way of full-duplex operation. However, the circulator is not appropriate to be used for wideband systems, because of its narrow operating bandwidth. Multiplexers provide isolation between transmit and receive channels by assigning a different frequency band to each channel and can operate over a wide bandwidth. Various kinds of multiplexers have been developed so far [10-12]. Microstrip multiplexer used for multi-frequency, full-duplex and phased-array antenna systems has been reported in [13]. But there is still a system requirement for even wider bandwidth than the multiplexer in [13] can offer. Because of the requirement of wide bandwidth, the parallel coupled microstrip bandpass filters used as channel filters of the multiplexer should have a way to suppress the harmonic passbands. Novel and simple techniques to suppress the harmonic passbands of the microstrip have been developed in this research.

Compared to mechanical steering, electronic steering of an antenna beam has many advantages such as rapidness, higher reliability, and the ability to be easily

incorporated with solid-state devices [14]. The electronic beam steering normally requires a phased-array antenna, phase shifters, and transmit/receive modules (T/R modules) and these components have become active research topics in communication and radar applications. One of the recent research interests is to increase the operation bandwidth of phased-array antenna transceiver systems [15]. In this dissertation, the operating frequency bandwidth of the T/R module has been extended to a very wide band from 10 to 35 GHz. The T/R module is an enabling component for wideband phased-array antenna transceiver systems for wide band communication applications. The extremely wideband T/R module is integrated with the wideband phased-array antenna and phase shifter to construct a phased-array antenna transceiver system.

Low-cost and multi-band radar systems are also demonstrated using ultra-wideband phased-array antennas. Two designs are presented, one operating from 3 to 12 GHz and the other from 8 to 20 GHz. A broadband monolithic microwave integrated circuit (MMIC) power amplifier (PA) is assembled and then integrated into this design in order to generate microwave power over the wide frequency range. System tests demonstrating pulse-radar target ranging and phased-array beam steering are performed with excellent results for each array design.

Finally, a microstrip patch antenna with more than one operating frequency is designed. Using pairs of spur-lines, two extra resonant frequencies can be excited between TM_{01} and TM_{02} mode of the rectangular microstrip patch antenna. Measurement results show good radiation patterns at three resonant frequencies and match well with the simulated ones.

1.2. Dissertation organization

This dissertation covers a variety of topics, which are modified microstrip parallel coupled-line structures for suppression of multi-spurious passbands, microstrip filters for millimeter-wave diplexer, microstrip multiplexer, multi-band transmit and receive module, phased-array radar, and multi-frequency microstrip patch antenna. The dissertation consists of eight chapters.

Chapter II presents two modified microstrip coupled-line bandpass filter structures for suppression of multi-spurious passbands. One incorporates spur-lines into the input and output resonators of the conventional microstrip parallel coupled-line bandpass filter. The other uses small resonators placed in the vicinity of the conventional microstrip parallel coupled bandpass filter. This modified parallel coupled bandpass filter is used in the multiplexer described in Chapter IV.

Chapter III introduces a new design for microstrip bandpass filters and its application to a millimeter-wave diplexer. Basically, parallel-coupled microstrip lines are utilized for bandpass response and non-uniform open-circuited stubs are added to tune the bandwidth of the passband and improve out-of-band rejection. The designed filters are connected to make a diplexer. The diplexer is designed to separate an input signal containing both 32 GHz and 35 GHz into two signals of 32 GHz and 35 GHz, respectively or to combine two signals at 32 GHz and 35 GHz into one signal.

Chapter IV describes a design procedure for a six channel multiplexer composed of parallel coupled-line microstrip bandpass filters. The passbands of the filters, *i.e.* channel frequencies, are 10, 12, 19, 21, 32, and 35 GHz. The operating frequency range

of the multiplexer is so wide that a method of harmonic suppression presented in Chapter II is used for the filters designed at 10 and 12 GHz.. The multiplexer developed in this research is used in the wideband transceiver system, which is discussed in the following chapter.

Chapter V discusses a multi-band, compact, and full-duplex beam scanning antenna transceiver system operating from 10 to 35. The system consists of ultra-wideband Vivaldi antennas, a multi-line PET-based phase shifter, a six-channel microstrip multiplexer described in Chapter IV, and monolithic microwave integrated circuit (MMIC) amplifiers. The beam scanning capability of the transceiver system is demonstrated at all six communication channels.

Chapter VI introduces a cost-effective implementation for extremely wideband phased-array radars. Two designs are introduced, one operating from 3 to 12 GHz and the other operating from 8 to 20 GHz. These designs incorporate ultra-wideband antipodal tapered slot antennas (ATSA), a novel cross-polarization suppressed array architecture, piezoelectric true time delay phase shifters, and broadband high-power monolithic amplifiers. The tests for pulse-radar target ranging and phased-array beam steering are performed for each array design.

Chapter VII presents a rectangular microstrip patch antenna with triple resonant frequencies. Two pairs of spur-lines are embedded in the non-radiating edges of the patch antenna to excite extra resonant frequencies.

Chapter VIII concludes this dissertation with a summary and discussion of the research accomplishments and recommendations for further studies.

CHAPTER II

MODIFIED MICROSTRIP PARALLEL COUPLED-LINE BANDPASS FILTER STRUCTURES FOR SUPPRESSION OF MULTI-SPURIOUS PASSBANDS

2.1. Introduction

Because of its planar structure, simple design, and easy implementation, the conventional microstrip parallel coupled-line bandpass filter has been widely used in RF front end of microwave and wireless communication systems since Cohn first proposed the structure in 1958 [16]. The filter is composed of half-wave length parallel coupled-line resonators but this type of filter has a disadvantage of having spurious passbands at the harmonics of the design frequency (f_0). These spurious passbands greatly limit the use of the microstrip parallel coupled-line bandpass filters in broadband systems. Since recent communication developments require a system that can operate over a multi-octave bandwidth, the spurious passbands at the harmonics ($2 f_0$, $3 f_0$, etc) of fundamental passband frequency could become a more serious problem

Many methods have been proposed to solve this problem. The most common type of method to suppress the first spurious passband is equalizing the even and odd mode phase velocities of the coupled-line. In [17] and [18], the two phase velocities are equalized by over-coupled resonators. The over-coupled resonator has an effect of

increasing the electrical length of the odd mode, which propagates faster than the even mode in the microstrip coupled-line. But this method can not suppress the second spurious passband which occurs at $3 f_0$. Another approach uses extra capacitors to slow down the odd mode phase velocity [19, 20]. In [21], and [22], square grooves are introduced in the coupled sections of the coupled-line filter to achieve identical electrical length of both even and odd mode propagations. But these methods also suppress only the first spurious passband. Recently, methods for suppressing both the first and the second spurious passbands were published but the methods require more complex design or fabrication procedures [23 - 25].

In this research, two modified microstrip coupled-line bandpass filter structures for suppression of multi-spurious passbands are presented. One incorporates spur-lines into the input and output resonators of the conventional microstrip parallel coupled-line bandpass filter and modifies the layout of the filter with the spur-lines for simultaneous suppression of the first and the second spurious passbands, which appears around $2 f_0$ and $3 f_0$, respectively. The other uses half-wave open-ended resonators placed near the edges of the conventional parallel coupled-line bandpass filter and bends the filter twice by 90 degrees.

2.2. Harmonic suppression with spur-lines

Two techniques are introduced in the design of a microstrip parallel coupled-line bandpass filter for suppression of both the first and the second spurious. First, spur-lines are incorporated into the conventional parallel coupled-line bandpass filter to suppress

the first spurious passband. Second, the layout of the filter with the spur-lines is modified for the suppression of the second spurious passband. Similar spur-lines have been incorporated into open-stub band stop filter for a better stop band rejection [26]. Another advantage of the proposed design in addition to the suppression of the spurious passbands is that the conventional parallel coupled-line bandpass filter is used without significant modifications. The design parameters used in the conventional microstrip parallel coupled-line bandpass filter can be used in the proposed filter with suppression of multi-spurious passbands. The new filter also has the advantage of reducing the overall length of the filter

2.2.1. Design

To demonstrate the design procedure for a microstrip parallel coupled-line bandpass filter with suppression of both the first and the second spurious passbands, a conventional microstrip parallel coupled-line bandpass filter centered at $f_0 = 2.45$ GHz is designed first following the well known procedures [27]. The filter has six coupling sections with a 10 % fractional bandwidth. The layout of the designed filter is shown in Fig. 1 and the physical dimensions of the layout are given in Table 1. The substrate employed has a relative dielectric constant $\epsilon_r = 10.2$ with thickness $h = 1.27$ mm.

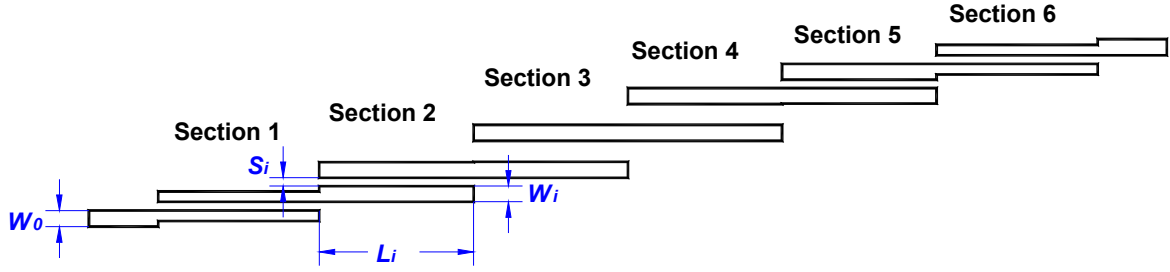


Fig. 1. Six-section conventional parallel-coupled microstrip bandpass filter centered at 2.45 GHz.

TABLE 1. Physical parameters for the filter shown in Fig.1. W_i , S_i , and L_i are the width, the separation between coupled-lines, and the length of the i th section, respectively. The input and output port strip width are $W_0 = 1.18$ mm, corresponding to 50 Ω .

(Unit: mm)

Sections	W_i	S_i	L_i
1 and 6	0.76	0.13	11.84
2 and 5	1.14	0.61	11.35
3 and 4	1.17	1.52	11.33

To suppress the first spurious passband at $2f_0$, spur-lines are incorporated in the coupling section 1 and 6 as shown in Fig. 2 (a). Bates [28] designed a microstrip spur-line band-stop filter with a bandwidth of order of 10 %, which can be fit in a microstrip line. Therefore, by incorporating spur-lines in the conventional bandpass filter the first spurious passband at $2f_0$ can be effectively suppressed. The initial length of the spur-line (a) and the gap size (b) at a center frequency f_0 can be determined from [28] as

$$a = \frac{2.997925 \times 10^8}{4f_0 \sqrt{K_{effo}}} - \Delta l_1 \quad (1)$$

where K_{effo} and Δl_1 are the odd mode effective dielectric constant and the effective

length extension due to the gap (b), respectively. The initial dimensions are optimized for better suppression of the first spurious passband using IE3D, a full wave electromagnetic simulator [29].

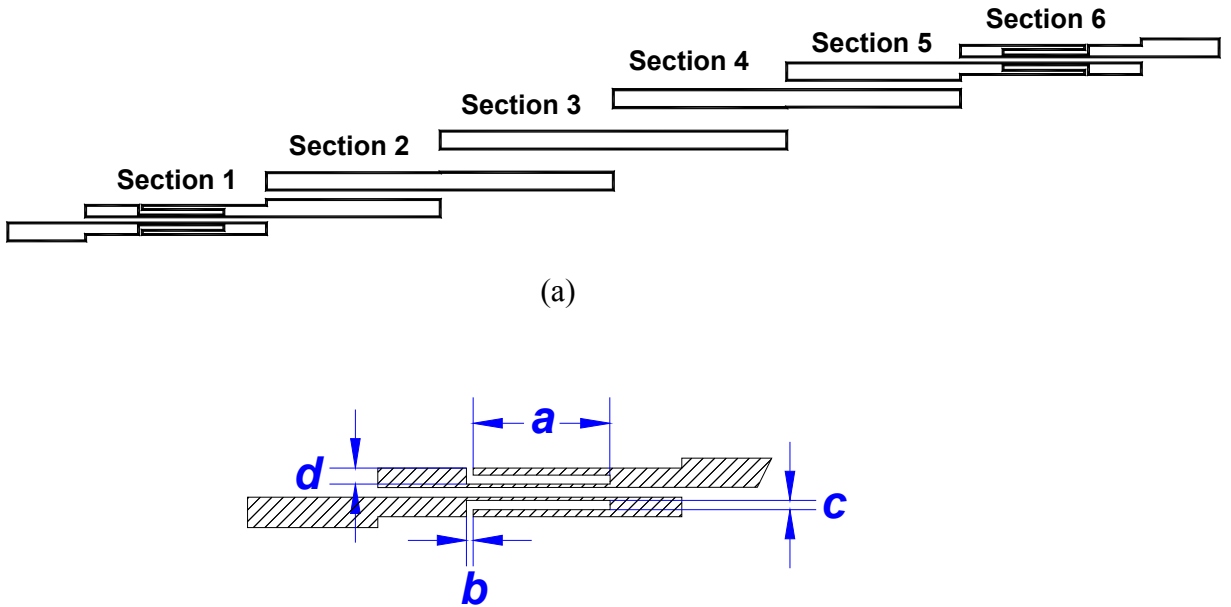


Fig. 2. Microstrip parallel coupled-line bandpass filter for suppression of the first spurious passband. (a) Layout of the filter incorporated with spur-lines. (b) Detailed view of the coupling section with spur-lines.

The optimized dimensions of the spur-line parameters of Fig. 2 (b) are: $a = 5.33$ mm, $b = 0.25$ mm, $c = 0.36$ mm, $d = 0.64$ mm. Fig. 3 shows the simulation results of the conventional parallel coupled-line bandpass filter and the modified filter shown in Fig. 2 (a). The first spurious passband is suppressed by more than 30 dB at $2f_0$. It can be observed that the second spurious passband at around $3f_0$ is also suppressed by the spur-line, although the suppression is not as much as the $2f_0$ case.

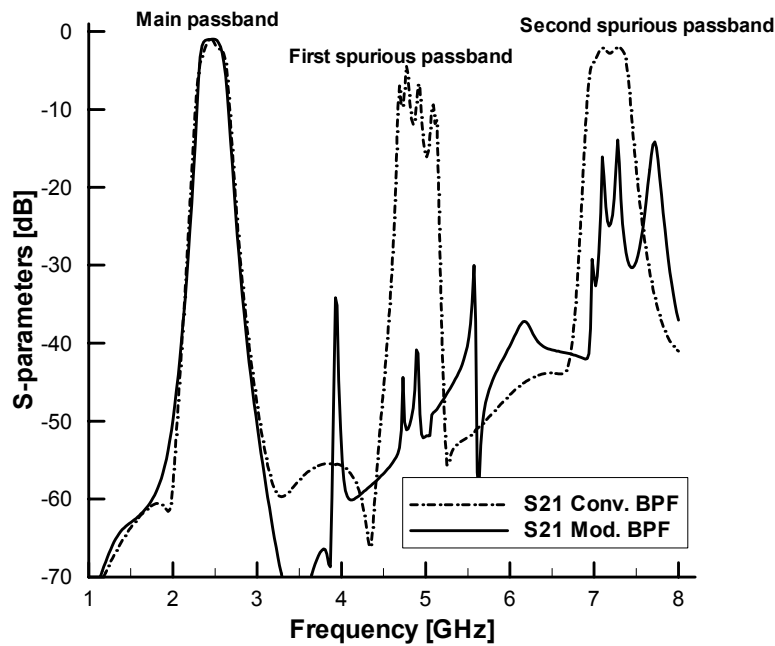
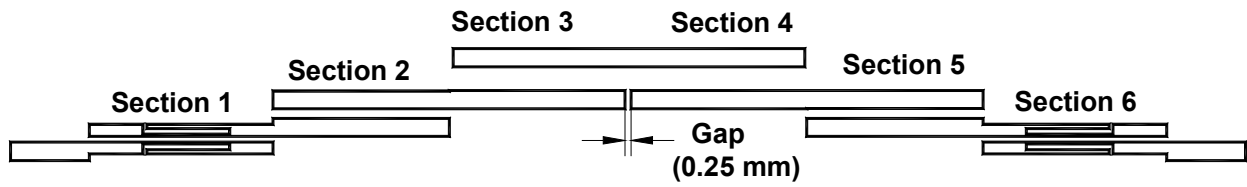
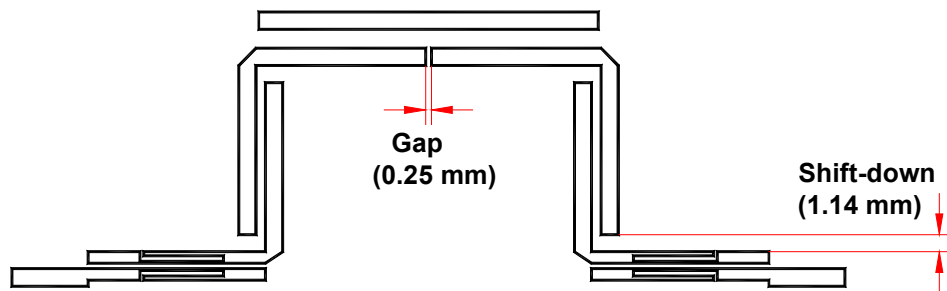


Fig. 3. Simulated frequency responses of the conventional parallel coupled-line bandpass filter and the modified bandpass filter shown in Fig. 2 (a).

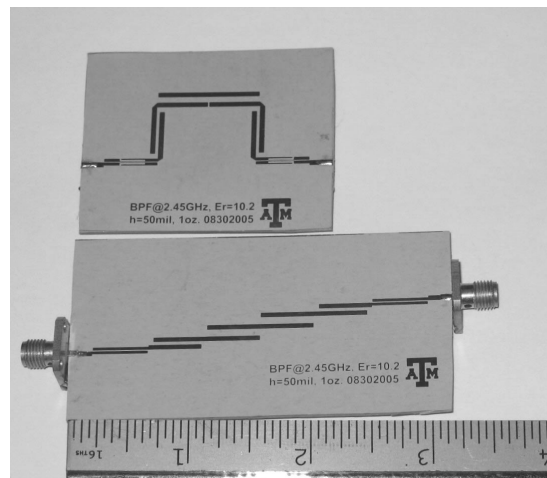
To achieve enough suppression of the second spurious passband at $3f_0$, the layout of the filters of Fig. 2 (a) is modified as shown in Fig. 4. Coupling sections 4, 5, and 6 of Fig. 2 (a) are flipped over vertically to become Fig. 4 (a) and a small gap of 0.25 mm is inserted between resonators of section 2 and 5 to prevent the two resonators from being connected. After flipping over, section 2 and 5 are bent by 90 degrees and slightly shifted down by 1.14 mm to preclude shorted resonators as shown in Fig. 4 (b). The photos of this new filter and the conventional filter are shown in Fig. 4 (c) for comparison.



(a)



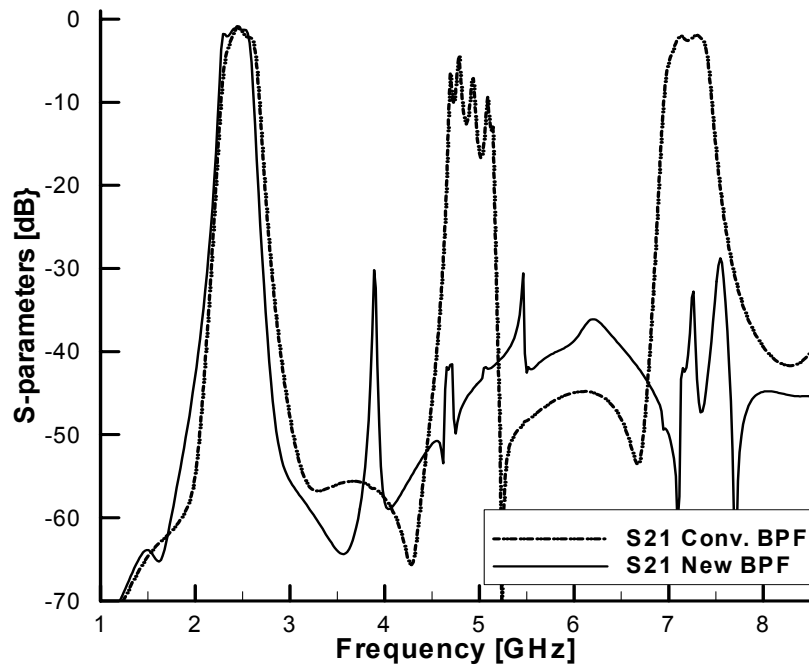
(b)



(c)

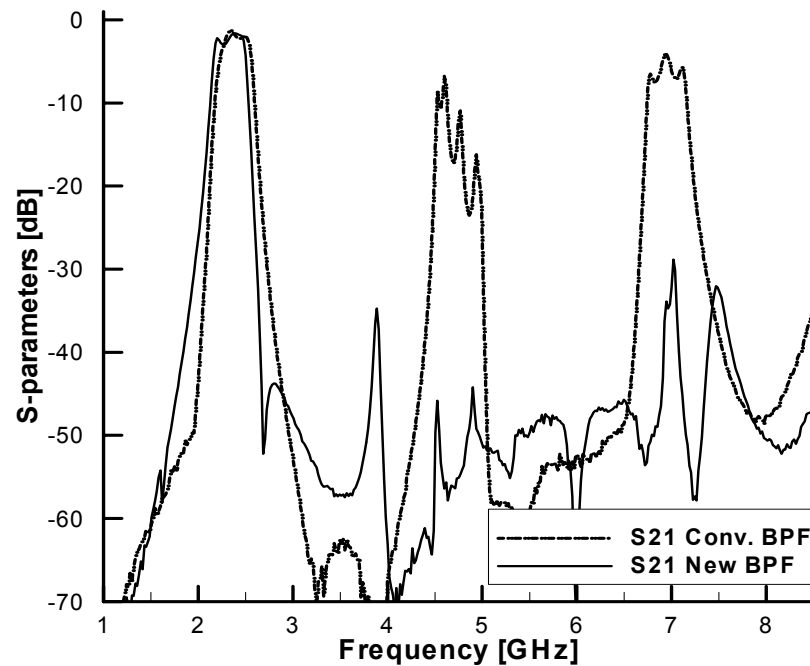
Fig. 4. Transformation of the filter shown in Fig. 2 (a) to obtain enough suppression of the second spurious passband. (a) Flipping vertically. (b) 90-degree bending and shifting down of sections 2 and 5. (c) Photos of the proposed new filter and the conventional filter. The top photo is for the new filter and the bottom photo is for the conventional filter.

Fig. 5 shows the simulated and measured frequency responses of the conventional parallel coupled-line bandpass filter and the filter proposed in this research as shown in Fig. 4 (b). By the flipping and bending procedures, the second spurious passband which does not appears exactly at $3f_0$ due to the dispersion effect is suppressed below -30 dB and the length of the filter can be reduced by 30 %. The measured insertion loss is 1.67 dB at 2.4 GHz. The simulation results match well with the measured results.



(a)

Fig. 5. Simulated and measured frequency responses of the conventional filter and the proposed filter. (a) Simulated results. (b) Measured performances.



(b)

Fig. 5. Continued.

2.3. Harmonic suppression with small resonators

Since all of the previously proposed methods for the harmonic suppression, which are mentioned in introduction of this chapter, demonstrate their performance for the filters designed around 2 GHz, it is not sure that they can work as well if the designed center frequency of the filter increases such that the harmonic frequencies are in the millimeter-wave region. Furthermore, when the harmonic frequencies are in the millimeter-wave region, the fabrication precision required for the methods mentioned earlier becomes more stringent. A novel and simple method is proposed in this research that requires neither change in the conventional filter design nor more precise fabrication

for suppression of spurious passbands even in the millimeter-wave region. Half-wave open-ended resonators are placed in the vicinity of the conventional parallel-coupled bandpass filter to suppress both the first and the second spurious passbands. In addition to placing the resonators, the conventional filter is bent twice for better suppression of the harmonic passbands. By bending the filter, a more compact filter can be obtained. There is no added complexity in fabrication compared to that of conventional filters. A parallel coupled-line bandpass filter centered at 12 GHz is designed using the proposed topology and measured for demonstration.

2.3.1. Filter design

The schematic diagram of a conventional parallel coupled-line microstrip bandpass filter is presented in Fig. 6. The filter is a five-section Chebyshev type bandpass filter with a center frequency (f_0) of 12 GHz and the passband bandwidth of 10%. The basic design methodology is the same as the conventional filter design procedure [27]. A better return loss can be achieved by decreasing the widths and the gap sizes of the input and output coupled resonators following the method used in [13]. The physical dimensions are listed in Table 2. The substrate is a 0.25-mm-thick Rogers 5880 Duroid substrate with a dielectric constant $\epsilon_r = 2.2$. Relatively thin substrate is used to reduce the radiation loss. The width of input/output lines is set to 0.84 mm making the characteristic impedance of the lines 50 Ω .

2.3.2. Harmonic suppression

First, to suppress the first spurious passband of the designed filter, one set of resonators which are half wavelength long at the second harmonic frequency ($2f_0$), is placed near the outer edge of the second and the fourth coupling sections as shown in Fig. 7. The 0.15-mm gap and 0.56-mm offset from the edge of the coupling section are decided by optimization process and consideration of etching tolerance. Fig. 8 is the simulated and measured frequency responses of the filter. The measured results show the first spurious passband is suppressed below -35dB .

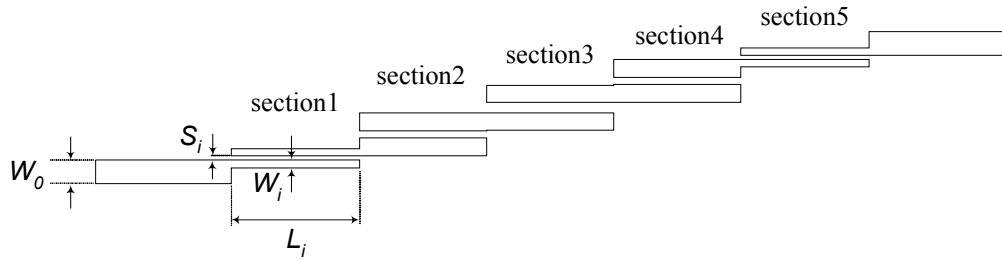


Fig. 6. Five-section conventional microstrip parallel coupled-line bandpass filter centered at 12 GHz.

TABLE 2. Physical parameters for the microstrip parallel coupled-line bandpass filter centered at 12GHz. The strip width of input/output ports (W_0) is 0.84 mm.

<i>Unit: mm</i>	W_i	S_i	L_i
Section 1 & 5	0.28	0.15	4.57
Section 2 & 4	0.64	0.28	4.52
Section 3	0.61	0.38	4.52

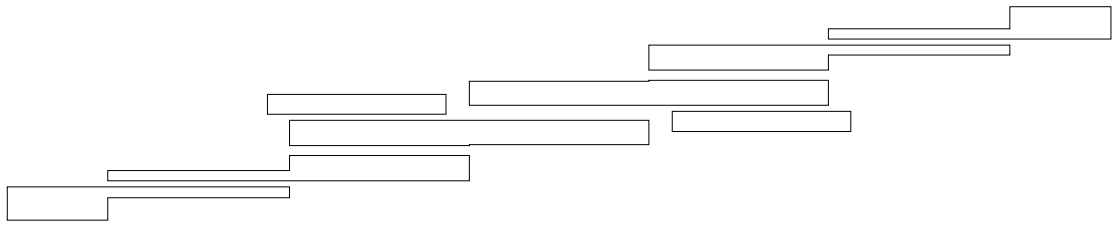
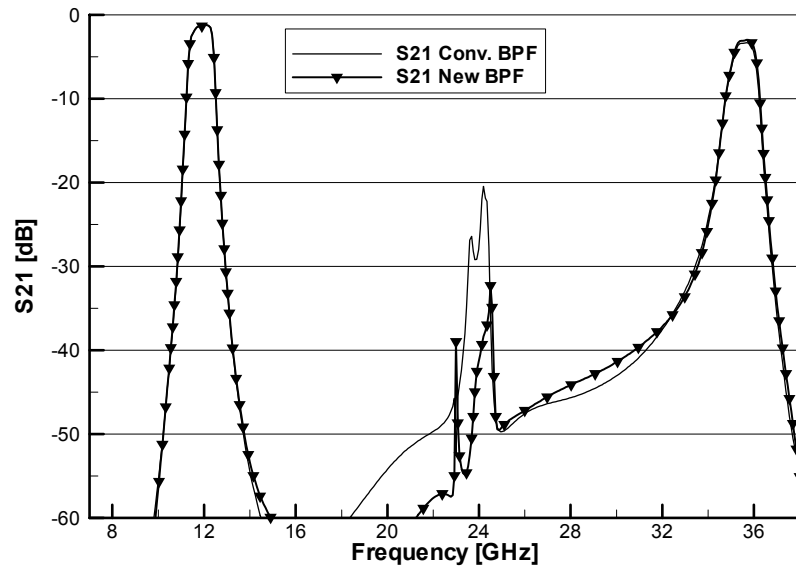
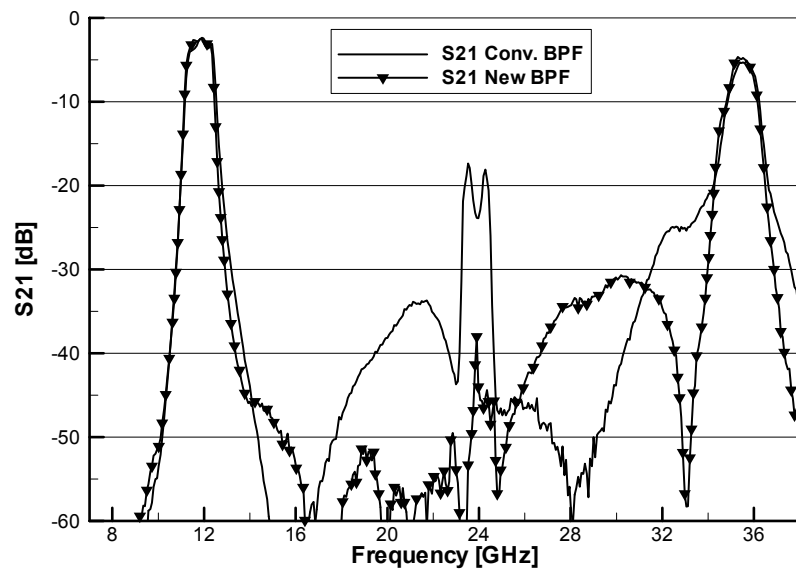


Fig. 7. Layout of the new filter with suppression of the first spurious passband.

For the suppression of the second spurious passband, which appears around $3f_0$, another set of resonators is placed near the edge of the first and the fifth coupling sections with a gap size of 0.15-mm as shown in Fig. 9. The length of the resonator is optimized to accurately suppress the second spurious passband. Furthermore, the resonators are modified to stepped-impedance resonators for better suppression.



(a)



(b)

Fig. 8. Simulated and measured frequency responses of the conventional filter and the new filter with suppression of the second harmonic passband. (a) Simulated responses. (b) Measured responses

It has been found from the simulation results that the suppression of the second spurious passband by using a set of resonator only is not enough, compared to the suppression of the first spurious passband. To obtain more suppression of the second spurious passband, the resonators of the coupling section 3 in Fig. 9 are bent by 90 degrees and their relative positions are changed so that the inner side of the coupling section becomes outer side as shown in Fig. 10. By bending and repositioning the resonators, the second spurious passband is better suppressed without affecting the main passband response. Besides the suppression of the spurious passbands, the total length of the filter can be shortened by bending. Fig. 11 shows the measured frequency responses of the finally designed bandpass filter with suppression of both the first and the second spurious passbands. The measured results in Fig. 11 show that the first spurious passband of the conventional filter is suppressed from -19.24 dB to -50.37 dB at 24.35 GHz and the second spurious passband is suppressed from -5.76 dB to -38.90 dB at 35.3 GHz. More than 30 dB suppression of both the first and the second harmonic passbands is achieved with the proposed method. There is no noticeable change in the main passband.

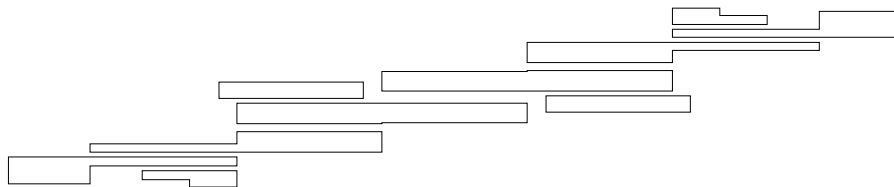
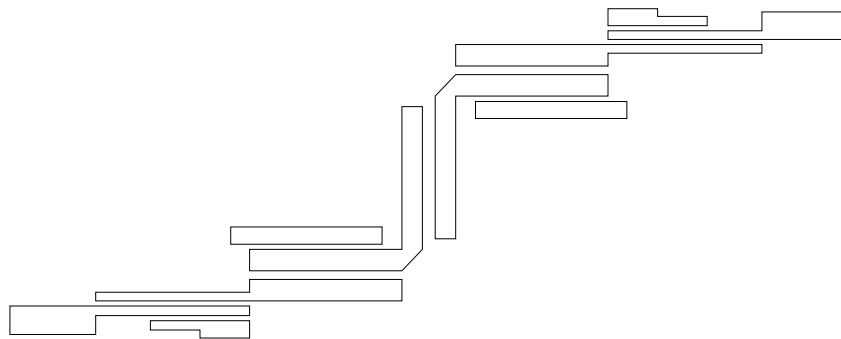
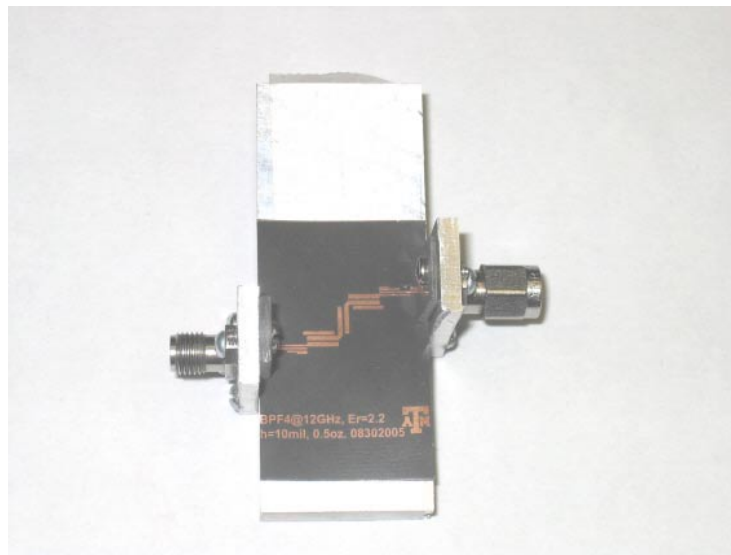


Fig. 9. Layout of the new filter with suppression of both the first and the second spurious passbands.

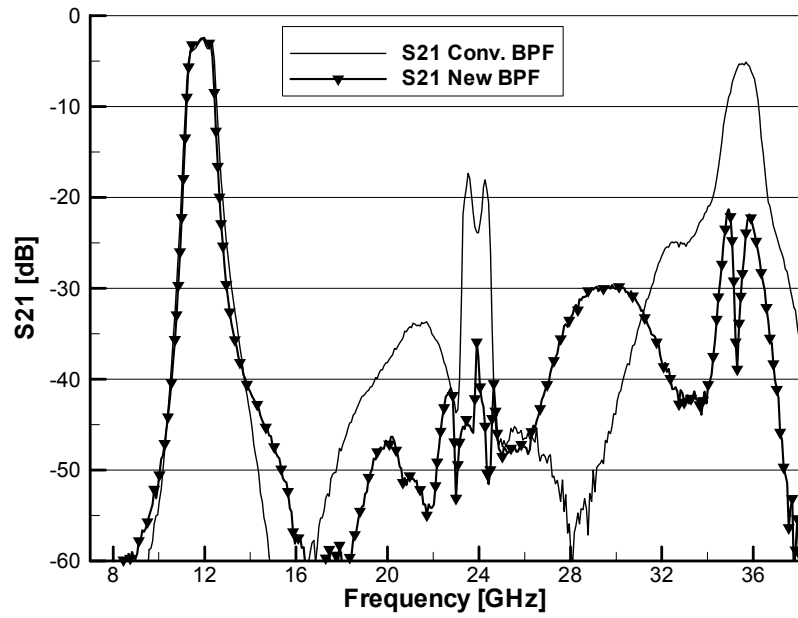


(a)

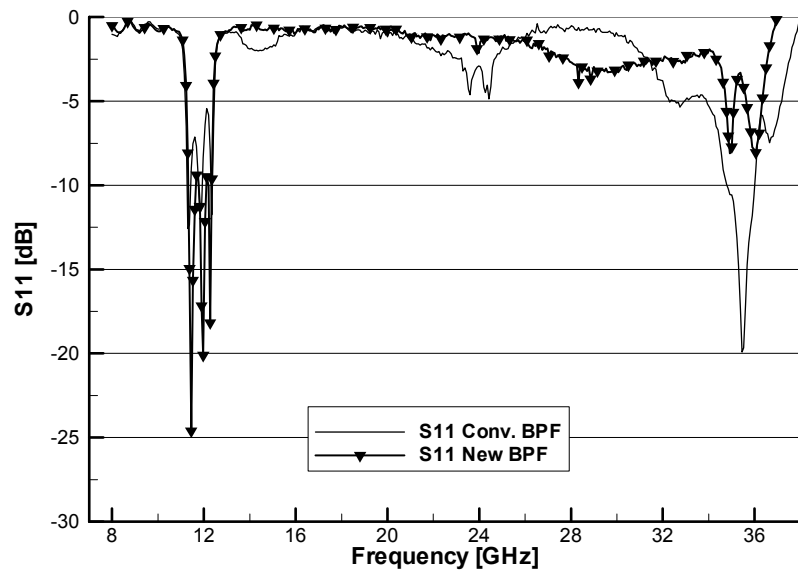


(b)

Fig. 10. (a) Layout of the new parallel-coupled microstrip bandpass filter. (b) Photo of the fabricated filter inside a test fixture.



(a)



(b)

Fig. 11. Measured results of conventional and new filter. (a) Insertion loss. (b) Return loss.

2.4. Conclusions

Two modified microstrip coupled-line bandpass filter structures for suppression of multi-spurious passbands have been introduced in this chapter. One structure incorporates spur-lines in the input and output resonators with simple transformation of the layout of the conventional parallel coupled-line microstrip bandpass filter to simultaneously suppress the first and the second spurious passbands, which appears near $2 f_0$ and $3 f_0$, respectively. Because of the transformation, the proposed filter becomes shorter than the conventional filter by 30 %. The insertion loss at the main passband is measured as 1.67 dB.

The other structure uses sets of half-wave length open-ended resonators placed near the coupling edges of the conventional filter to suppress the spurious passbands at harmonic frequencies. Discontinuities and repositioning of the coupling section caused by bending the filter give more suppression of the second spurious passband. This structure is used in the multiplexer design described in Chapter IV.

The measurement results show that both of the new filter structures suppress the first and the second spurious passbands below -30 dB and the main passband does not show any noticeable difference from that of the conventional microstrip parallel coupled-line bandpass filter.

CHAPTER III

STUB-TUNED MICROSTRIP BANDPASS FILTERS FOR MILLIMETER-WAVE DIPLEXER DESIGN*

3.1. Introduction

One of the essential components in RF front end of most communication systems is a diplexer. Diplexers are usually composed of two bandpass filters with different passband frequencies, whether they are contiguous or not [30]. The fast growth of the wireless communication technology has brought communication systems operating in millimeter-wave range. In millimeter-wave range, the filters used for diplexers are normally made of metal waveguide, because of its low insertion loss and high isolation. Other technologies like micromachining techniques are also used for filter design in this frequency range [6 - 8].

Microstrip line is a good candidate for filter design due to its advantages of low-cost, easy fabrication, compact-size, light weight, planar structure and easy integration with other components on a single circuit board. In millimeter-wave range, however, much attention has not been given to microstrip lines for filter and diplexer designs, because of their relatively high loss in this frequency range. Only a few literatures are reported so far [9]. Despite their relatively high loss in millimeter-wave range,

* © 2005 IEEE. Parts of this chapter are reprinted, with permission, from S. Hong and K. Chang, "Stub-tuned microstrip bandpass filters for millimeter-wave diplexer design," *IEEE Microwave & Wireless Components Lett.*, vol. 15, No. 9, pp. 582 - 584, Sep. 2005.

microstrip filters and their application to diplexer design still remain as an attractive research topic due to their aforementioned merits.

Generally, the use of thick substrate for microstrip circuits can make the width of a microstrip line wider for a given characteristic impedance. It is, therefore, desirable to use relatively thick substrate in the millimeter-wave range to reduce the resistive losses. But the use of thick substrate causes circuits composed of resonators to radiate strongly if their resonance frequencies are in millimeter-wave range [31]. Although edge-coupled half-wavelength resonators are the popular building block of microstrip bandpass filters, the filters with half-wavelength resonators will radiate strongly when the center frequency is designed to be in millimeter-wave range. The strong radiation tends to cause high insertion loss preventing microstrip filters from being used in the millimeter-wave range.

To reduce the resistive loss and the radiation from the resonators, the design in this research uses a relatively thick substrate and avoids the use of edge-coupled half wavelength resonators. With the use of thick substrate, the design can avoid the fabrication of many thin lines and narrow coupling gaps, which cause the high loss and difficulty in etching accurately. Instead of using half-wavelength resonators, the passband formed between neighboring stop bands of open-circuited stub is utilized for bandpass response. Additional open-circuited stubs are then placed on the input and output lines for the diplexer application. Diplexers composed of filters with open-circuited stubs were studied by Henryk [32] and Strassner and Chang [33]. But they are not appropriate for a phased-array transceiver system, because they cannot block low

frequency and/or DC signals needed for MMIC biases. In this research, a gap is inserted in the center stub of filters and it plays a key role in blocking the DC signals. Since there is only one gap in each filter, the filter can tolerate variation in the gap size caused by etching process better than the filters composed of edge-coupled half wavelength resonators.

3.2. Filter and diplexer design

The simulated response of the parallel-coupled microstrip lines to be used in the filter design is shown in Fig. 12. The substrate used is 0.51-mm thick RT/Duroid 5880 from Rogers with a relative dielectric constant $\epsilon_r = 2.2$. As can be seen from Fig. 12, the insertion loss becomes smaller as the frequency increases, making the lines suitable for bandpass filter design in the millimeter-wave range.

Two bandpass filters were designed for the center frequency of 32 GHz and 35 GHz, respectively. The filter centered at 32 GHz is denoted as transmit (Tx) filter and the filter with center frequency of 35 GHz is denoted receive (Rx) filter. Every simulation and optimization was done using IE3D [29].

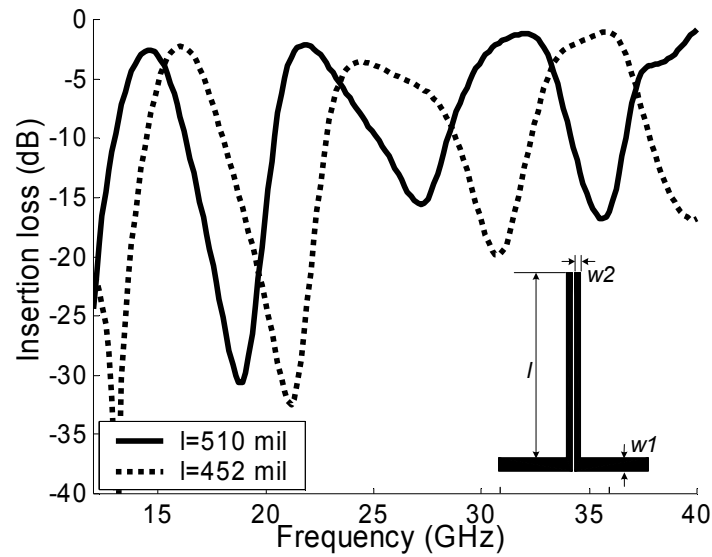


Fig. 12. Simulated frequency responses of parallel-coupled lines. ($w_1 = 0.91$ mm, $w_2 = 0.43$ mm, gap = 0.2 mm).

The out-of-band rejection of the coupled lines is less than 20 dB and should be improved. To do this, open-circuited stubs are added, their positions are optimized, and the width of upper side of the stubs is made thicker than that of lower side. Moreover, the lengths of the third stubs of the Tx filter and the third and the fourth stubs of the Rx filter from the center are slightly changed as shown in Fig. 13 (a) and (b). The gap sizes are optimized as 0.15 and 0.2 mm for the Rx and Tx filter, respectively. Simulation results show that the performances of the filters are stable with the gap size variation of -0.1 to $+0.2$ mm.

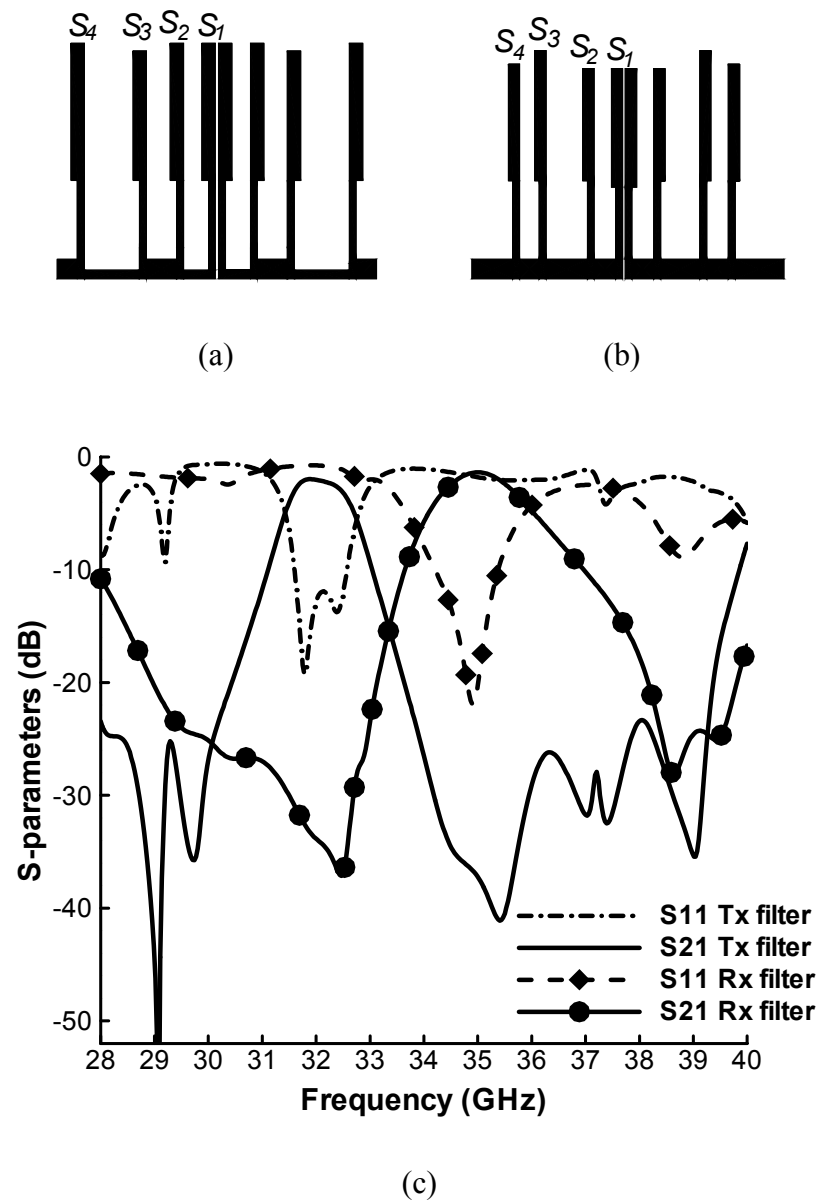


Fig. 13. Layouts of the designed bandpass filters and their simulated responses (a) Tx filter centered at 32 GHz. (gap = 0.2 mm). (b) Rx filter centered at 35 GHz. (gap = 0.15 mm). (c) Simulated responses of the two filters.

For the Tx filter, the upper frequency side skirt became smoother than that of lower side even after the methods mentioned above were applied. To make the slope

steeper, the widths of input and output lines of Tx filter are perturbed as shown in Fig. 13 (a), which has the effect of incorporating a low pass filter. Fig. 13 shows the layouts of the designed filters and simulated results of the filters. The two filters have the insertion losses of about 2 dB and their return losses are bigger than 15 dB. The rejection of filters at each other's passband is more than 30 dB. The physical dimensions are listed in Table 3.

TABLE 3. Physical parameters for the designed filter. (Unit: mm)

Tx filter	Stub length/width (Thick part)	Stub length/width (Thin part)	Connecting line between this and next stub (length/width)
S ₁	8.03/0.84	5.26/0.43	1.55/0.51
S ₂	8.03/0.84	4.62/0.43	1.88/1.14
S ₃	7.57/0.84	5.26/0.43	3.43/0.51
S ₄	8.03/0.84	4.62/0.43	-/1.14
Rx filter	Stub length/width (Thick part)	Stub length/width (Thin part)	Connecting line between this and next stub (length/width)
S ₁	6.96/0.71	4.22/0.43	1.35/1.14
S ₂	6.58/0.71	4.60/0.43	2.57/1.14
S ₃	7.62/0.71	4.60/0.43	1.09/1.14
S ₄	6.83/0.71	4.60/0.43	-/1.14

Having designed the two bandpass filters, they are connected to make a diplexer as shown in Fig.14. In millimeter-wave range, a little change in the length between the junction and each filter makes significant variations in the return loss and the insertion loss of the diplexer. The lengths are optimized such that each filter in the diplexer should look like an open circuit to the other filter at its center frequency. At the input and output ports of the diplexer, stepped impedance transformers are added to improve the return

loss at each port. The width of each port is 1.55 mm, which is corresponding to the width of 50 Ω microstrip line at the operating frequency of the diplexer.

Fig. 15 shows the comparison of the simulated and measured frequency responses of the diplexer. Due to the discontinuity caused by the junction, the insertion loss of each filter in the diplexer is slightly increased from the insertion loss of the filter itself. The diplexer was measured using K-connectors as shown in Fig. 16 and an HP 8510C network analyzer. To remove the effect of the connectors, the measured results are calibrated using a Thru-Reflect-Line (TRL) calibration. The measured insertion loss is 3.5 dB at 32 GHz and 3.2 dB at 35 GHz. The return loss is more than 10 dB at both 32 GHz and 35 GHz. The isolation is more than 30 dB for the two frequencies. The passband has a bandwidth of about 2 GHz at 32 GHz and 1.3 GHz at 35 GHz.

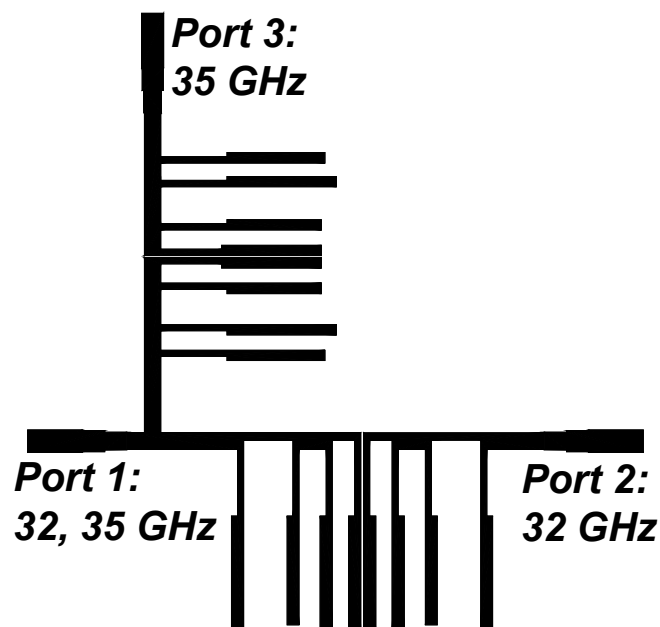


Fig. 14. Layout of the designed diplexer.

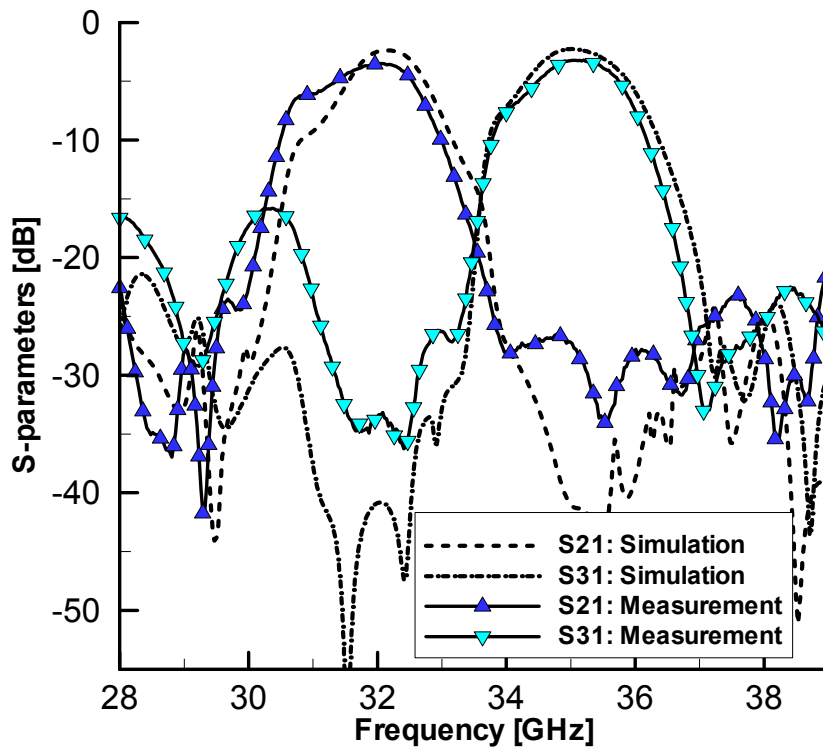


Fig. 15. Simulated and measured frequency responses of the diplexer.

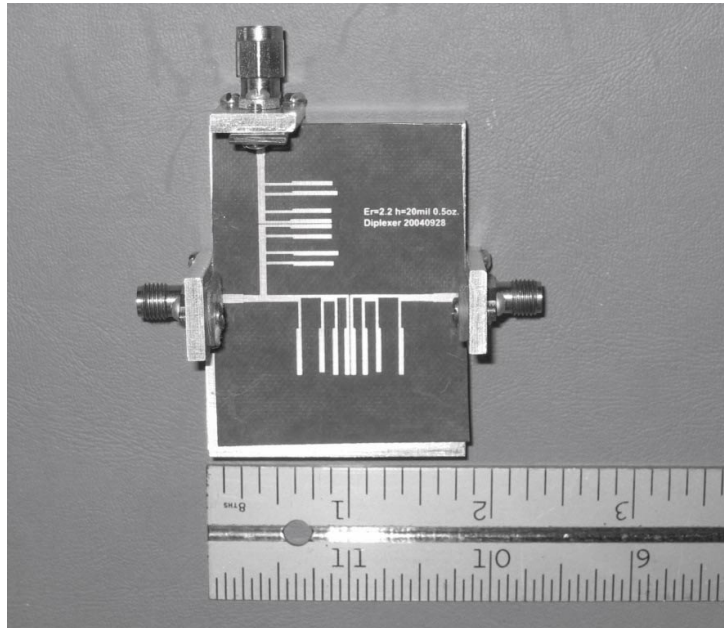


Fig. 16. Photo of the fabricated diplexer inside a test fixture.

3.3. Conclusions

Two microstrip bandpass filters are designed and they are connected to form a diplexer in millimeter-wave range. The diplexer takes an input signal from port 1 and separates 32 GHz signal to port 2 and 35 GHz signal to port 3. The diplexer was fabricated and measured to verify the design. The simulated and measured data matches well with each other. The insertion loss is 3.5 dB for port 2 and 3.2 dB for port 3, which is good for the relatively thick substrate used for the diplexer. The diplexer can be used in a phased-array transceiver system operating in millimeter wave range.

CHAPTER IV

A 10—35-GHZ SIX-CHANNEL MICROSTRIP MULTIPLEXER FOR WIDEBAND COMMUNICATION SYSTEMS*

4.1. Introduction

Today, it is required that satellite, mobile, and other communication systems operate in full-duplex mode. The systems are also required to operate over a wide band or multi-frequency bands. To meet these requirements, the system should be able to transmit and receive signals simultaneously over its operating frequency range and must have a way to provide high degree of isolation between transmit and receive paths to prevent the receiver from being degraded by the leakage from the transmitter and to maintain good signal to noise ratio. Multiplexers provide isolation between transmit and receive channels by assigning a different frequency band to each channel and can operate over a wide bandwidth. Microstrip multiplexer used for multi-frequency, full-duplex and phased-array antenna systems has been reported in [13].

In this research, a compact, six-channel, wideband multiplexer is developed. The design of the filters constituting the multiplexer will be presented first then the procedure of constructing the multiplexer will be explained. The multiplexer is

* © 2006 IEEE. Parts of this chapter are reprinted, with permission, from S. Hong and K. Chang, “A 10—35-GHz six-channel microstrip multiplexer for wide-band communication tuned microstrip bandpass filters for millimeter-wave diplexer design,” *IEEE Trans. Microw. Theory Tech.*, vol. 54, No. 4, pp. 1370 - 1378, Apr. 2006.

composed of six microstrip parallel coupled-line bandpass filters and can offer full duplex operation over an extremely wide frequency range from 10 to 35 GHz. Because of the wide operation bandwidth of the multiplexer, the bandpass filters centered at lower frequencies, *i.e.* 10 and 12 GHz should be able to reduce the spurious passbands at the harmonic frequencies of the designed passband frequency (f_0). Many methods have been proposed to suppress the spurious passbands inherent to the microstrip parallel coupled-line bandpass filters [17 - 25]. In this research, a novel and simple method presented in Chapter II is used to suppress the spurious passbands of the bandpass filters centered at 10 and 12 GHz. With the method presented, the conventional microstrip parallel coupled-line bandpass filters can be used without any changes. Instead of modifying the filter itself, small half wavelength resonators are placed in the vicinity of the conventional filter. The small resonators invoke matching conditions for the wave propagating through the filter at the harmonic frequencies, perturb the current distribution on the coupled-lines of the filter and reject the spurious passbands. A transmission line model is used to predict the extra resonances caused by the added resonator.

The construction of the multiplexer by connecting each microstrip bandpass filter requires a great deal of effort, because there are many optimization variables and even a slight change in the length of any microstrip line connecting each filter will change the frequency responses of the multiplexer. The initial condition for optimization is important to avoid the local minima and reduce the optimization time. The procedure of designing the multiplexer, taking into account of these considerations, is presented in

section 4.

When connected with wideband MMIC amplifiers and phased-array antenna as shown in Fig. 17, the multiplexer routes transmitting signals at 10, 19, and 32 GHz from the power amplifiers and then sends the amplified signals to the phased-array antenna. We call this path as a transmit path. On the other hand, in the receive path, it receives signals at 12, 21, and 35 GHz from the antenna and routes them to the low noise amplifiers. A bandwidth of at least 500 MHz is required for each channel. The multiplexer presented in this research should have many applications in full-duplex multi-band communication systems and radar systems.

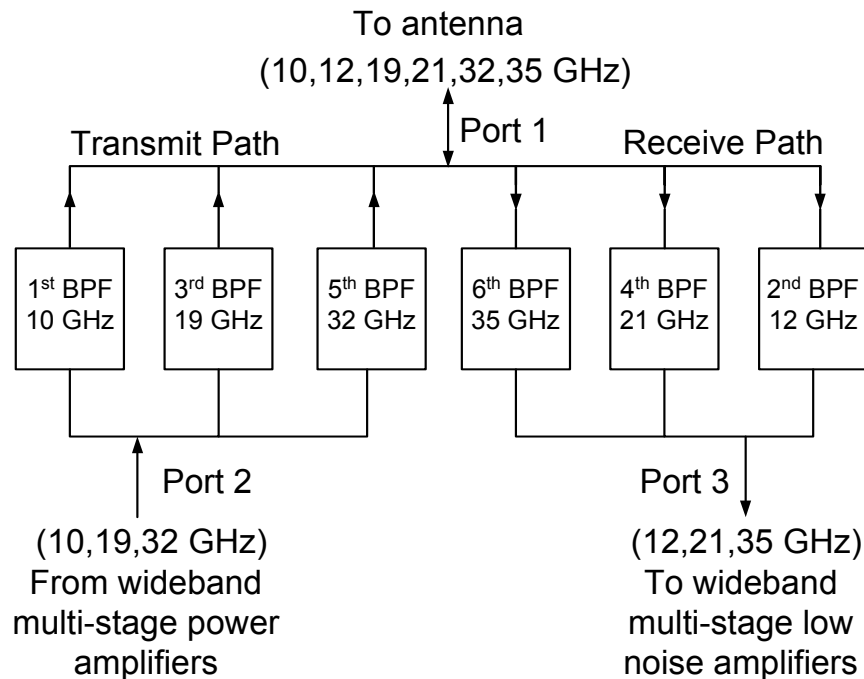


Fig. 17. Block diagram of the multiplexer.

4.2. Channel filter design

To construct a six-channel multiplexer, six bandpass filters shown in Fig. 17, whose passbands are corresponding to each channel of the multiplexer, should be designed first. In this research, conventional microstrip parallel coupled-line bandpass filter composed of half wavelength resonators is chosen for the channel filter of the multiplexer, because of its compactness, easy fabrication and low cost. However, the radiation from the filter with half wavelength resonators increases as the designed center frequency of the filter operates in the millimeter-wave region, causing high insertion loss. The loss due to the radiation becomes severe if a thick substrate is used. For this reason, a thin 0.25-mm substrate is selected for the filter design. The actual substrate used is 0.25-mm thick RT/Duroid 5880 from Rogers with a relative dielectric constant $\epsilon_r = 2.2$. All six filters have five coupling sections and a bandwidth of about 10%. The basic design procedure follows the conventional parallel coupled-line filter design methods [16] and the designed filters are optimized using IE3D. The coupling sections of the filters are symmetrical with respect to the third section, that is, the first and the second sections have same physical dimensions as the fifth and fourth sections. Fig. 18 shows the physical layout of the designed filters and the actual dimensions of each filter are summarized in Table 4. The width of input/output lines is set to 0.84 mm making the characteristic impedance of the lines 50Ω .

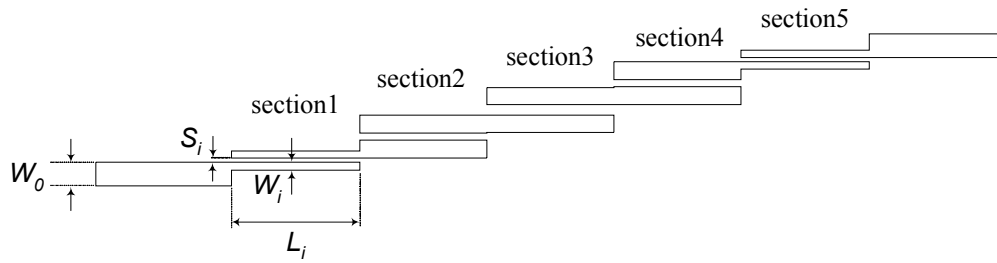


Fig. 18. Layout of the designed filters. ($W_0 = 0.84$ mm)

The three filters centered at 10, 19, and 32 GHz are placed in the transmit path of the multiplexer and their simulated responses are shown in Fig. 19. The three filters in the receive path of the multiplexer have center frequencies of 12, 21, and 35 GHz, respectively and their simulated responses are shown in Fig. 20. Table 5 shows the simulated insertion losses of the designed filters. The insertion loss of the filter is less than 2 dB even in the millimeter-wave region, although it has higher losses at 32 and 35 GHz due to the higher dielectric and radiation loss.

TABLE 4. Dimension of designed microstrip parallel coupled-line bandpass filters.
(Unit: mm)

Center Freq.	10 GHz			12 GHz		
Section	W_i	S_i	L_i	W_i	S_i	L_i
1 and 5	0.28	0.15	5.46	0.28	0.15	4.57
2 and 4	0.61	0.25	5.46	0.64	0.25	4.52
3	0.48	0.46	5.46	0.61	0.38	4.52
Center Freq.	19 GHz			21 GHz		
Section	W_i	S_i	L_i	W_i	S_i	L_i
1 and 5	0.28	0.15	2.84	0.28	0.15	2.56
2 and 4	0.51	0.25	2.79	0.51	0.25	2.51
3	0.28	0.46	2.87	0.28	0.46	2.59
Center Freq.	32 GHz			35 GHz		
Section	W_i	S_i	L_i	W_i	S_i	L_i
1 and 5	0.28	0.15	1.65	0.28	0.15	1.47
2 and 4	0.51	0.35	1.60	0.51	0.38	1.50
3	0.28	0.51	1.68	0.28	0.51	1.50

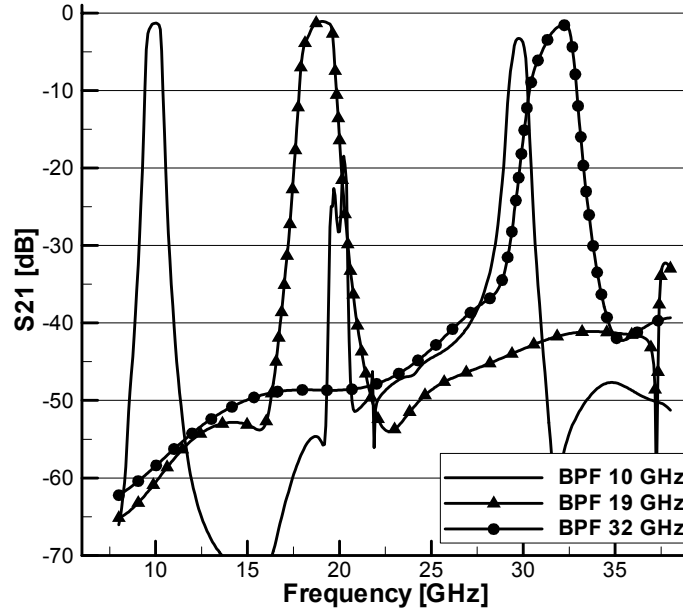


Fig. 19. Simulated frequency responses of the designed filters to be placed in the transmit path of the multiplexer. The designed frequencies are 10, 19, and 32 GHz, respectively.

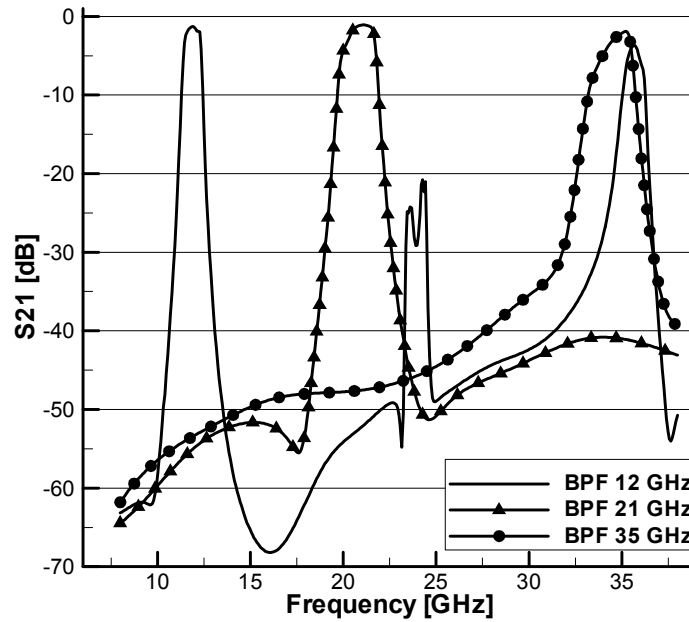


Fig. 20. Simulated frequency responses of the designed filters to be placed in the receive path of the multiplexer. The designed frequencies are 12, 21, and 35 GHz, respectively.

TABLE 5. Simulated insertion loss (IL) of the designed bandpass filters.

Center Freq.(GHz)	IL (dB)	Center Freq.(GHz)	IL (dB)
10	1.3	12	1.3
19	1.1	21	1.1
32	1.6	35	1.9

4.3. Harmonic suppression of the channel filters

In Fig. 19, it can be seen that the spurious passband responses of the filter designed at 10 GHz appear around the harmonic frequencies of 20 and 30 GHz and overlap in part with the passbands of filters designed at 19 and 32 GHz, respectively. Same

phenomenon happens for the filter designed at 12 GHz as can be seen in Fig. 20, but at the third harmonic frequency, the level of the insertion loss is close to that of the filter designed at 35 GHz and the overlapping bandwidth occupies about the half of the passband of the filter designed at 35 GHz. Unfortunately, the spurious responses at $2f_0$ and $3f_0$ are inevitable for the microstrip parallel coupled-line filters composed of half wavelength resonators. If the spurious passbands are not suppressed properly, these overlapping passbands can provide signals at 32 and 35 GHz with multiple paths or a loop path, causing signal distortions when all the filters are connected together to form a multiplexer.

Many methods have been reported to suppress the spurious passbands at the harmonic frequencies but every method has its own merits and disadvantages. To mention a few, the method in [21] provides different lengths for the even and the odd modes to suppress the spurious passbands only at $2f_0$. The method in [23] uses a uniplanar compact photonic-bandgap (UC-PBG) structure to reject the spurious passbands at both $2f_0$ and $3f_0$. But the physical dimensions of the microstrip parallel coupled-line bandpass filter should be redesigned and additional etching and accurate alignment are required because of the UC-PBG structure in the ground plane. A novel and simple method presented in Chapter II is used to suppress the spurious passbands of the bandpass filters centered at 10 and 12 GHz.

To show the basic idea of the method presented in Chapter II, a half-wavelength open-ended microstrip resonator and a half wavelength microstrip parallel coupled-line shown in Fig. 21 are investigated first at its resonant frequency f_r . The input impedance

Z_{in} of a lossless half wavelength resonator when one end is terminated with open circuit is

$$Z_{in} = -jZ_0 \cot(\beta(l+l_e)) = jX_{in} \quad (2)$$

where l is the physical length of the resonator corresponding to the half wavelength and l_e is the additional length due to the effect of the open end [34]. The input impedance of a microstrip parallel coupled-line can be computed from the ABCD matrix of the line. The ABCD matrix of a parallel coupled-line can be expressed as [35]

$$A = \frac{Z_{0e} \cot \theta_e + Z_{0o} \cot \theta_o}{Z_{0e} \csc \theta_e - Z_{0o} \csc \theta_o} = D \quad (3a)$$

$$B = \frac{j}{2} \frac{Z_{0e}^2 + Z_{0o}^2 - 2Z_{0e}Z_{0o}(\cot \theta_e \cot \theta_o + \csc \theta_e \csc \theta_o)}{Z_{0e} \csc \theta_e - Z_{0o} \csc \theta_o} \quad (3b)$$

$$C = \frac{2j}{Z_{0e} \csc \theta_e - Z_{0o} \csc \theta_o} \quad (3c)$$

where Z_{0e} is the even mode characteristic impedance, Z_{0o} is the odd mode characteristic impedance of the coupled transmission line, θ_e is the even mode electrical length, and θ_o is the odd mode electrical length of the line.

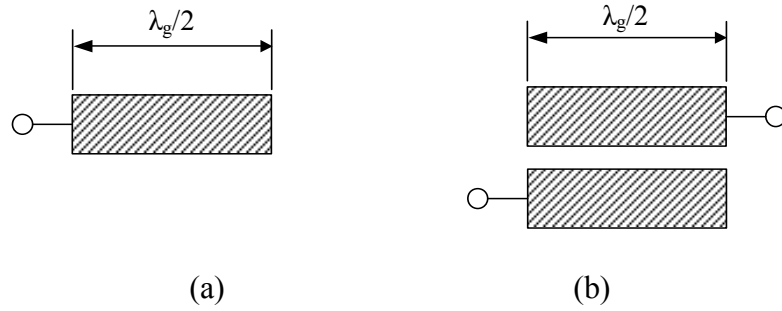


Fig. 21. Half wavelength resonators; (a) Single microstrip line. (b) Parallel-coupled microstrip line. (λ_g is the guided wavelength)

For a two-port network, if one of its ports is terminated with a load impedance of Z_L , the input impedance ($Z_{in,c}$) seen from the other port can be calculated from the ABCD matrix of the network. Therefore, when one of the ports is terminated with an open circuit, the input impedance of the coupled line in Fig. 21 (b) can be calculated as

$$Z_{in,c} = -j \frac{Z_{0e} \cot \theta_e + Z_{0o} \cot \theta_o}{2} = jX_{in,c} \quad (4)$$

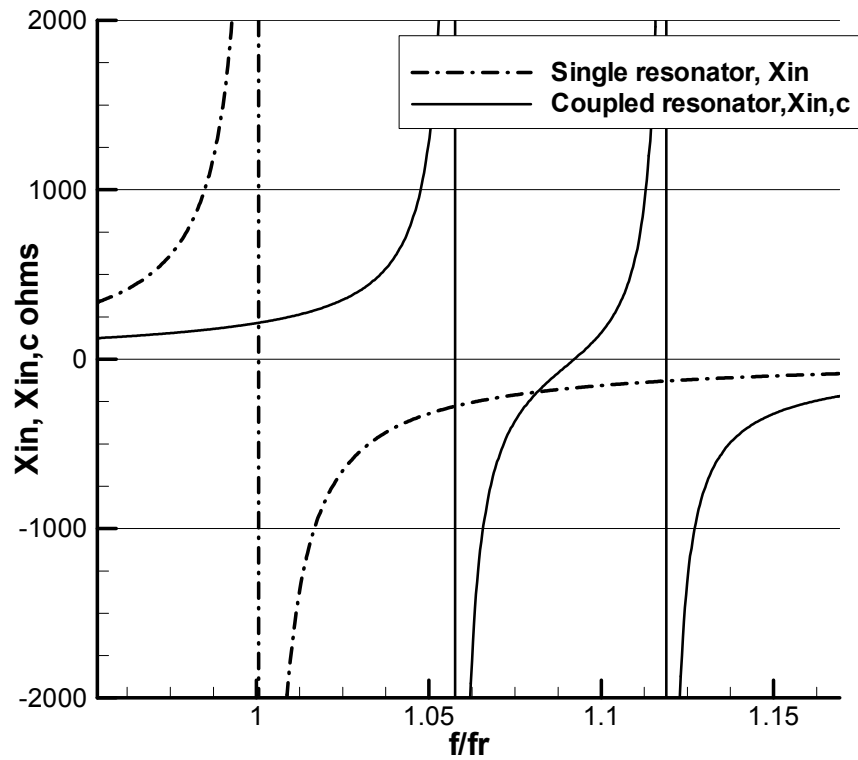


Fig. 22. Variations of X_{in} and $X_{in,c}$ with frequency.

Fig. 22 shows the frequency responses of X_{in} and $X_{in,c}$ calculated by (2) and (4). As can be seen in the figure, $X_{in,c}$ has an additional resonance near the resonant frequency of X_{in} .

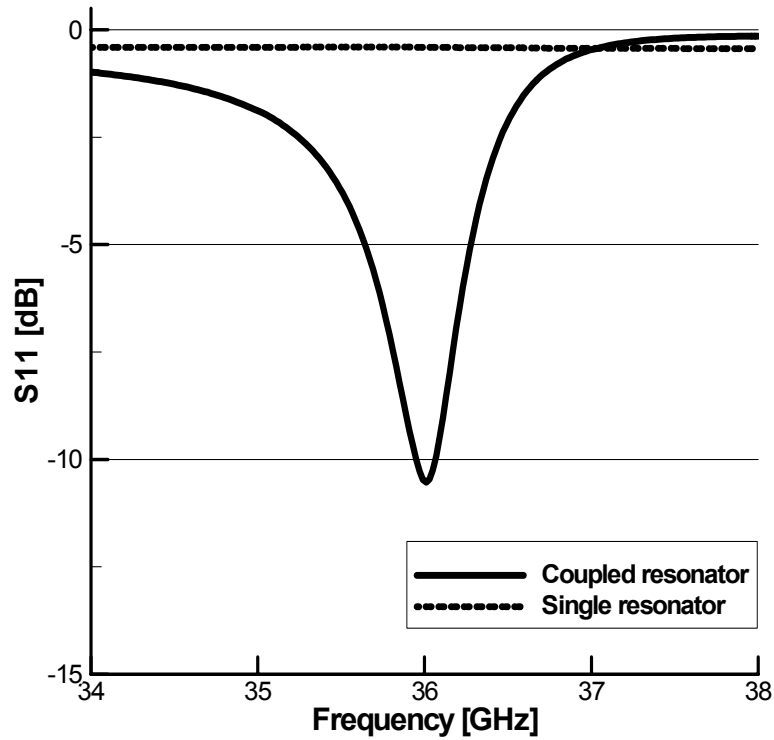


Fig. 23. S11 responses of the single microstrip resonator and the coupled resonator.

Due to this additional resonance, there is a frequency where $X_{in,c}$ becomes zero and this zero hinders a wave in traveling through the filter at that frequency. The frequency of the zero can be predicted from (4) as

$$Z_{0e} \cot \theta_e = -Z_{0o} \cot \theta_o \quad (5)$$

Therefore, it is possible to suppress the spurious passband by placing an open-circuited resonator near resonators of a microstrip parallel coupled-line bandpass filter

and adjusting the resonant frequency of so-formed coupled lines such that the frequency where the $X_{in,c}$ becomes zero, can be close to the harmonic frequency of the microstrip bandpass filter. The method is verified by full-wave simulation as shown in Fig. 23. Because of the good return loss at the harmonic frequency, which is 36 GHz in this simulation, it is difficult for the resonators of the filter to sustain the standing wave necessary for the passband at 36 GHz. The small resonator placed near the coupling section, therefore, can be considered as a matched load at the harmonic frequency of 36 GHz and the 10 dB return loss is contributed mainly by ohmic loss. The change in the input impedance of the resonators by forming a coupled line makes better return loss and give rise to matching condition to the resonator of the filter at the desired frequency as shown in Fig. 23. At the harmonic resonance frequency, standing waves exist on the resonators of the conventional microstrip parallel coupled-line bandpass filter and the standing waves cause the spurious passband. The matching condition introduced by the coupled line of the proposed filter prevents the standing waves from existing on the proposed filter at the harmonic frequency and thus suppresses the passband at that frequency. To suppress the harmonics passband, the method is applied to the filter designed at 12 GHz.

To suppress the second harmonic passband of the filter centered at 12 GHz with its layout shown in Fig. 18, open-circuited resonators are placed near the outer edge of first, third and fifth coupling sections as shown in Fig. 24. For the third coupling section, two resonators are placed for symmetry. The length of the resonators is half wavelength at the second harmonic frequency of 24 GHz. For the third harmonic suppression, a

resonator is placed near the edge of the second and the fourth coupling sections with a length of one-half wavelength at the third harmonic frequency ($3f_0$) of the filter. The gap size of the coupled line is decided as 0.15 mm after the optimization process.

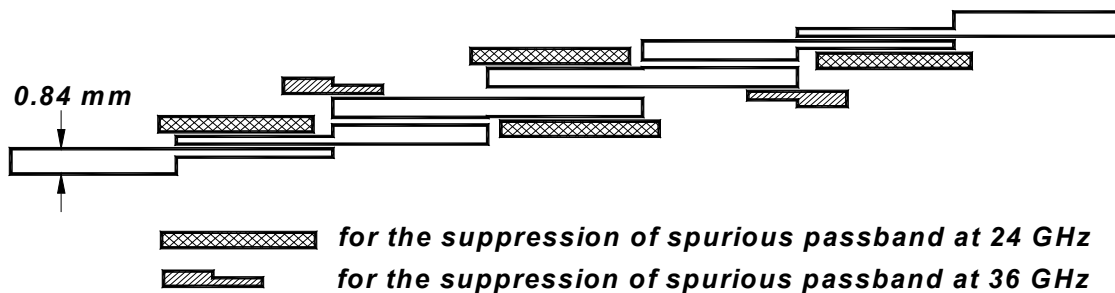
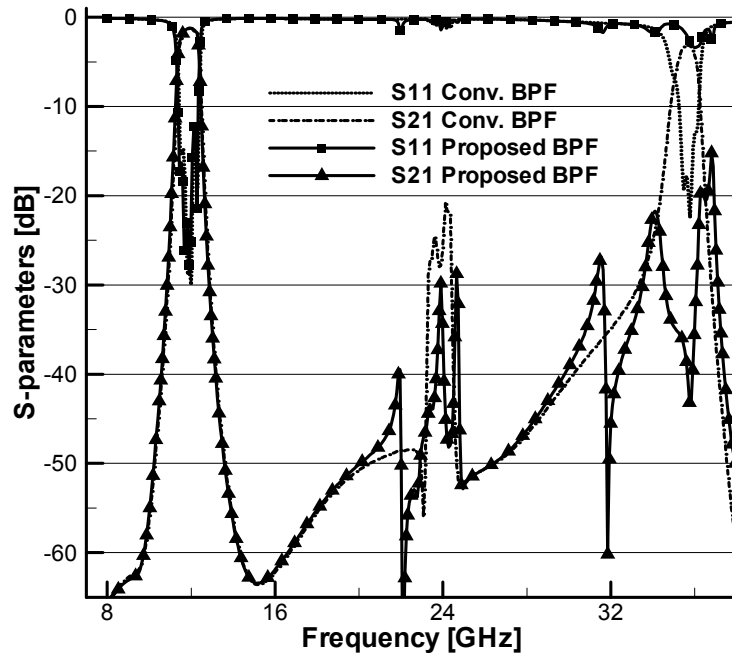


Fig. 24. Proposed parallel-coupled microstrip bandpass filter designed at 12 GHz with suppression of both the second and the third harmonic responses.

As mentioned earlier in this section, the third harmonic passband of the filter designed at 12 GHz is more problematic when operating with the filter designed at 35 GHz. The resonators for suppressing the third harmonic passband is, therefore, modified to stepped impedance resonator and their position is optimized to have wider suppression and rejection bandwidth. Fig. 24 shows the final layout of the proposed microstrip parallel coupled-line bandpass filters centered at 12 GHz.

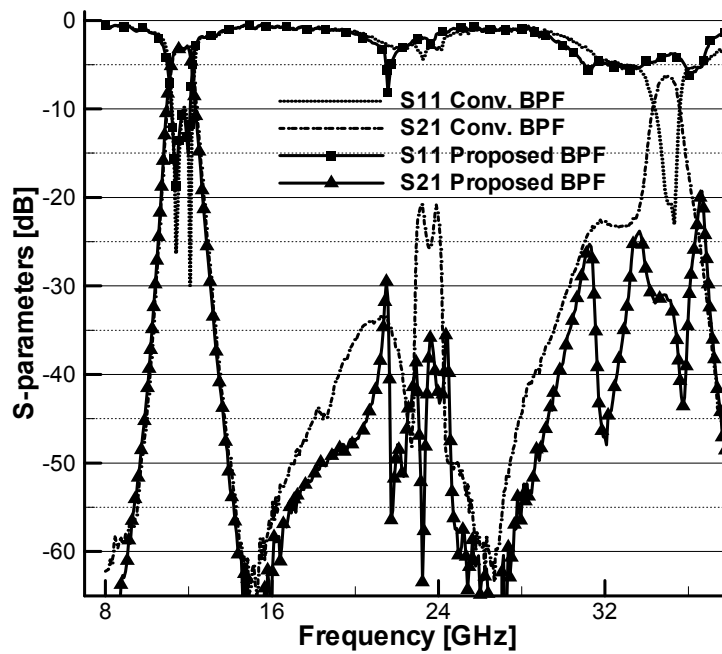
Fig. 25 shows the simulated and the measured frequency responses of the conventional and the proposed microstrip parallel coupled-line bandpass filters. The measured result shows that the second harmonic passband of the conventional filter is suppressed below -35 dB and the third harmonic passband is suppressed from -7.6 dB to -42.5 dB at 35.7 GHz. Over 30 dB suppression for the third harmonic passband is

achieved with the proposed method. It should be emphasized that the main passband is almost the same for the conventional and the proposed filters. The same procedure is applied to the filter designed at 10 GHz.



(a)

Fig. 25. Simulated and measured performances of the conventional and proposed filters.
(a) Simulated results. (b) Measured results.



(b)

Fig. 25. Continued.

4.4. Multiplexer design and measurement

Although several multiplexer design methods have been published so far, [36, 37], they are mainly applicable to the manifold multiplexing technique and, generally, practical multiplexers need some tuning after fabrication. The multiplexer presented in this chapter is composed of microstrip bandpass filters. Unlike the waveguide multiplexers, the microstrip multiplexer has higher loss [9] and is difficult to tune after fabrication. Therefore, precise design should be carried out before fabrication. In spite of these drawbacks, the reasons for selecting the microstrip filter as channel elements are its compact size, light weight, low cost fabrication, and easy integration with other

microstrip circuits in a system. Some of the circuits in the system that will be integrated with the multiplexer include phase shifters, MMIC amplifiers and microstrip feed wideband antennas. The configuration of the multiplexer is shown earlier in Fig. 17. There are two groups of filters for transmit and receive paths and each group has three filters corresponding to each passband channel. Because of the grouping of filters, the variable range of the length of the line between each filter becomes limited, which makes the design of the multiplexer more difficult than the design of manifold multiplexer.

Since the multiplexer presented here covers an extremely wide bandwidth and the filters are composed of half wavelength resonators, the physical dimensions vary a lot from filter to filter. Fig. 26 shows the relative sizes of the filters in the transmit path group. The size variation of the filter is another obstacle to the design of the wideband multiplexer, especially for compact multiplexers. To make the final multiplexer more compact, the filters centered at lower frequencies are bent and the method presented in section 3 is applied to suppress the spurious passbands as in Fig. 27.

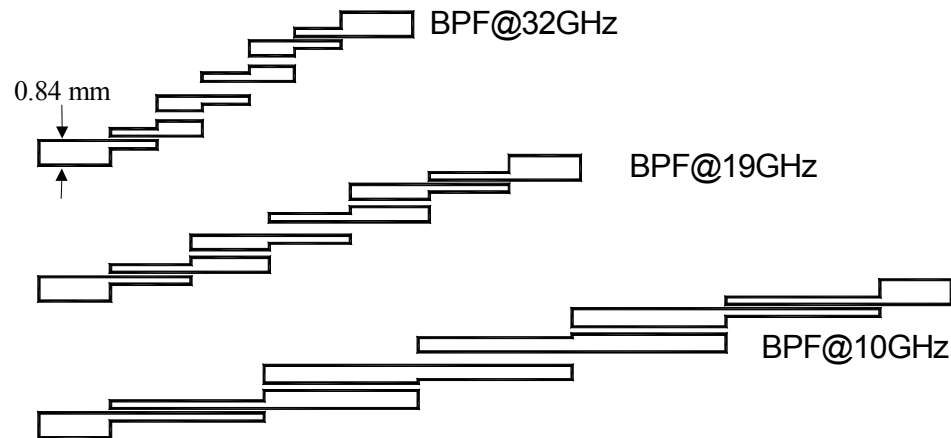


Fig. 26. Relative sizes of filters in the transmit path.

Compared with the results in Fig. 25 for the unbent proposed filters, the simulated results in Fig. 28 show that the bent filter has almost the same main passband response and slightly better suppression of the spurious passbands at the second and third harmonic frequencies ($2f_0$, $3f_0$). By bending a resonator of the filter, the structure is perturbed and more difficult to form the passband at the third harmonic frequency. The filters for the mid frequency bands, which are 19 and 21 GHz, are tilted by 20 degrees for compactness of the multiplexer.

With all the filters corresponding to each channel designed, the next step in designing a multiplexer is to connect filters together with the requirements of compact size, low insertion loss, high return loss at each channel, and good isolation between channels. This procedure is normally done by optimization. However, when the number of channel increases, the number of optimization variables increases more and it is extremely difficult and time consuming for a full-wave electromagnetic simulator to optimize all variables. Therefore, the method used in this research uses both a full-wave and a circuit simulator. The full-wave simulator used is IE3D [29] and the circuit simulator is Microwave Office [38]. Before the optimization procedure, to reduce the optimization time and the possibility of falling into a local minimum, a guideline for the initial lengths of the microstrip lines connecting each filter has to be found. Fig. 29 shows the variation of the frequency response of the channel filter with the length between the filters. The filters centered at 10 and 35 GHz are selected because they are the two extreme cases and have the longest and the shortest resonators among the channel filters in the multiplexer, respectively.

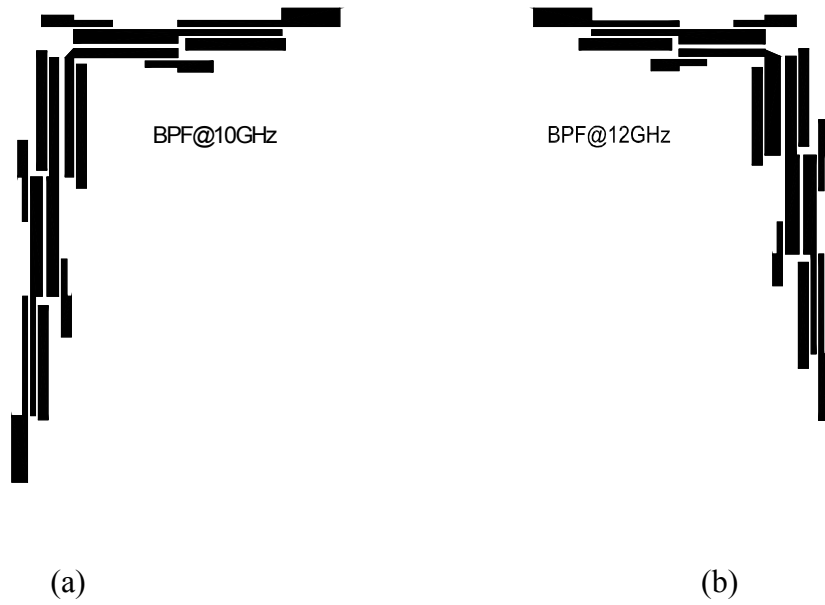
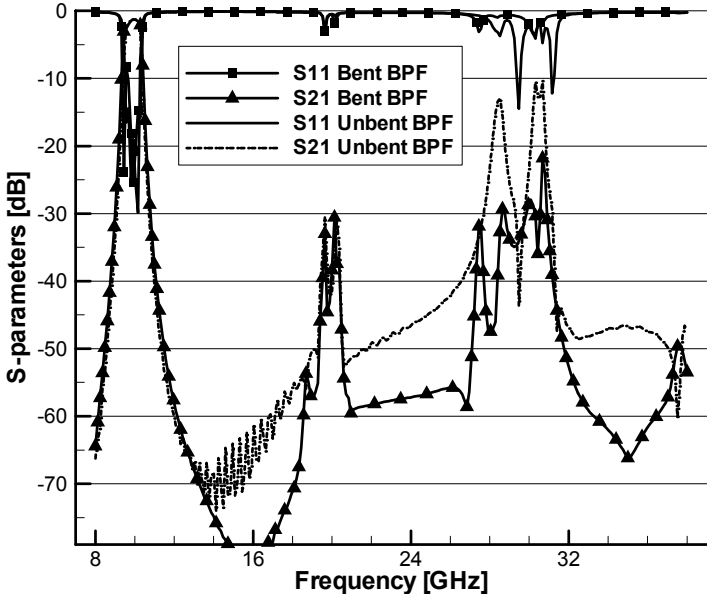
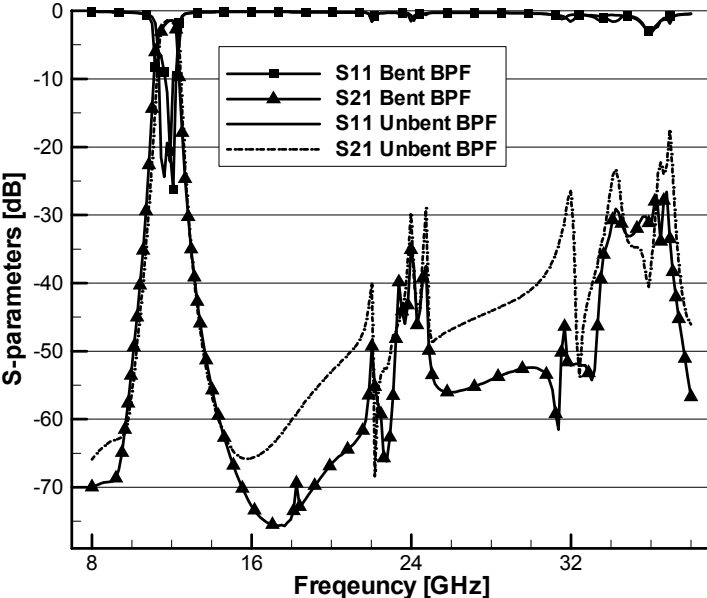


Fig. 27. Layouts of bent filters designed at (a) 10 GHz and (b) 12 GHz.



(a)



(b)

Fig. 28. Performance comparisons between the unbent and bent proposed filters (a) Designed at 10 GHz. (b) Designed at 12 GHz.

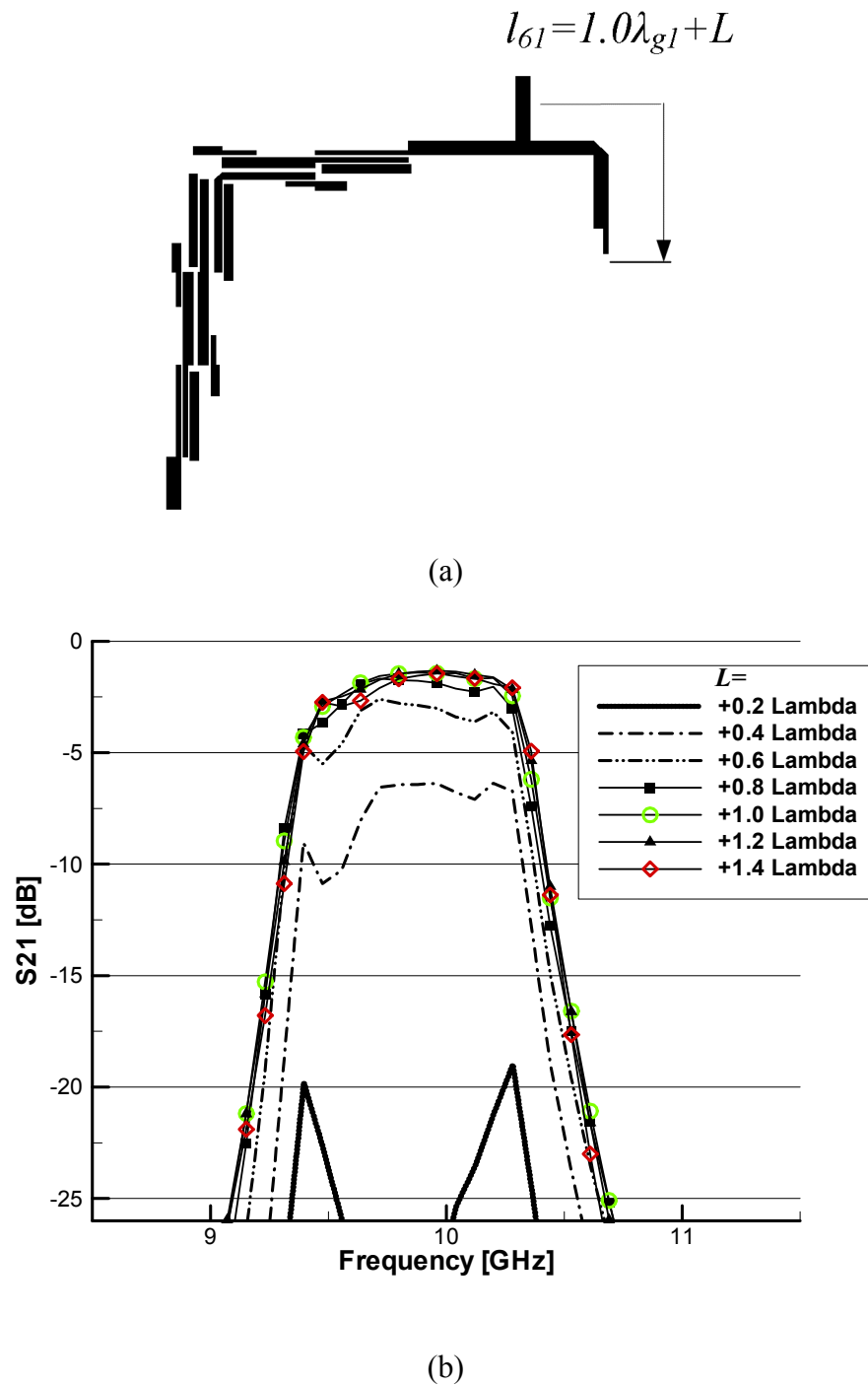
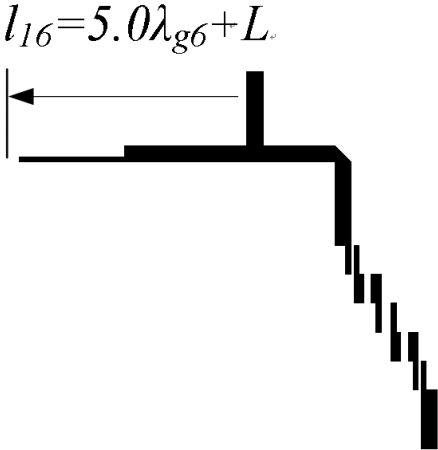
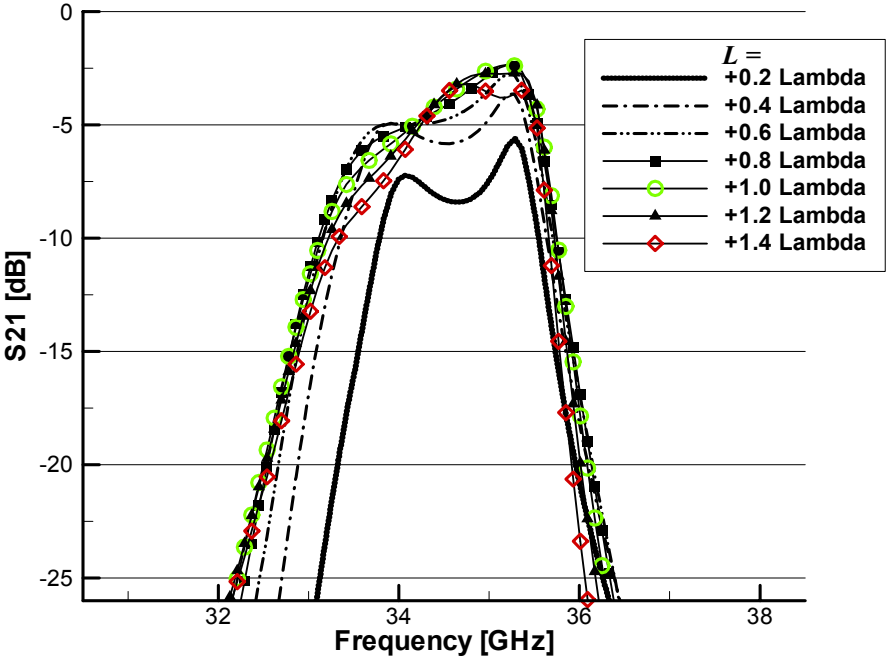


Fig. 29. Variation of the frequency response of the channel filter with the length between the filters. (a) Filter centered at 10 GHz. (b) Simulated insertion loss of the filter centered at 10 GHz. (c) Filter centered at 35 GHz. (d) Simulated insertion loss of the filter centered at 35 GHz.



(c)



(d)

Fig. 29. Continued.

Fig. 29 shows the insertion loss does not change much if the L is between 0.7 and 1.3 wavelengths. It can be reasoned that the length of the line L (from the feed line of a filter to the first resonator of other filters) should be in the range of even multiples of the quarter wavelength at the center frequency of the filter and ± 0.3 wavelength for the line to act like an open stub. For example, if the L in Fig. 29 (a) is one wavelength λ_{g1} , the total length of l_{61} becomes four quarter wavelengths, resulting in the best insertion loss. Therefore, from many simulation results, it is found that for an acceptable insertion loss the length of the line L should be

$$2n \frac{\lambda_{gk}}{4} - 0.3\lambda_{gk} < l_{jk} < 2n \frac{\lambda_{gk}}{4} + 0.3\lambda_{gk}, \quad n = 1, 2, 3, \dots \quad (6)$$

where l_{jk} means the length from the feed line of the k^{th} filter to the end of the first resonator of the j^{th} filter and λ_{gk} is the guide wavelength at the center frequency of the k^{th} filter in Fig. 17. Therefore, the best choice is to set the lengths of the connecting lines such that (6) is satisfied for all possible l_{jk} 's for $j \neq k$. For example, l_{61} is considered as l_{63} and l_{65} at the same time for the filters in the transmit path and each length should satisfy (6) for λ_{g1} , λ_{g3} and λ_{g5} simultaneously. Unfortunately, it is almost impossible to satisfy the above condition for all six filters, keeping the length as short as possible for a compact multiplexer. It turns out to be a good choice to apply (6) to the lines connecting filters designed at lower and higher frequencies, that is 10, 12, 32,

and 35 GHz and resort to computer optimization for the final lengths of all l_{jk} 's. The complete design procedure of the multiplexer is illustrated by the flow chart in Fig. 30 and explained step by step as follows.

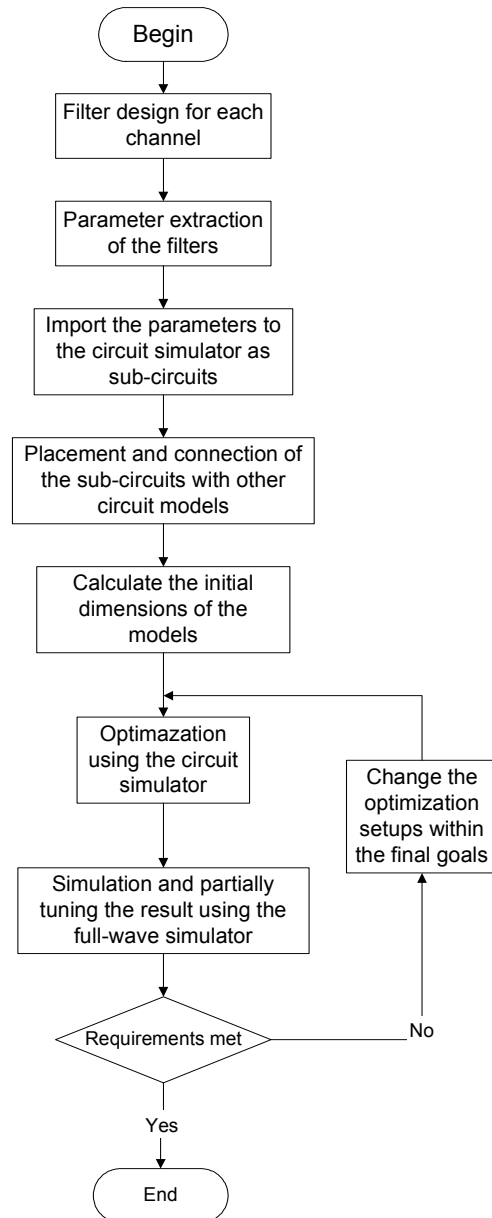


Fig. 30. Flow chart of multiplexer design.

- Step 1) Design each channel filter
- Step 2) Extract the S-parameters of each designed channel filter using the full-wave simulator for the entire operating frequency range of the multiplexer.
- Step 3) Import the extracted S-parameters of each filter using the circuit simulator as a sub-circuit
- Step 4) Place and connect the sub-circuits corresponding to each channel filter with circuit models like microstrip lines, bend, and junctions, provided by the circuit simulator. The placement should be done with the consideration about the actual layout of the filters inside the multiplexer.
- Step 5) Set the initial line lengths connecting filters designed at lower and higher frequencies according to the equation (6). Care should be taken in setting the variable range of the length such that the final results should be physically realizable.
- Step 6) Set the optimization goals and run the optimization with a proper maximum iteration.
- Step 7) Verify the optimized result using the full-wave simulation. If the performance is acceptable, it is the final design. If it is not acceptable, tune the design using the full-wave simulator or change the optimization setups slightly within the goals and rerun the optimization.

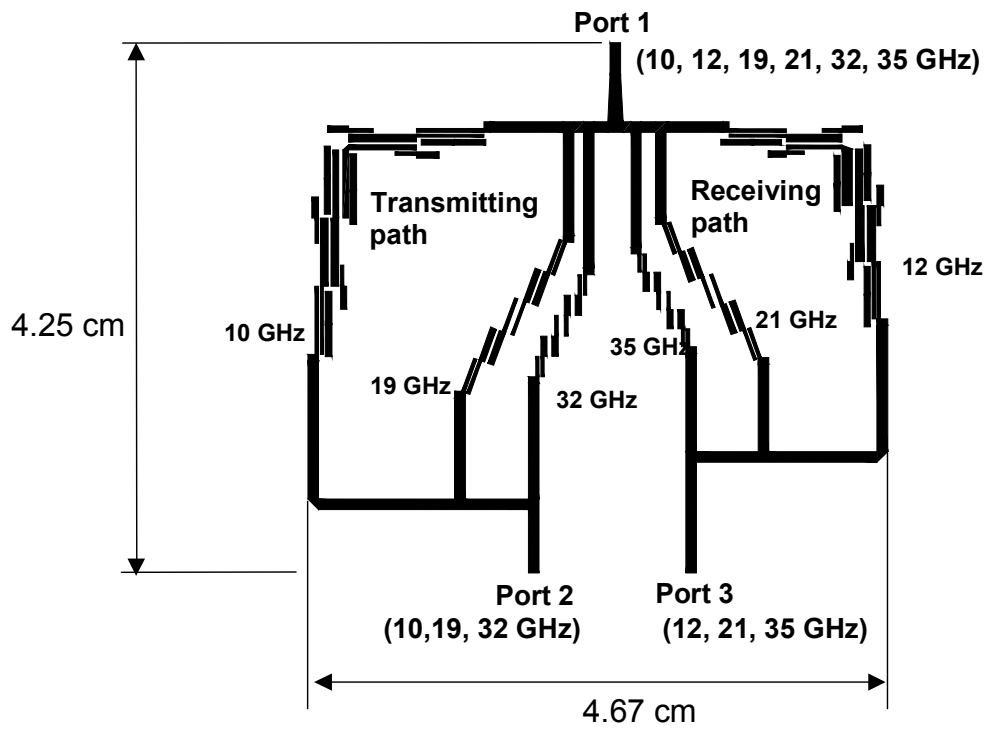
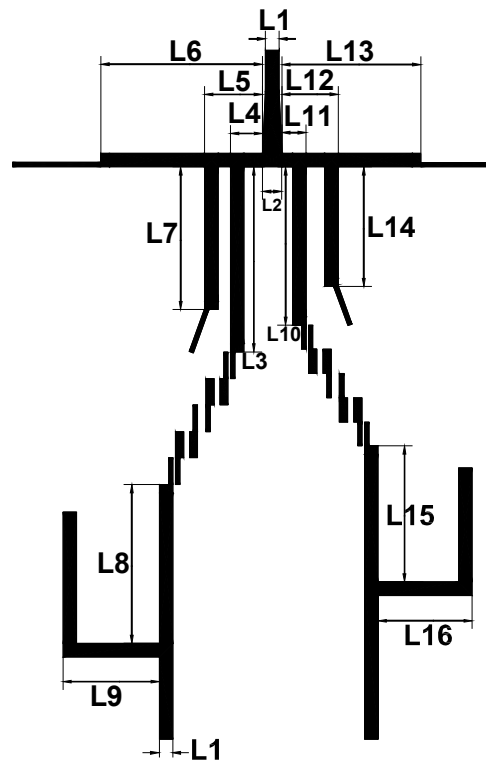


Fig. 31. Physical layout of the designed six-channel microstrip multiplexer.

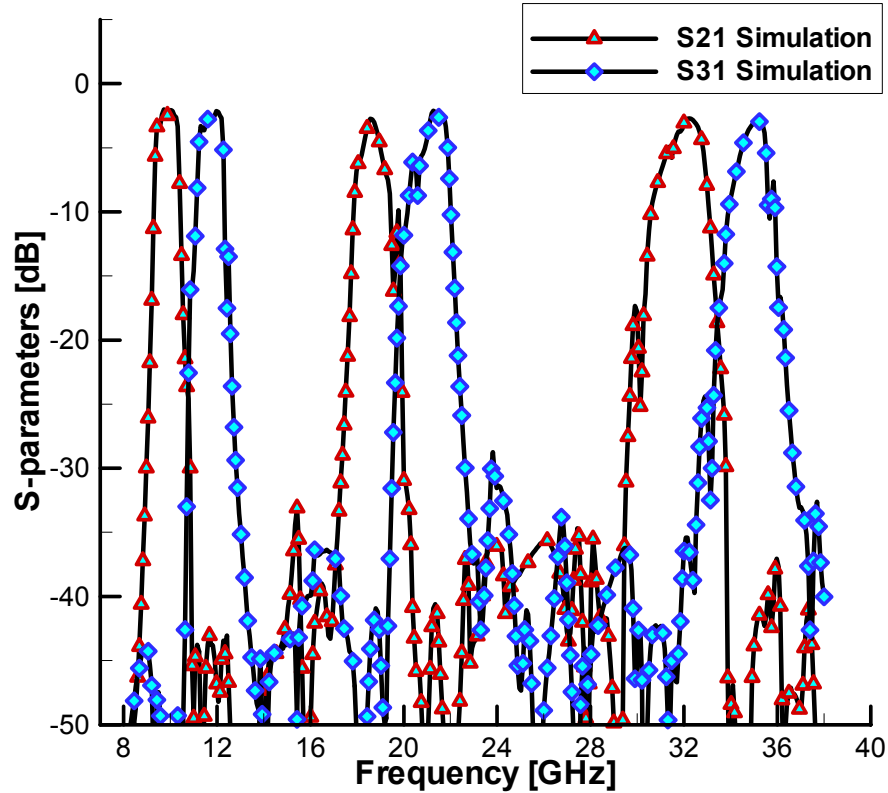


L1	<i>0.84</i>	L5	<i>3.58</i>	L9	<i>5.97</i>	L13	<i>8.59</i>
L2	<i>1.19</i>	L6	<i>9.98</i>	L10	<i>9.78</i>	L14	<i>7.39</i>
L3	<i>11.43</i>	L7	<i>8.81</i>	L11	<i>1.50</i>	L15	<i>8.41</i>
L4	<i>1.98</i>	L8	<i>9.80</i>	L12	<i>3.48</i>	L16	<i>5.82</i>

Fig. 32. Physical dimensions of the distances for the interconnecting lines between the channel filters. (Unit: mm)

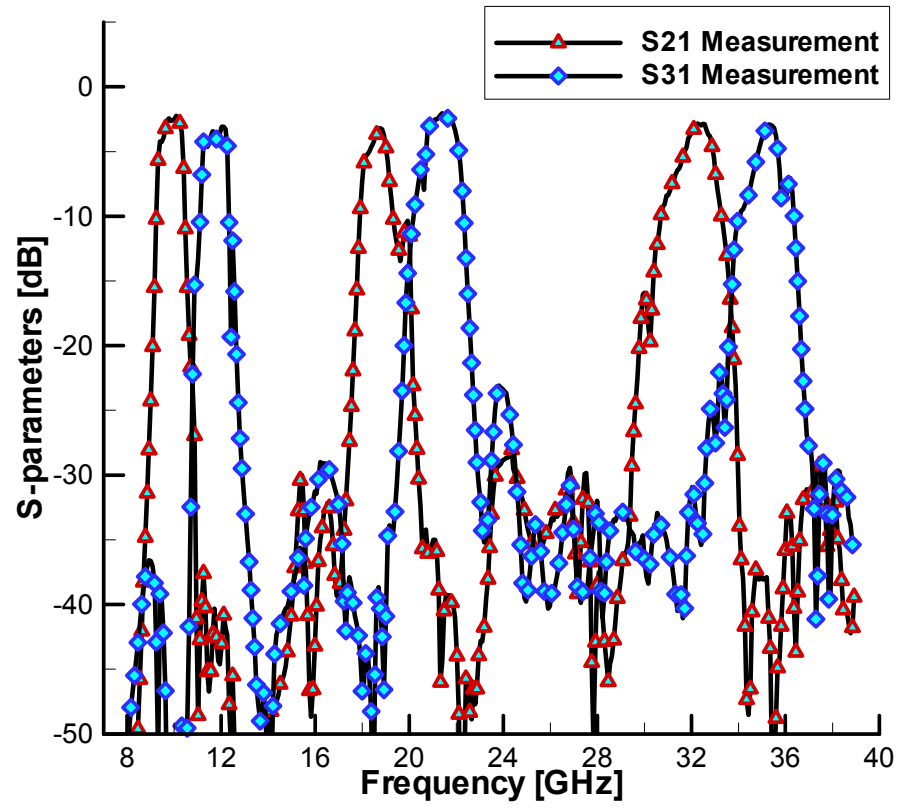
The layout of the designed multiplexer following the procedure is shown in Fig. 31 and the physical dimensions are shown in Fig. 32. The designed multiplexer is measured with the HP 8510C Network Analyzer and the measured results are plotted in Fig. 33 together with the simulation results. To remove the effect of the connectors, the

measured results are calibrated using a Thru-Reflect-Line (TRL) calibration. Referring to the block diagram in Fig. 17, the measured insertion losses are 2.2, 3.1, 3.2, 2.0, 2.8, and 3.0 dB at 10, 12, 19, 21, 32, and 35 GHz, respectively. The insertion loss at 35 GHz is smaller than that of the diplexer reported in [9]. The isolation for any channels between port 2 and 3 shown in Fig. 17 is more than 30 dB. A good agreement between the simulation and measurement results is achieved.



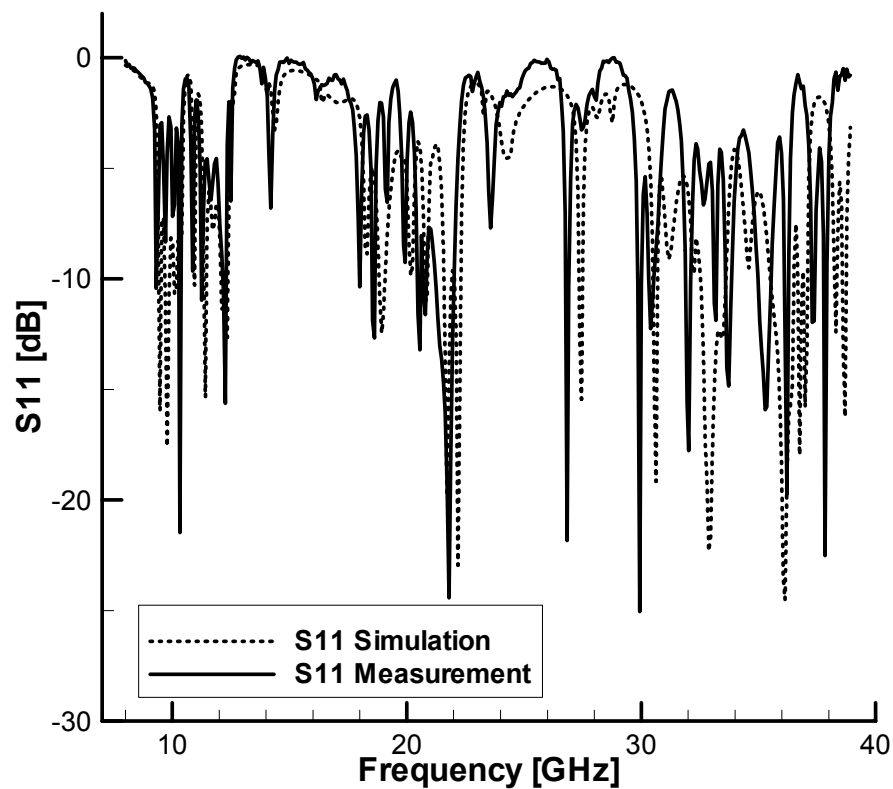
(a)

Fig. 33. Simulated and measured frequency responses of the six-channel multiplexer. (a) Simulated responses for S21 and S31, (b) Measured responses for S21 and S31, and (c) Simulated and measured responses for S11.



(b)

Fig. 33. Continued.



(c)

Fig. 33. Continued.

4.5. Conclusions

A 10–35-GHz six channel microstrip multiplexer for wideband communication systems has been presented. The multiplexer is composed of the microstrip parallel coupled-line bandpass filters. Since the operating frequency range is extremely wide, the channel filters centered at lower frequencies should have a way to suppress the spurious passbands at their harmonic frequencies. A new method of suppressing the spurious

passbands has been presented. The method is simple and does not require any changes to the design of the conventional microstrip parallel coupled-line filters. The method is applied to the filters centered at 12 GHz and verified to be effective by both simulation and measurement.

The design procedure for the microstrip multiplexer has been presented together with a rule of initial setup for optimization. The multiplexer designed does not need tuning after fabrication and measurement results show good performance over the entire operating frequency range. The insertion losses are between 2.0 and 3.2 dB. The return losses are better than 10 dB for all six channels although for some of the channels, the bandwidth for the return loss better than 10 dB is narrow. The multiplexer developed in this chapter is used in the wide-band transceiver system described next chapter and should have many applications in multi-band communication systems requiring full-duplex operation.

CHAPTER V

**A MULTI-BAND, COMPACT, AND FULL-DUPLEX BEAM
SCANNING ANTENNA TRANSCEIVER SYSTEM OPERATING
FROM 10 TO 35 GHZ***

5.1. Introduction

Recent development trend in both commercial and military wireless communication systems calls for a system that can operate over multi-frequency bands. A wideband phased-array antenna transceiver system is an active research topic to answer such a technological demand. Phased-array antenna transceiver systems have been widely used in variety of areas like medical imaging, vehicle collision avoidance radar, remote sensing applications, radars, and satellite communication systems [39], [40] since the concept of the phased-array was proposed in 1889 [41]. But the bandwidth of phased-array antenna system is limited by several components in the system. Recently, a phased-array antenna transceiver system operating over a bandwidth more than 10 GHz was reported [15].

Wideband Transmit/Receive (T/R) module, wideband antenna element, wideband phase shifter and control circuit, and phased-array architectures are the basic

* © 2006 IEEE. Parts of this chapter are reprinted, with permission, from S. Hong, S.-G. Kim, M. R. Coutant, C. T. Rodenbeck, and K. Chang, "A multiband, compact, and full-duplex beam scanning antenna transceiver system operating from 10 to 35 GHz," *IEEE Trans. Antennas Propag.*, vol. 54, No. 2, pp. 359 - 367, Feb. 2006.

components required to build a phased-array antenna transceiver system operating in multi-frequency bands. Compactness of a system is another important issue in wireless communication system designs, especially in satellite communication systems, where the cost for launch per kilogram of mass is comparable to the cost for the satellite development itself [42]. Moreover, satellite communication systems normally require full-duplex operation. The system should transmit and receive signals simultaneously. These requirements for a compact phased-array antenna transceiver system, which can operate in full-duplex mode beyond the current bandwidth limit, motivate this research. For full-duplex operation, microstrip multiplexers presented in Chapter IV are used to provide isolation between transmit and receive paths of the T/R module. The multiplexer connected with MMIC amplifiers plays a key role in achieving full-duplex operation over an ultra-wideband frequency range from 10 to 35 GHz.

Among many types of wideband antennas, Vivaldi antenna is chosen for this research as an antenna element of the phased-array antenna system, because of its relatively high gain for a given cross section [43] and compact size for a wide frequency band. Vivaldi antenna is a continuously scaled, gradually curved, and end-fire traveling wave antenna with unlimited operating frequency range in theory. But the actual bandwidth is limited by its size and the transition mechanism [44]. In this research, Vivaldi antennas operating from 8 to 35 GHz are designed and arranged as a 1 x 4 *H*-plane array. The beam steering capability of the antenna array is demonstrated using a piezoelectric transducer (PET) controlled phase shifter. The array is integrated with the wideband T/R module to demonstrate the multi-frequency operation of phased-array

antenna transceiver system introduced in this chapter and to show the possibility of building a larger array.

This research expands the bandwidth of a transceiver system in [15] by more than 10 GHz. The resulting operation bandwidth of the system is unprecedented. Furthermore, the transceiver system in this chapter has made remarkable progress by increasing the number of channels from 4 to 6 while decreasing the size by 84 %. The six-channel multiplexer which is made of microstrip filters and operating from 10 to 35 GHz is never published before.

5.2. Wideband T/R module

The wideband T/R module consists of two multiplexers and cascaded MMIC amplifiers. The multiplexer routes 10, 19, and 32 GHz signals to transmit path and 12, 21, and 35GHz to receive path. The layout of the designed six-channel multiplexer is shown in Fig. 31 and its simulated and measured frequency responses are shown in Fig. 33.

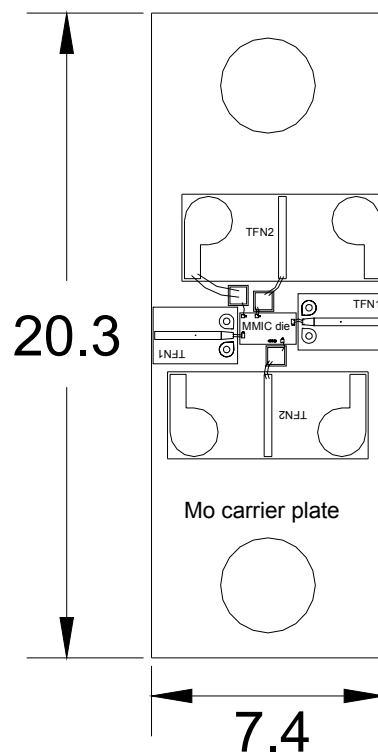


Fig. 34. Assembly diagram of the MMICs. (Unit: mm)

The T/R module uses a 10—32-GHz power amplifier (PA) and a 12—35-GHz low noise amplifier (LNA). These amplifiers are built using monolithic microwave integrated circuits (MMICs) available from TriQuint Semiconductor. The parts selected are listed in Table 6 together with the nominal performance specifications for each ultra-broadband MMIC chip. To form the transmit path, two TGA4832s are cascaded. The receive path consists of two TGA4830s and one TGA 4832.

TABLE 6. MMIC selections for the T/R module. All parts are manufactured by TriQuint Semiconductor. Performance for the LNA is listed at 12, 21, and 35 GHz; performance for the PAs is listed at 10, 19, and 32 GHz.

Frequency (GHz) <i>LNA/PA</i>	Performance	
	LNA (TGA4830)	PA (TGA4832)
10/12	Gain = 13 dB P_{out} @ P1dB = 11.5 dBm Noise Figure = 2.5 dB	Gain = 13 dB P_{out} @ P1dB = 19 dBm
19/21	Gain = 12.7 dB P_{out} @ P1dB = 10.4 dBm Noise Figure = 3.2 dB	Gain = 12.8 dB P_{out} @ P1dB = 18.3 dBm
32/35	Gain = 12 dB P_{out} @ P1dB = 10 dBm Noise Figure = 3.8 dB	Gain = 12.5 dB P_{out} @ P1dB = 16 dBm

The MMIC amplifiers are assembled on molybdenum (Mo) carriers with alumina Thin Film Networks (TFNs) interfacing to the outside world as shown in Fig. 34. This type of assembly is commonly used in industry for the testing of single MMIC die. The assembly is more easily implemented than a full module, which is composed of five MMICs, while allowing easy interchangeability and testing of the MMIC die. Single layer chip capacitors provide RF grounding in close proximity to the MMIC. The molybdenum alloy closely matches the thermal coefficient of expansion for gallium arsenide and provides thermal dissipation for the MMIC. 0.25-mm-thick alumina TFNs with 50- Ω microstrip lines interface the MMIC RF input and RF output to adjacent stages. Thin 0.25-mm-thick alumina is used to keep the RF bond wires between the

MMIC and the TFN as short as possible lowering the added inductance in the RF path. TFNs also interface the DC bias pad on the MMIC to the power supply wires. Components are attached to the Mo carrier plates using conducting epoxy.

The measured performance of the assembled TGA4830 and TGA4832 are shown in Figs. 35 and 36. The return loss is less than 10 dB at some frequencies. This is attributed to the imperfection of the bond wires, test fixture and connections. With these assemblies a T/R module is built to prove the module design and full-duplex operation in integration with the phased antenna array.

The layout of the T/R module is shown in Fig. 37. One multiplexer is placed between the end of the cascaded MMIC amplifier assemblies and the antenna array and another mirror-imaged multiplexer is connected at the other end of the cascaded MMIC amplifier assemblies. Between the two multiplexers, two TGA4830 and one TGA4832 amplifiers are cascaded in the receive path, while two TGA4832s are used in the transmit path. Because the RF ports of each MMIC assembly are not DC blocked on-chip, external DC blocking capacitors must be placed in the RF path between dies in both the receive and the transmit paths. 100-pF single layer capacitors were mounted onto the 50- Ω TFNs using conductive epoxy.

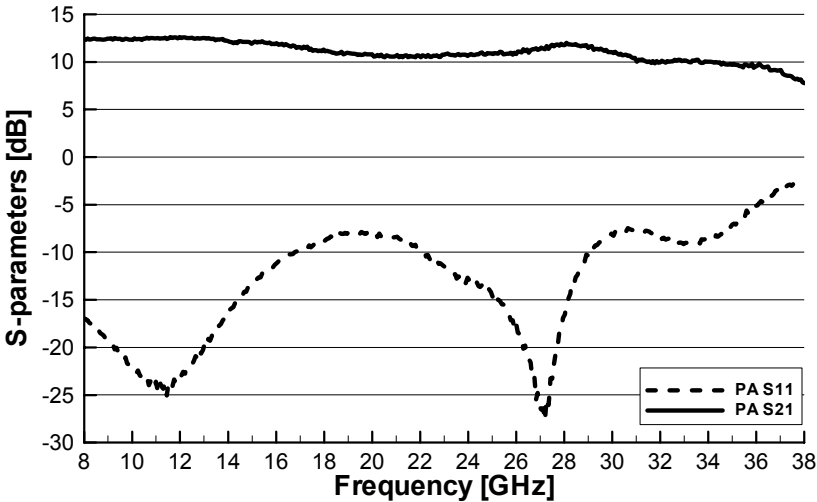


Fig. 35. Small-signal S-parameters of TGA4832 assembly.

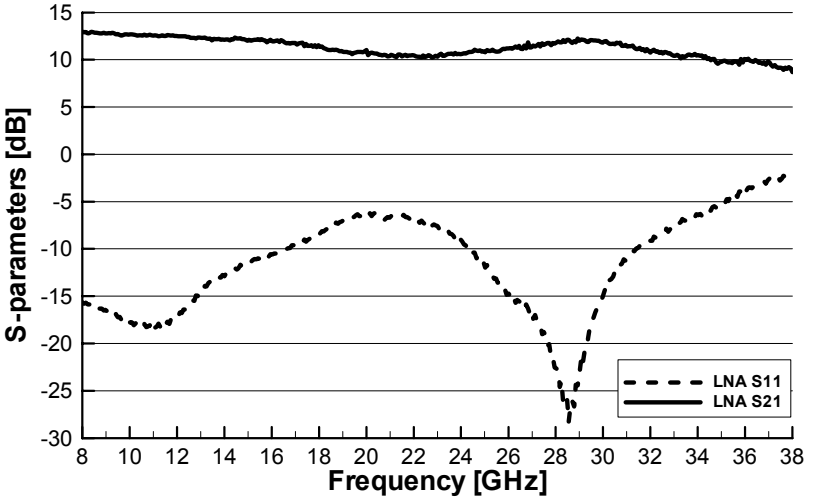


Fig. 36. Small-signal S-parameters of TGA4830 assembly.

Bond wires connect the capacitor to the adjacent TFN. DC blocks are not needed between the die and the multiplexers because the edge coupled filters block DC current.

Since the multiplexer is made of copper microstrip lines, gold wires used in bonding machines can not be connected to the multiplexer. Therefore, the tips of port 2 and port 3 of the multiplexer shown in Fig 31 are plated with gold. With gold plating, the multiplexer and the RF TFNs of the MMIC assemblies can be connected with bond wires.

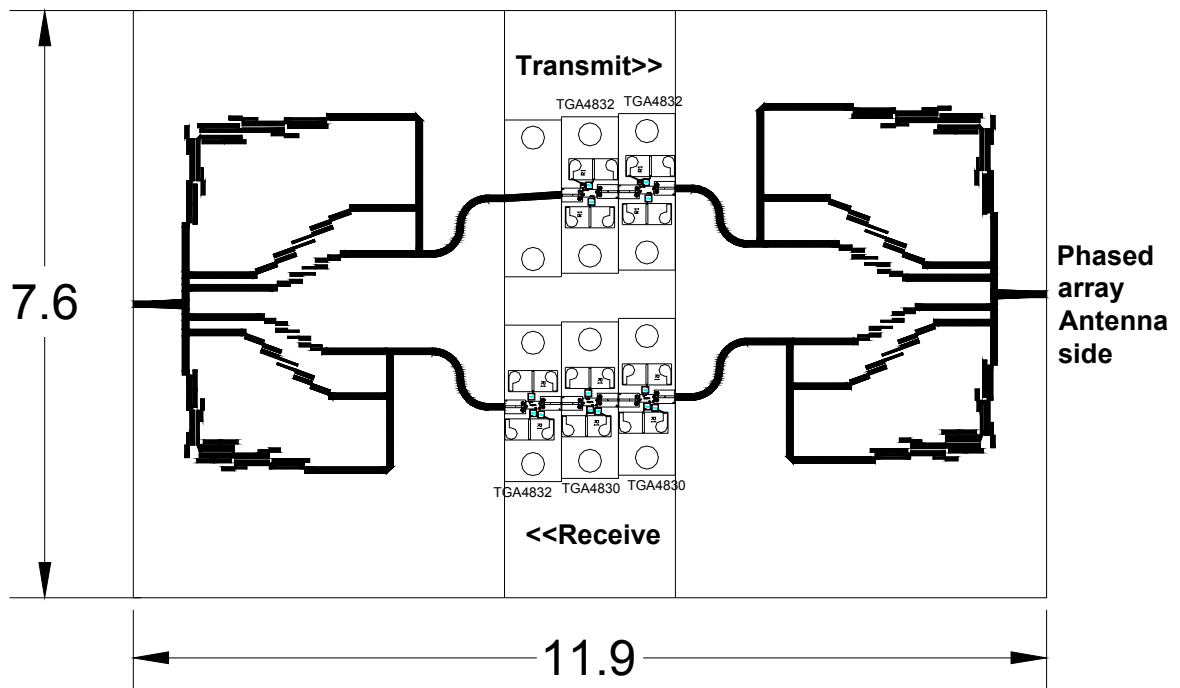


Fig. 37. Layout of the T/R module composed of two multiplexers, two TGA4832s and three TGA4830s. (Unit: cm).

The calculated noise figures of the T/R module at each receiving frequency are 7.42 dB at 12 GHz, 8.41 dB at 21 GHz, and 11.22 dB at 35 GHz, respectively. The

measurements were done at 12 and 35 GHz only, because of the availability of the equipment. The measured noise figures are 8.05 dB at 12 GHz and about 12 dB at 35 GHz. Although the measured noise figures are slightly higher than the calculated ones, they agree very well with the calculated ones.

5.3. Antenna and array

This section describes the design of the antenna elements, phase shifters, and antenna arrays. These components are illustrated in the photograph shown in Fig. 38. K-connectors are used to connect components for their good performance up to 40 GHz.

The key components are a 1 x 4 *H*-plane array of antipodal tapered slot antennas and a multi-line PET-based phase shifter. In addition, there is a 1 x 4 wideband microstrip power divider and a space adapter. These components are inexpensive, can be easily operated over wide bandwidths, and can be scaled depending on the requirements of the design. The space adapter located between the antenna array and phase shifter is used to adapt the narrow antenna spacing to the wide spacing for the phase shifter circuits. These components are inexpensive, can be easily operated over wide bandwidths, and can be scaled depending on the requirements of the design.

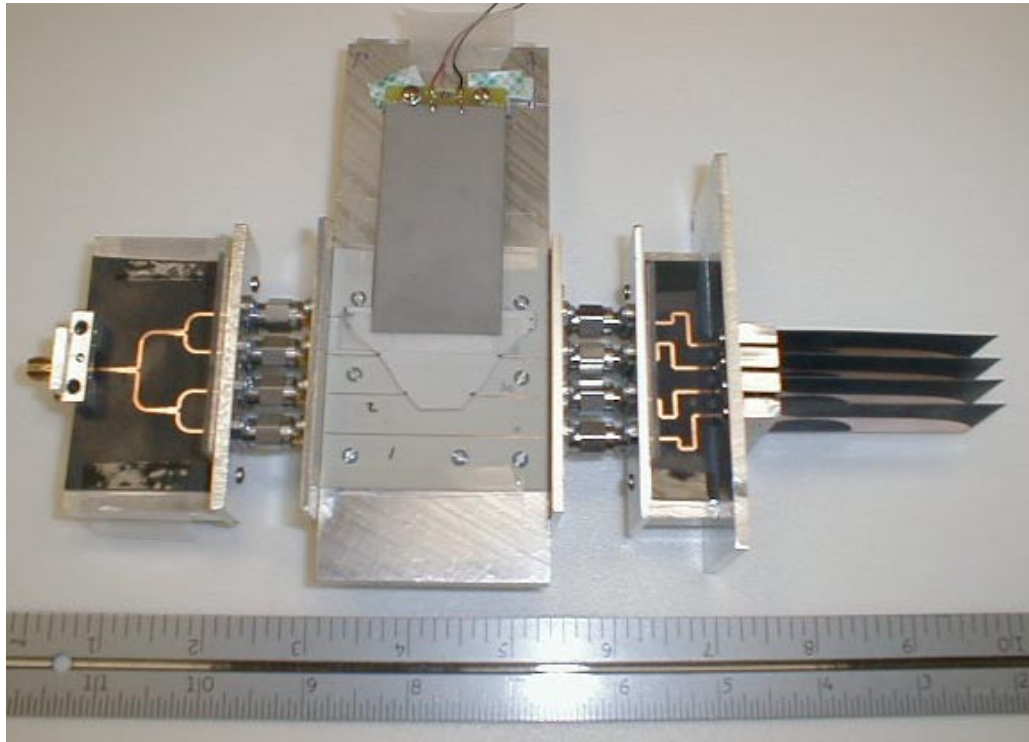


Fig. 38. Configuration of a 1 x 4 H -plane phased-array operated by a PET-controlled phase shifter. From left to right are 1 x 4 power divider, PET controlled phase shifter, space adapter, and 1 x 4 H -plane antenna array.

The geometry of an antipodal tapered-slot antenna (ATSA) is shown in Fig. 39. The antenna can achieve very wideband performance due to its elegant transition from microstrip line [44, 45]. The substrate for design is selected to provide mechanical rigidity while keeping the effective thickness within $0.005\lambda_0$ to $0.03\lambda_0$ across the operating bandwidth. The effective thickness (t_{eff}) can be calculated as $t_{eff} = t(\sqrt{\epsilon_r} - 1)$, where t is the physical thickness of a substrate [46]. The slot flare length (l) and width ($2d+w$) of the designed ATSA are 4.32 and 2.54 cm, respectively. The microstrip transition at the input is tapered circularly to parallel-strips for the antenna feed. The

antenna length l is chosen according to the empirical guidelines of [46] while also considering the practical stability of the antenna. The flare is tapered exponentially with the opening rate determined using recursive optimization in CST Microwave Studio® [47]. Fig. 40 shows that the simulated and measured return losses of the designed ATSA are better than 10 dB across the 8 to 35 GHz bands.

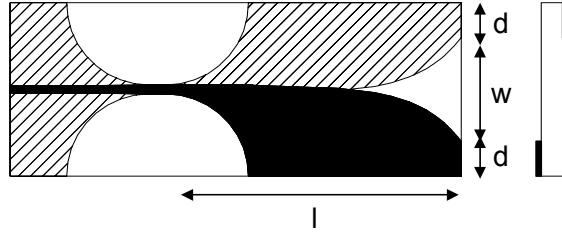


Fig. 39. Schematic illustrating an antipodal tapered-slot antenna (ATSA).

A PET-controlled multi-line phase shifter is also shown in the photograph of Fig. 38. A dielectric perturber is attached to a PET actuator and suspended above a series of microstrip lines. The perturber's triangular shape creates a progressive phase shift that can be varied by using the PET to adjusting the height of the perturber above the microstrip lines. The progressive phase shift between any two neighboring microstrip lines can be calculated as:

$$\Delta\phi = \Delta L \cdot \frac{2\pi}{\lambda_o} \left(\sqrt{\epsilon_{eff1}(f)} - \sqrt{\epsilon_{eff2}(f)} \right) \quad (7)$$

where ΔL is the progressive length of the perturber above the microstrip lines and $\epsilon_{eff1}(f)$ and $\epsilon_{eff2}(f)$ are the effective relative permittivities of the perturbed and unperturbed

microstrip line, respectively [48]. Equation (7) represents a true time delay (TTD) phase shift capable of linear operation over a wide range of frequencies.

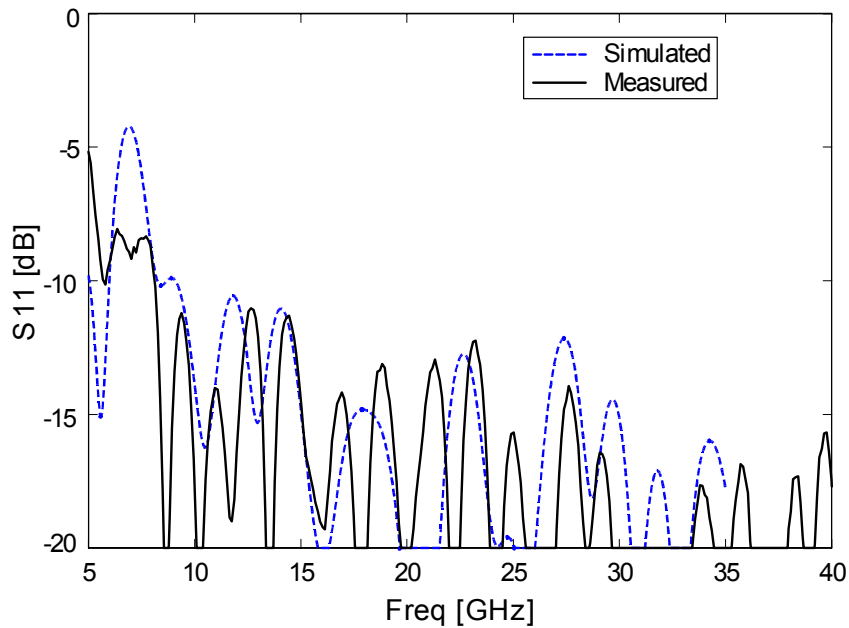
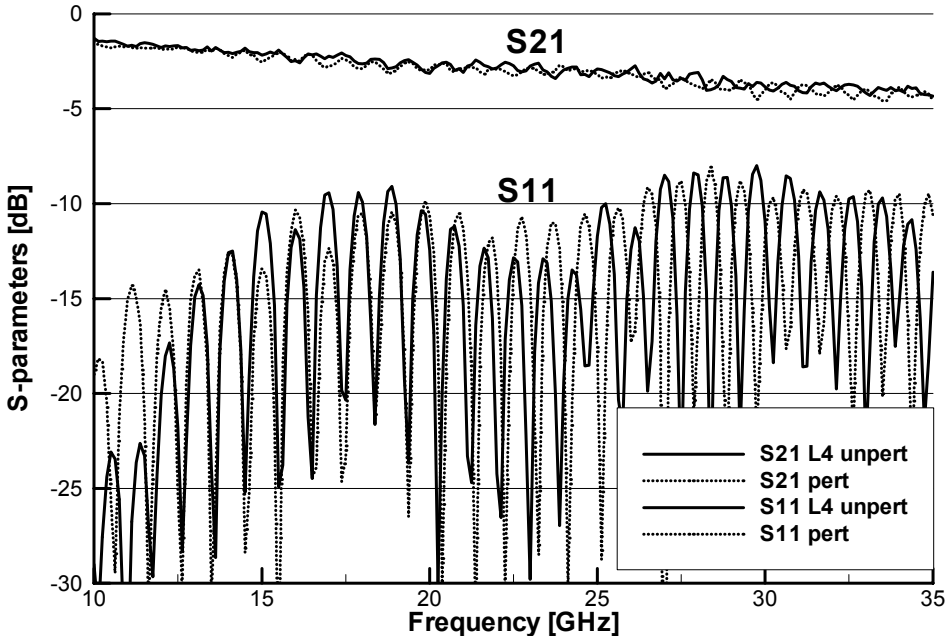


Fig. 40. Simulated and measured return loss of the ATSA.

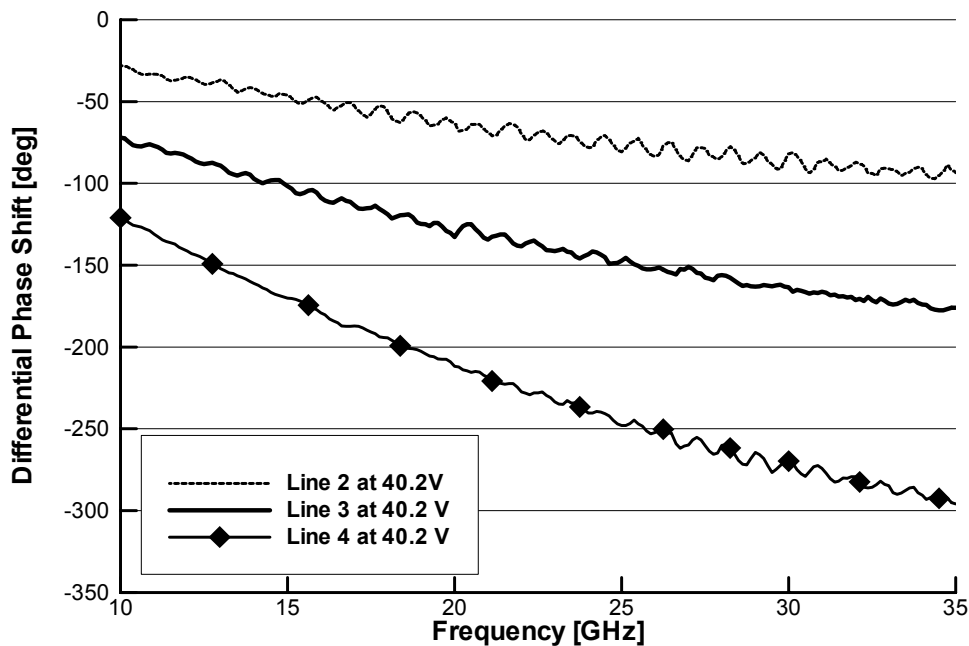
The phase shifter is designed to operate over the 10 - 35 GHz bands. The PET-controlled phase shifter is fabricated on RT/Duroid 6010 ($\epsilon_r = 10.2$) with the thickness of 0.38 mm. A dielectric material of 1.27-mm-thick TMM10 ($\epsilon_r = 10.2$) is used as a perturber. The maximum progressive phase shifts of 90° at 35 GHz is designed to achieve the scan angles of 20° . Fig. 41 shows the measured S -parameters and differential phase shifts for the fabricated phase shifter. The differential phase shifts are the phase shifts of the second, third and fourth lines relative to the first line of the phase shifter. The first line is not affected by the perturber and sets the phase reference. The return loss

is better than 10 dB for the operating frequency range, and the insertion loss is less than 4 dB at 35 GHz with full perturbation. This insertion loss includes the losses due to the connectors and line lengths.



(a)

Fig. 41. Measured performance of the phase shifter. (a) S-parameters. (b) Differential phase shift.



(b)

Fig. 41. Continued.

The 1 x 4 *H*-plane phased-arrays of the type shown in Fig. 38 are designed using the ATSA elements and phase shifters discussed earlier. The arrays are fed by using a wideband Chebyshev power divider. The array spacing is chosen sufficiently small to prevent grating lobe formation when the beam is steered in the *H*-plane at the highest operating frequency. The array spacing is 6 mm, corresponding to $0.2 \lambda_0$ at 10 GHz and $0.7 \lambda_0$ at 35 GHz.

In addition, the ATSA elements are placed in an alternating “mirrored” array architecture [49]. Though able to provide very wideband performance, ATSA elements and arrays traditionally suffer from high cross polarization levels due to the placement of

the tapered slot flares on different layer of the same substrate. This problem can be eliminated, however, by mirroring the elements in the array, as shown in Fig. 42. Doing so places a null in the cross-polarization pattern in the direction of the co-polarization maximum. This array approach, which is adopted in this research, can also be applied to two-dimensional arrays.

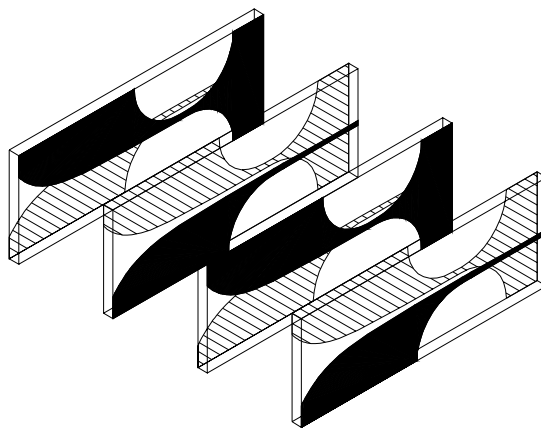
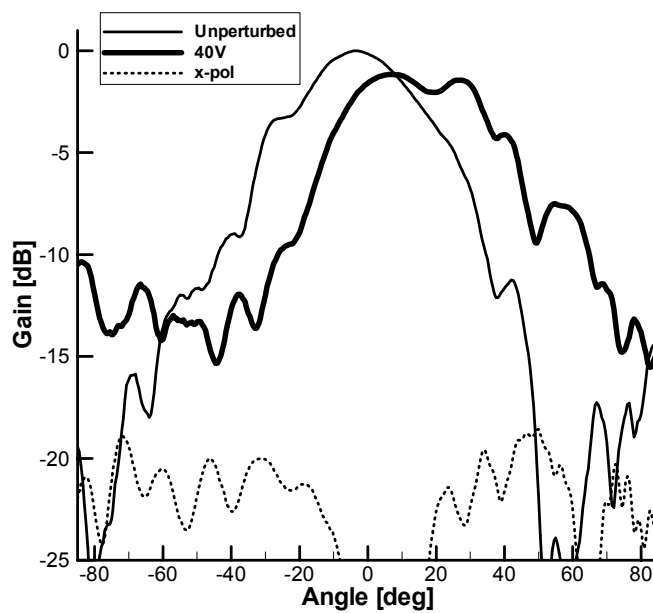


Fig. 42. Mirrored ATSA array architecture.

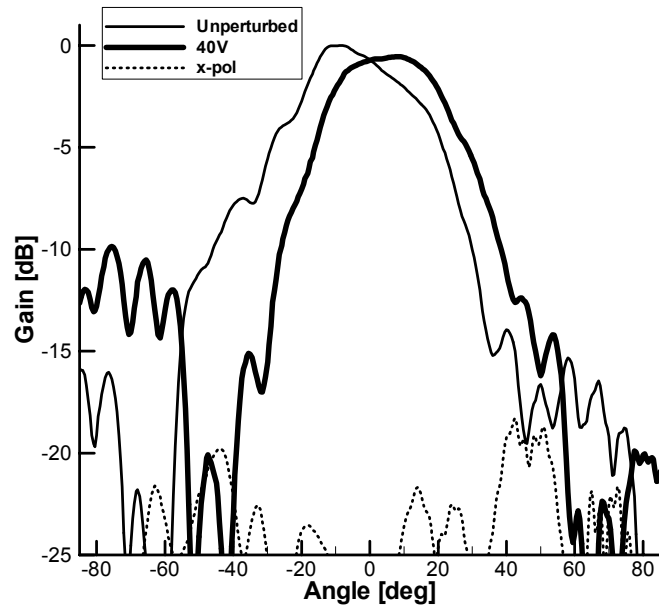
Fig. 43 shows the normalized steered beam patterns measured at 10, 12, 19, 21, 32, and 35 GHz. The unperturbed cases represent the antenna patterns measured without any external bias to the PET-controlled phase shifter. When 40 V external bias is applied to the PET-controlled phase shifter, each beam is steered more than 20 degrees from broadside in the H-plane. An additional perturber can be added to steer the beam in both directions [15]. Cross-polarization level for the unperturbed case is less than 20 dB below the co-polarization. This excellent linear polarization is due to the mirrored array arrangement described earlier. When the main beam of a co-polarized pattern is steered,

the null point of a cross-polarized pattern is also steered. Therefore, the null point of a cross-polarized pattern is always at the main beam direction maintaining the reduced cross-polarization level.

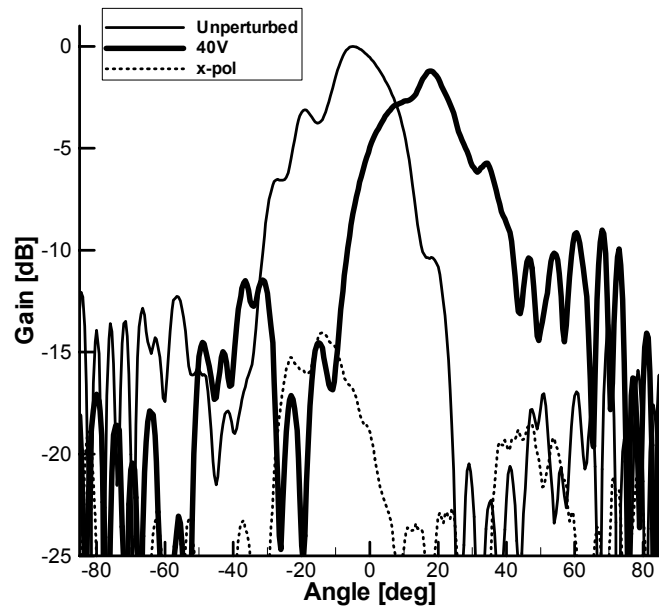


(a)

Fig. 43. Measured beam steering patterns at (a) 10 GHz. (b) 12 GHz. (c) 19 GHz. (d) 21 GHz. (e) 32 GHz. (f) 35 GHz.

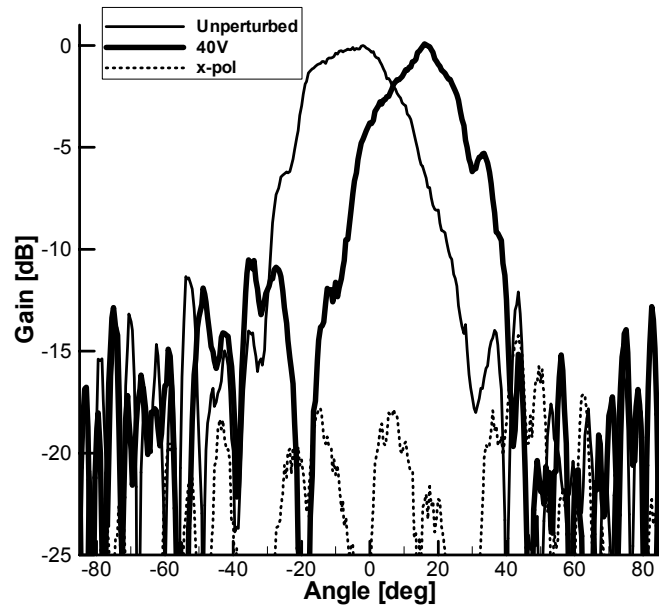


(b)

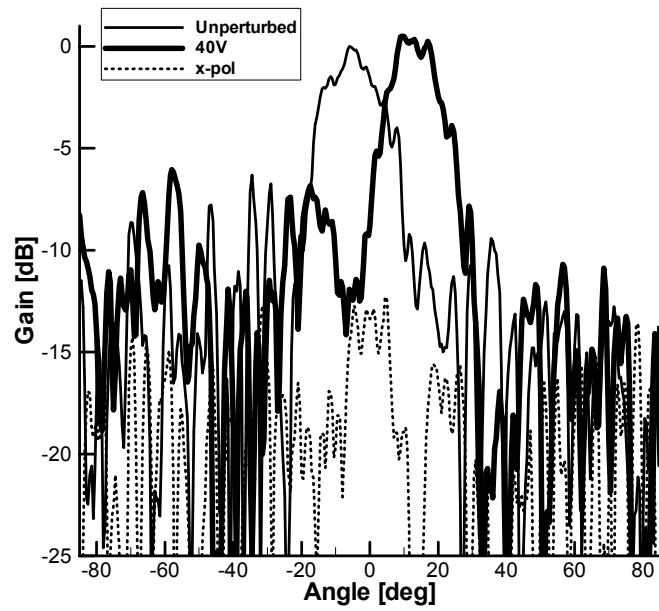


(c)

Fig. 43. Continued.

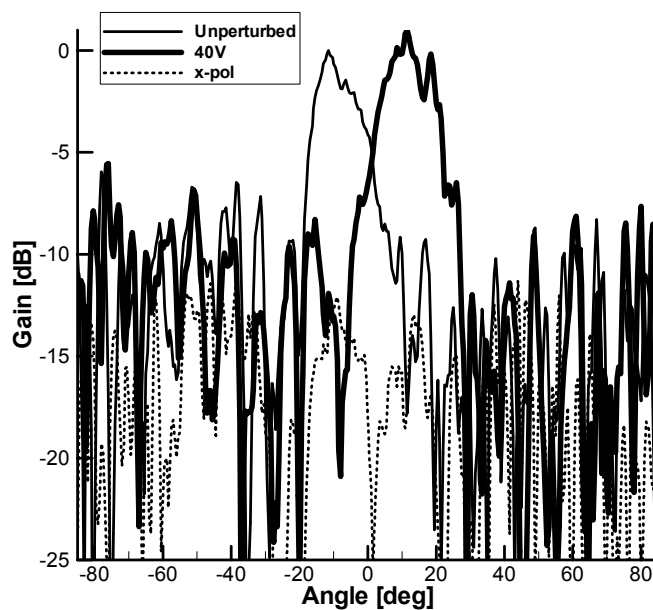


(d)



(e)

Fig. 43. Continued.



(f)

Fig. 43. Continued.

5.4. System integration and test

To demonstrate the functionality of the phased-array antenna in integration with the T/R module over the designed frequency range of 10 - 35 GHz, the antenna array and the T/R module are connected together as a phased-array antenna transceiver system. The transceiver system built for the functional test is shown in Fig. 44. Before the T/R module is connected with the antenna array, the gain of the T/R module is measured alone using the 8510C network analyzer. Fig. 45 shows the measured results of the T/R module, which is composed of a multiplexer, cascaded MMIC amplifiers, and a second multiplexer as shown in Fig. 37. The gains of transmit path composed of two PAs at the peaks of passbands are 16.4, 9.9 and 5.4 dB and for the receive path, the gains are 19.9,

16.6, and 3.7 dB at the peak of each passband, respectively.

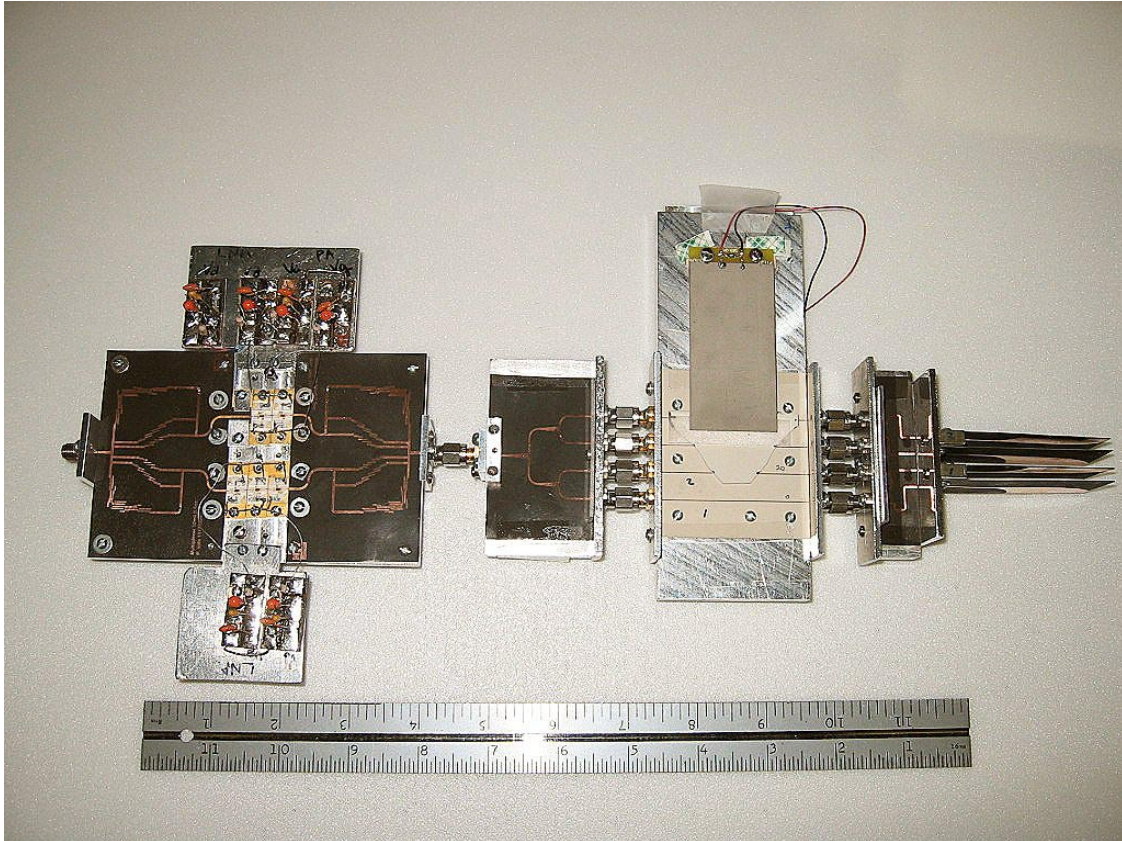


Fig. 44. Photograph of the phased-array antenna transceiver system composed of phased-array antenna and T/R module.

Because two MMIC amplifiers are cascaded in the transmit path while the receive path has three stage MMIC amplifiers, the gains at 10 and 19 GHz are smaller than those of receive path at 12 and 21 GHz. The gain drops severely in the millimeter wave region because the losses caused by the connectors, bonding wires connecting MMIC assemblies, bonding wires between the MMIC assembly and the multiplexer, and the capacitors epoxied onto the TFNs increases much as the frequency goes into the

millimeter-wave region, especially beyond 35 GHz. Another cause of the loss is degradation of the RF TFNs by many times of wire bondings during the test. The performance can be improved by using better MMIC amplifiers and avoiding the use of capacitors between them.

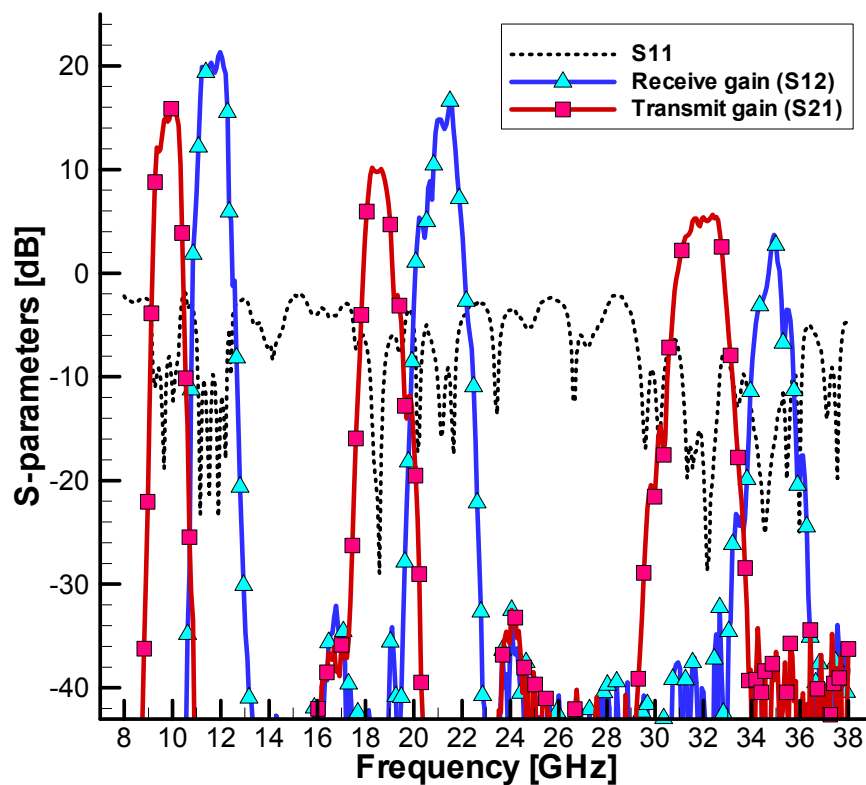


Fig. 45. Measured frequency responses of the T/R module.

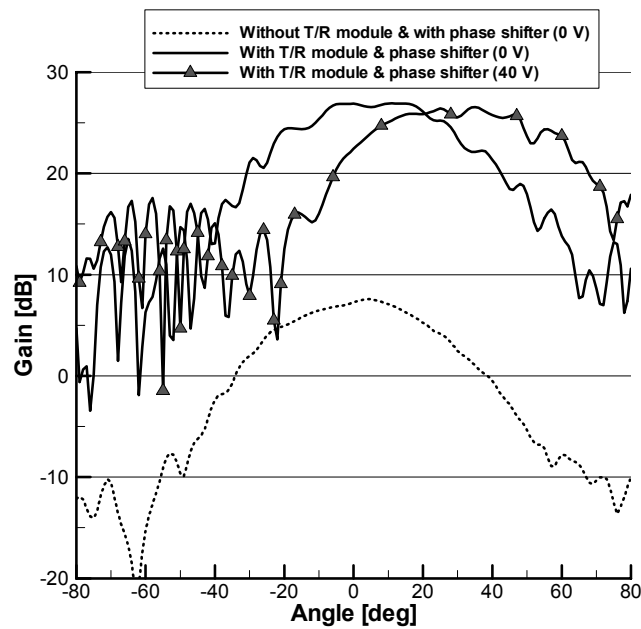
If each antenna element has its own T/R module connected to itself, the phase shifter can be placed behind the T/R module for better output power and lower noise figure. In this case, the noise figure will be dominated by the noise figure of the first

amplifier of the T/R module and the loss of the phase shifter will have little effect. However, four T/R modules will be required instead of one.

The antenna patterns for all the six frequencies corresponding to the passbands of the T/R module were measured in the anechoic chamber of Texas A&M University. In the receive site of the chamber, an antenna is mounted on a rotator and connected to a mixer of the receiver system. In the transmit site, an antenna is fixed with a HP 8349B wideband amplifier connected to it. For the measurement of the transceiver system, the transceiver system is mounted on the rotator, connected to the mixer of the receiver system. A standard horn placed in the transmit site transmits signals. The receive patterns of the transceiver system are measured first at three receive frequencies of 12, 21, and 35 GHz. Then the transmit patterns of the transceiver system at three transmit frequencies of 10, 19, and 32 GHz are measured after changing the positions of the standard horn and the transceiver system. To show the beams steering characteristics of the whole system, the radiation patterns with T/R module and 40 V bias applied to the phase shifter are measured. The measured patterns are shown in Figs. 46 and 47 in comparison with the antenna patterns without the T/R module. Table 7 shows measured gains of the antenna array with and without T/R module at its beam peak and the measured gain of the T/R module at each operating frequency. As can be seen in the Table 7, the gain of the array system increased by the gain of the T/R module.

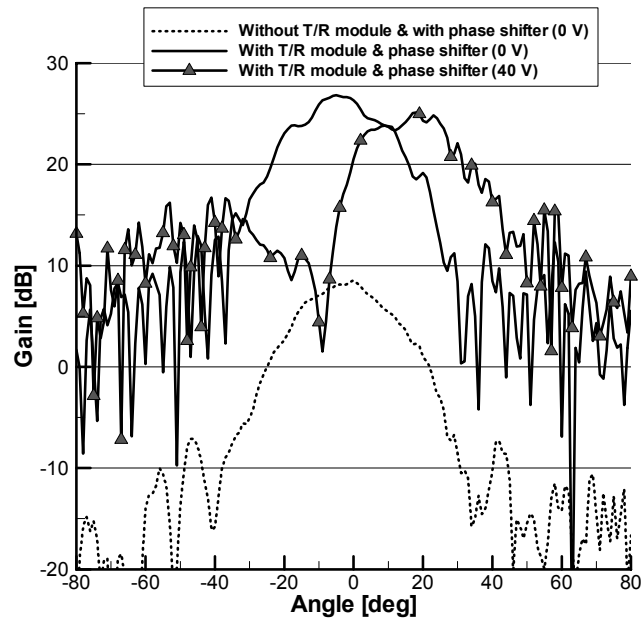
TABLE 7. Measured gain of the antenna array with and without T/R module and the measured gain of T/R module at each operating frequency. (T and R denote transmit and receive frequencies, respectively).

Channel [GHz]	10	12	19	21	32	35
Gain [dB]	T	R	T	R	T	R
Array without T/R module and with phase shifter	4.7	7.6	7.1	8.7	4.6	4.5
Array with T/R module and phase shifter	22.0	26.6	16.8	25.8	10.5	8.4
T/R module	16.4	19.9	9.9	16.6	5.4	3.7

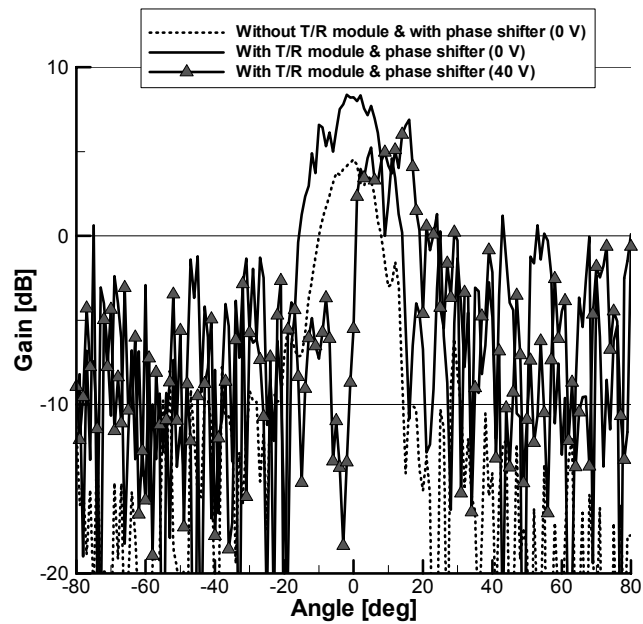


(a)

Fig. 46. Measured receive patterns of the phased-array antenna transceiver system for the receiving frequencies. (a) 12 GHz. (b) 21 GHz. (c) 35 GHz.

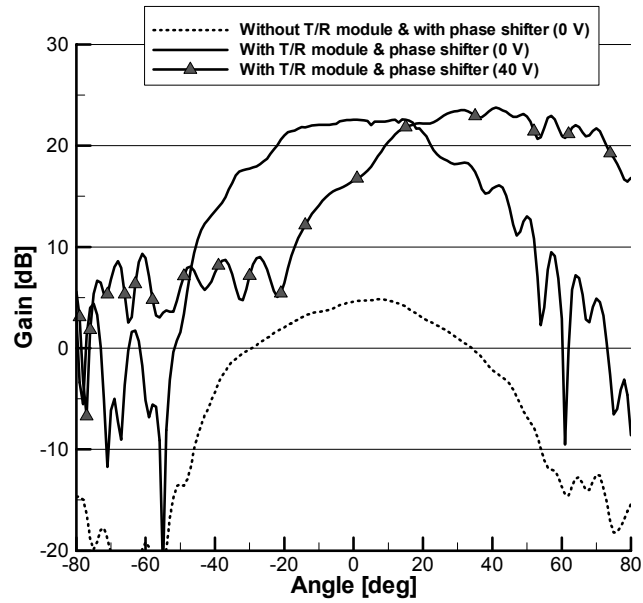


(b)

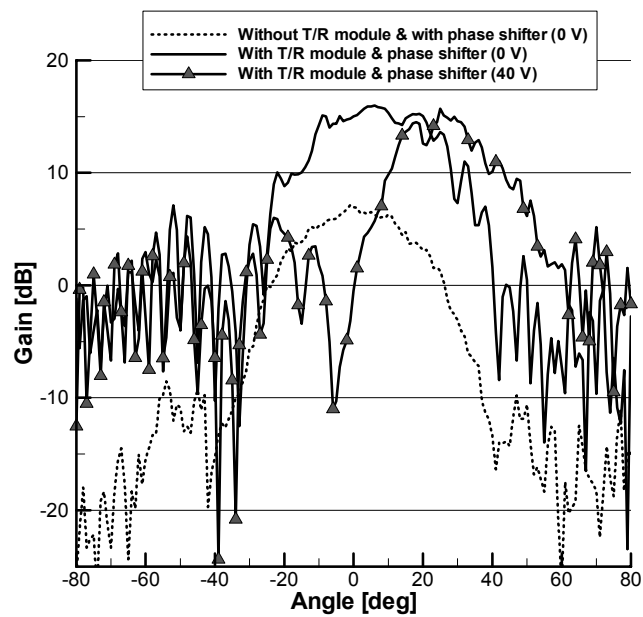


(c)

Fig. 46. Continued.

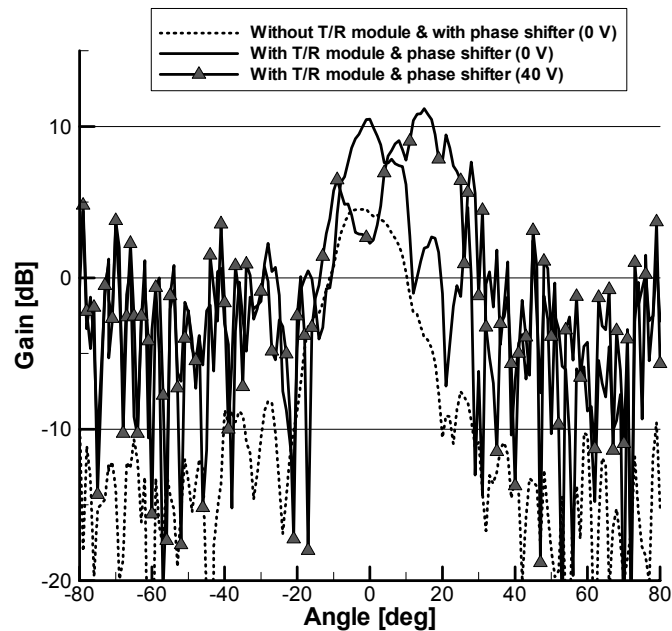


(a)



(b)

Fig. 47. Measured transmit patterns of the phased-array antenna transceiver system for the transmitting frequencies. (a) 10 GHz. (b) 19 GHz. (c) 32 GHz.



(c)

Fig. 47. Continued.

5.5. Conclusions

A 10—35-GHz, compact, multi-frequency, and full-duplex phased-array antenna transceiver system has been demonstrated. The system is possible by virtue of the components operating over a wide frequency range. The antenna elements, phase shifter, multiplexers and MMIC amplifiers, all operate over the 10 to 35 GHz frequency range. Full-duplex operation of the six-channel multiplexer and the beam scanning capability of the ultra-wideband Vivaldi antenna have been demonstrated. Finally, the phased-array antenna transceiver system was built by connecting the phased-array antenna block and the T/R module. It has been demonstrated that the whole transceiver system transmits

signal at 10, 19 and 32 GHz and receives signal at 12, 21 and 35 GHz with a beam scanning ability. The transceiver system should have many applications in wideband satellite communication systems and radar systems

CHAPTER VI

ULTRA-WIDEBAND LOW-COST PHASED-ARRAY RADARS*

6.1. Introduction

Rapid progress in telecommunication and radar technology is placing increasing demands on wireless system performance and functionality. Personal communications systems, for example, can now accommodate multiple functions and protocols [e.g., Global Positioning System (GPS), Universal Mobile Telecommunication system (UMTS), Personal Communication System (PCS)] within a single RF front end. A parallel process of convergence is beginning to take place within the military arena. Modern naval and aerospace vehicles are required to provide a large and increasing number of sensing functions, leading to a proliferation in the number of onboard phased arrays and radar systems. To reduce the number and collective cost of these systems, current research programs seek to integrate multiple systems and functions operating in different frequency bands into a single ultra-wideband system [50].

Although broadband phased array systems are a longstanding topic of interest [51], progress has recently been made using ultra-wideband tapered slot antennas together with true-time delay phase shifters [52, 53]. In [15], a low-cost four-channel 10—21-GHz phased array transceiver was demonstrated for communications applications.

* © 2005 IEEE. Parts of this chapter are reprinted, with permission, from C. T. Rodenbeck, S.-G. Kim, W.-H. Tu, M. R. Coutant, S. Hong, and K. Chang, "Ultra-wideband low-cost phased-array radars," *IEEE Trans. Microw. Theory Tech.*, vol. 53, No. 12, pp. 3697 - 3703, Dec. 2005.

In this research, extremely wideband phased array antennas are demonstrated as an enabling technology for low-cost multi-band and multi-function radar systems. Two designs are presented, one operating from 3 to 12 GHz and the other operating from 8 to 20 GHz. Both the 3—12- and 8—20-GHz systems cover frequencies commonly used for military radar and imaging. In addition, the 3—12-GHz system covers the frequencies designated by the US Federal Communications Commission for civilian ultra-wideband radar applications such as ground penetration, through-wall imaging, surveillance/security, and medical imaging [54]. Both designs use antipodal tapered-slot antennas (ATSA) in a novel mirrored array architecture to achieve ultra-wideband performance and low cross polarization. Beam steering is achieved across the complete operating bandwidths using low-cost piezoelectric transducer (PET) phase shifters. A broadband monolithic microwave integrated circuit (MMIC) power amplifier (PA) integrated into these designs addresses the traditional challenge of broadband microwave power generation. The PA operates over the 2—20-GHz decade with more than 29 dBm of output power and 15.8 dB of gain.

System tests demonstrating pulse-radar target ranging and phased-array beam steering are performed with excellent results for each array design. This approach is scalable in size and function for application to a variety of systems, with extended bandwidth and reduced cost in comparison with the state-of-the-art. These results are accordingly expected to stimulate further advances in microwave front-end designs for multi-function RF phased arrays and radars.

6.2. Antennas, array, and phase shifters

The design of the antenna elements, phase shifters, and antenna arrays are described here. The assembled subsystem of the radars is illustrated in the photograph shown in Fig. 48. The subsystem is composed of a multi-line PET-based phase shifter and a 1×4 H -plane array of ATSAs, whose geometry is already shown in Fig. 39 of Chapter V. Two different designs of ATSA elements are used to cover the respective 8—20- and 3—12-GHz bands. Table 8 lists the design parameters for both models, identified as “Design A” and “Design B”. Different sizes for the elements are used in Designs A and B in order to provide a satisfactory tradeoff between scan range and element gain for each of the respective bands

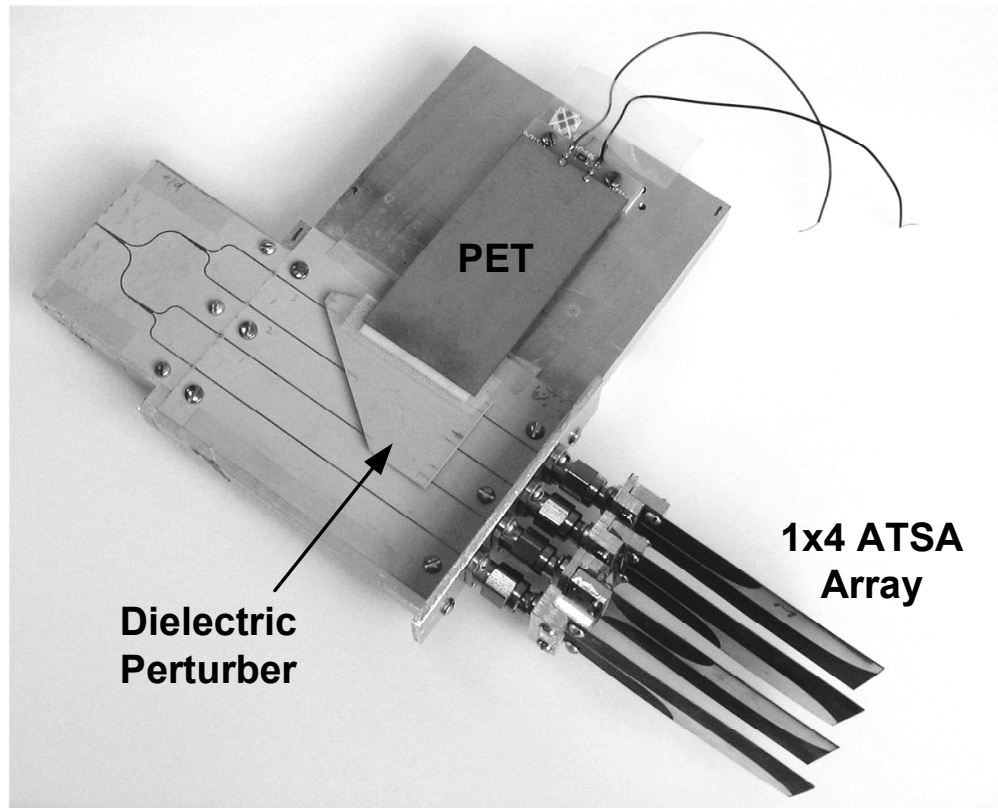


Fig. 48. Configuration of a 1 x 4 *H*-plane array operated by a PET-controlled phase shifter. The 8—20-GHz design is shown.

Fig. 49 shows that the measured return losses of the designed ATSAs are better than 10 dB across the 8—20- and 3—12-GHz bands. The measured gain of Design A is 4.9 dBi at 8 GHz, 6.8 dBi at 12 GHz, and 7.8 dBi at 20 GHz. The measured gain of Design B is 4.3 dBi at 3 GHz, 8.2 dBi at 7 GHz, and 13.8 dBi at 12 GHz.

Two PET-controlled multi-line phase shifters are designed to operate over the 8—20- and 3—12-GHz bands. Complete design parameters are given in Table 9. The maximum progressive phase shifts of 100° at 20 GHz and 80° at 12 GHz are designed to achieve scan angles of 30° and 20° , respectively. Fig. 50 shows the measured S-

parameters and differential phase shifts for the 8-20 GHz design. The return loss is better than 10 dB for the operating frequency ranges, and the insertion loss is less than 4 dB at 20 GHz with full perturbation. This insertion loss includes the losses due to the connectors, power divider, and line lengths. Fig. 51 shows the measured differential phase shifts for the 3-12 GHz design.

TABLE 8. Dimensions of the designed ATSA's.

Design Parameter	Design A	Design B
Frequency range (GHz)	8-20	3-12
Substrate dielectric constant, ϵ_r	2.2	2.33
Substrate thickness (mm)	0.38	0.79
SLOT LENGTH, L (MM)	43.2	130
Edge width, d (mm)	5.1	15
Slot width, w (mm)	15.2	80

TABLE 9. Dimensions of the designed phase shifters.

Design Parameter	Type A	Type B
Frequency range (GHz)	8-20	3-12
Substrate dielectric constant, ϵ_r	10.2	2.2
Substrate thickness (mm)	0.38	0.38
Perturber dielectric constant, ϵ_r	9.2	10.2
Perturber thickness (mm)	1.27	1.27
Incremental length of the perturber over the microstrip line, ΔL (mm)	15	17

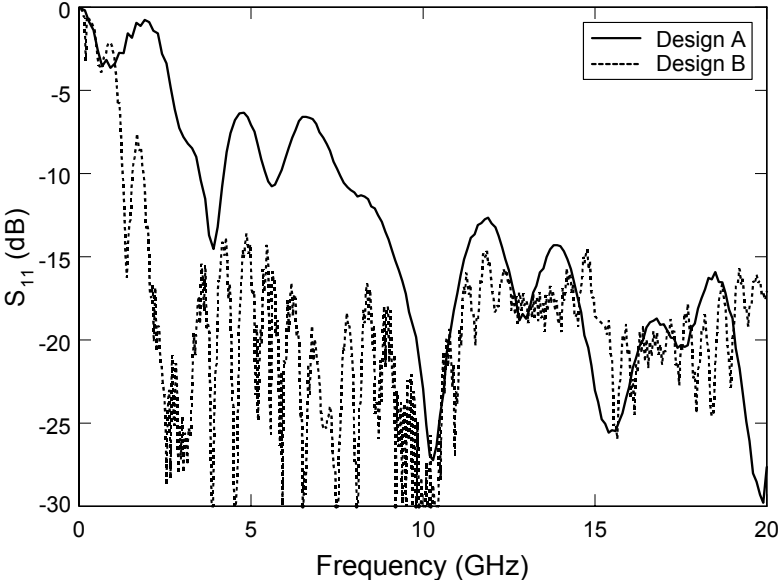
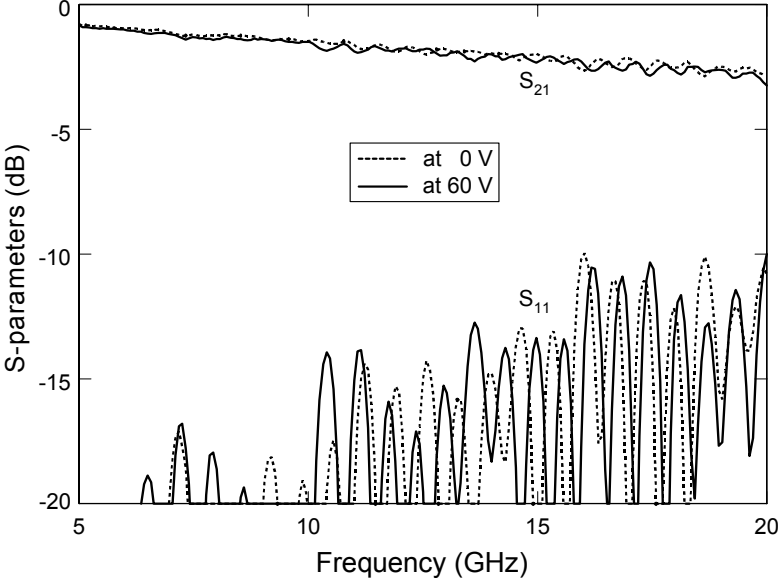
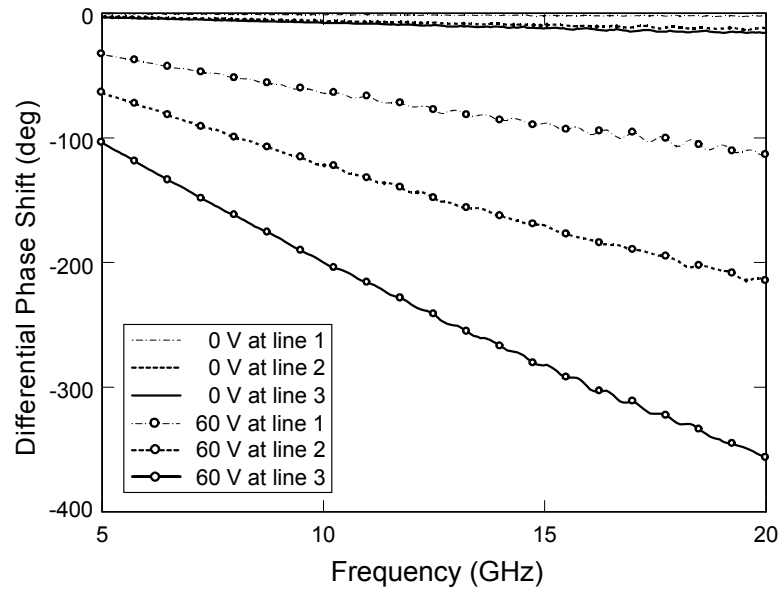


Fig. 49. Measured return loss of the ATSAs.



(a)

Fig. 50. Measured performance of the phase shifter operating from 8 to 20 GHz. (a) S-parameters. (b) Differential phase shift.



(b)

Fig. 50. Continued.

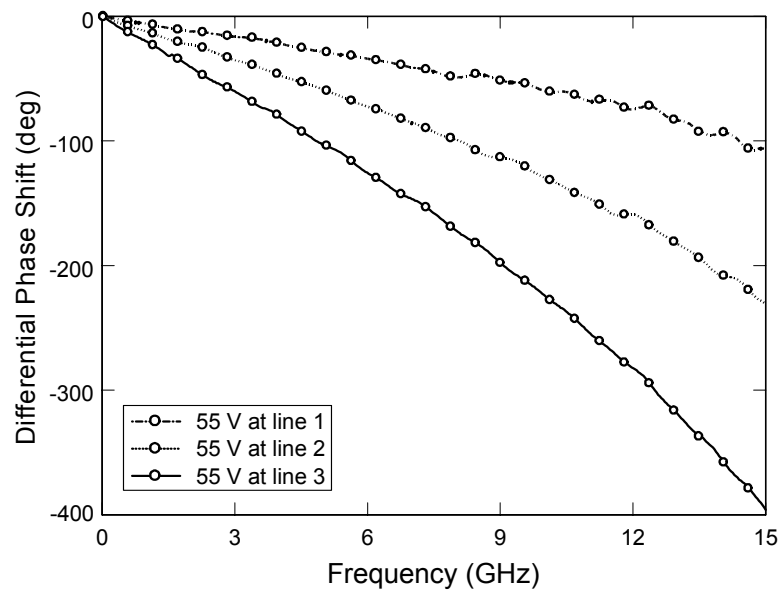


Fig. 51. Measured differential phase shift of the phase shifter operating from 3 to 12 GHz.

The arrays are fed using wideband Chebyshev power dividers. The array spacing is chosen to be sufficiently small to prevent grating lobe formation when the beam is steered in the H -plane at the highest operating frequency. The array spacing in the 8—20-GHz design is 9.4 mm, corresponding to $0.25 \lambda_0$ at 8 GHz and $0.63 \lambda_0$ at 20 GHz. The spacing in the 3—12-GHz case is 18 mm, meaning $0.18 \lambda_0$ at 3 GHz and $0.72 \lambda_0$ at 12 GHz. The measured gain of Design A at broadside scan is 4.8 dBi at 8 GHz, 6.5 dBi at 12 GHz, and 8.9 dBi at 20 GHz. For Design B at broadside scan, the measured array gain is 9.2 dBi at 3 GHz, 12.4 dBi at 7 GHz, and 14.4 dBi at 12 GHz.

6.3. 2—20-GHz MMIC-based amplifiers

The goal of this research is to demonstrate low-cost, ultra-wideband phased arrays for pulse radar applications. Such a demonstration would not be possible, however, without a broadband power amplifier (PA) for the transmitter and low-noise amplifier (LNA) for the receiver. To meet this need, a 2—20-GHz MMIC-based PA and LNA are assembled and incorporated within the system. Fig. 52 illustrates the method of integration. Each MMIC amplifier is solder-mounted on a gold/nickel-plated molybdenum carrier, which is also used in Fig. 34 of Chapter V. Same procedures as explained in the section 2 of Chapter V, are applied to assemble the MMIC module shown in Fig. 52. LNA MMICs covering the 2—20-GHz decade are currently available from multiple vendors. In this system, two Velocium ALH102C LNA chips are used to build up the receive LNA for the radar. Across the 2—20-GHz band, gain of each device varies from 8 to 12 dB, and noise figure varies from 2 to 4 dB. The power dissipation

totals 220 mW for both chips.

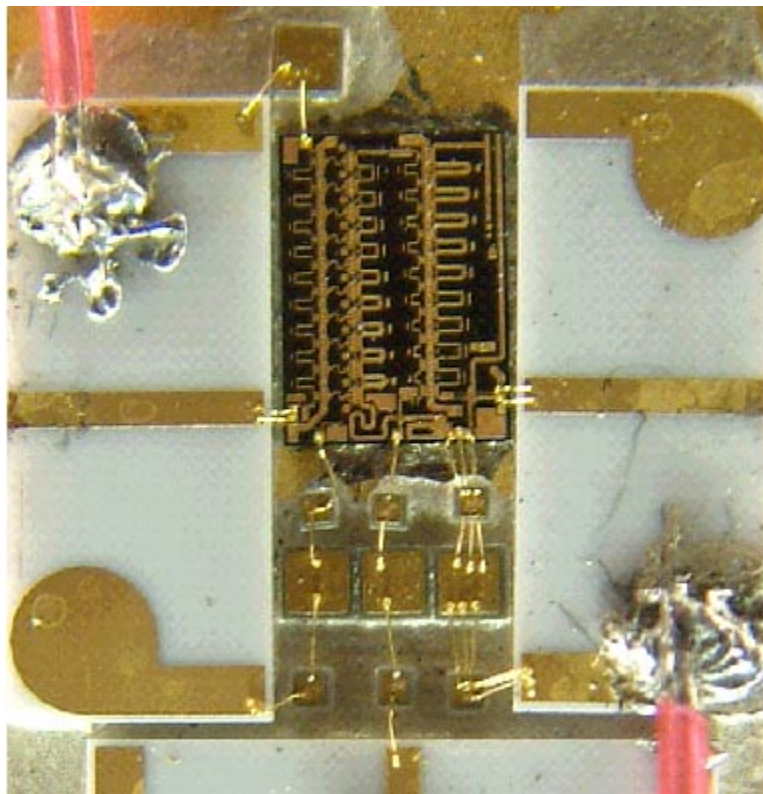


Fig. 52. A photograph of the assembled PA module including the TGA2509 MMIC, the 50- Ω lines at the input and output, and the bias networks.

High-power MMIC amplifiers operating from 2 to 20 GHz have only recently begun to enter the commercial market. This system uses the TriQuint TGA2509 MMIC power amplifier. This chip provides over 29 dBm of power with at least 15.8-dB gain across the 2–20-GHz band, performance that surpasses previously published results for amplifiers of this class [55 - 57]. The layout of the chip is included in Fig. 52. The chip size is 7.5 mm². The first stage of this distributed amplifier utilizes cascode cells to

enhance the gain while providing an option for automatic gain control. The second stage utilizes common source cells to provide high output power over the entire band. Both stages employ capacitive division on each cell to extend the upper band edge to 20 GHz. Gate bias is provided through the gate termination resistor, while the drain bias is provided through an on-chip low-pass network. The drain voltage is 12 V, and total power consumption is 13.2 W. As illustrated in Fig. 53 small-signal gain exceeds 15.8 dB and saturation power exceeds 29 dBm over the entire 2—20-GHz band.

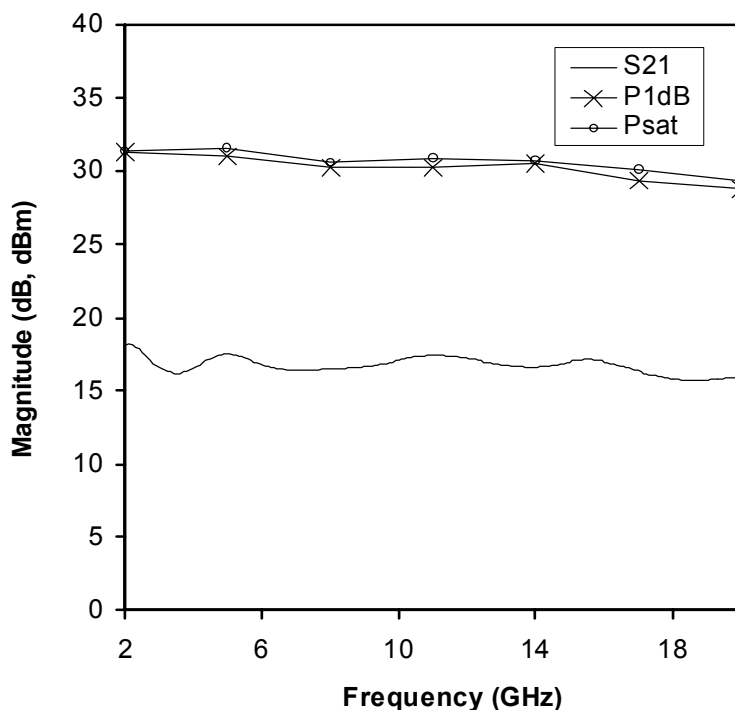


Fig. 53. Gain and output power of the PA MMIC versus frequency.

6.4. System tests

For system-level measurements, the PET-controlled antenna arrays are incorporated with the MMIC-based amplifier modules and tested using the setup shown in Fig. 54. A pulse-modulated synthesized source feeds an HP 8349B wideband driver amplifier that in turn feeds the 2—20-GHz PA module. The PA drives the PET-controlled phased array previously shown in Fig. 48. An identical PET-controlled array is used for the receiver so that both phased arrays can be controlled using the same bias voltage. Alternatively, a single antenna array can be used with the addition of a wideband duplexer switch. The receiving phased array feeds the 2—20-GHz LNA module, which in turn feeds an HP8472B Schottky diode detector and an IF amplifier. The detected waveform is compared with a timing signal to determine target range.

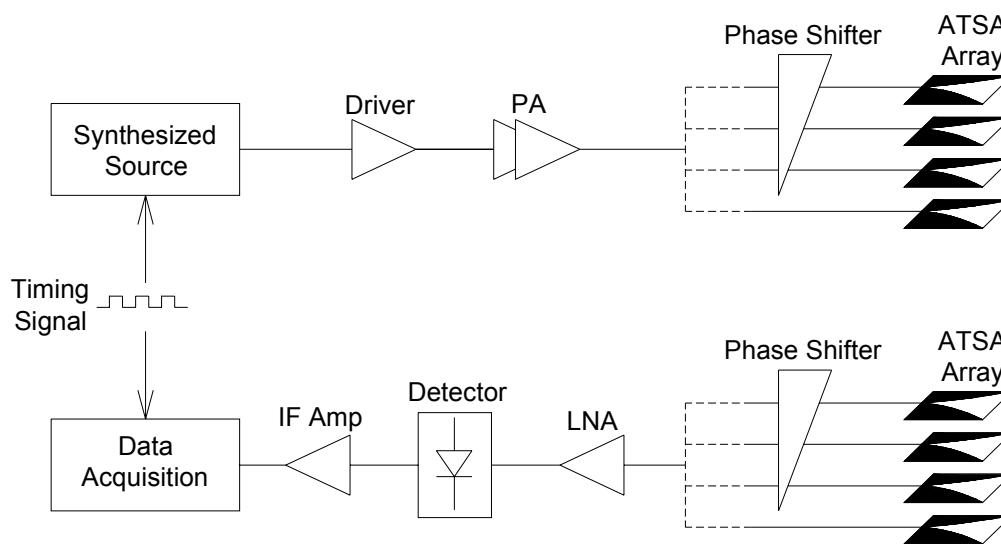


Fig. 54. System block diagram illustrating the test setup for the beam-steerable pulse radar.

A movable 1 x 1 m aluminum reflector serves as the target. The transmitter sends a pulse-modulated signal onto the target, and the receiver picks up the return signal. The distance between the target and the radar is varied, and the radar detects the variation in this distance by measuring the time delay between the received signal and the timing signal. This experimental setup is shown in Fig. 55. The results presented in this research use an RF transmit signal that is pulse modulated at a pulse-repetition frequency (PRF) of 20 MHz and at a duty cycle of 10 %. All measurements are taken inside a 9-m indoor range.

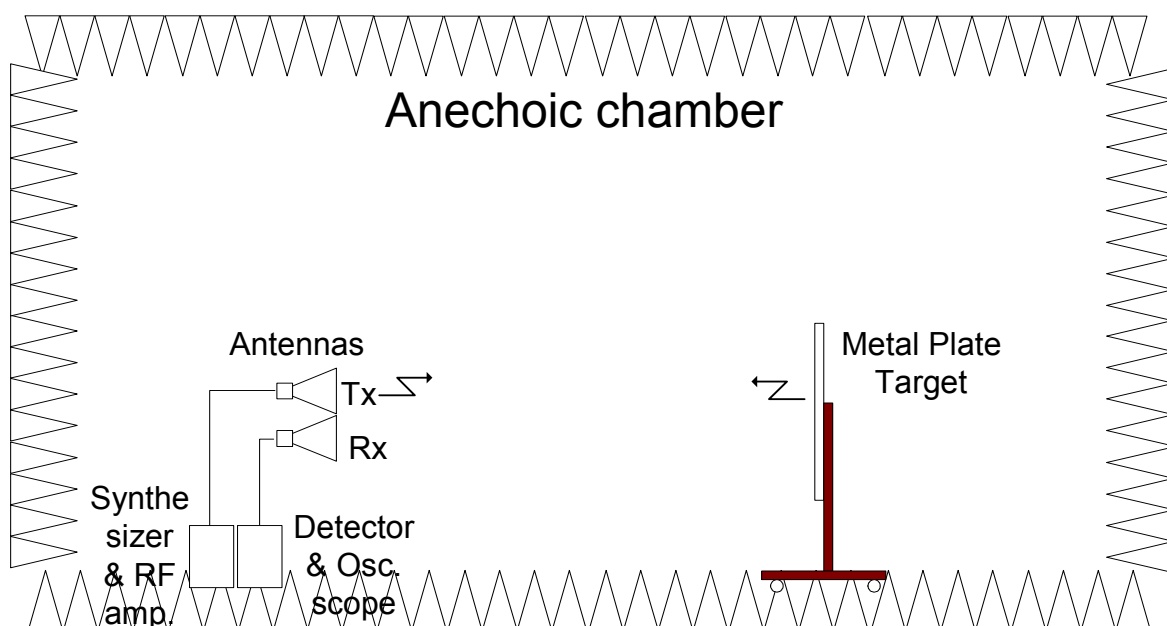


Fig. 55. Experimental setup for the radar target range test.

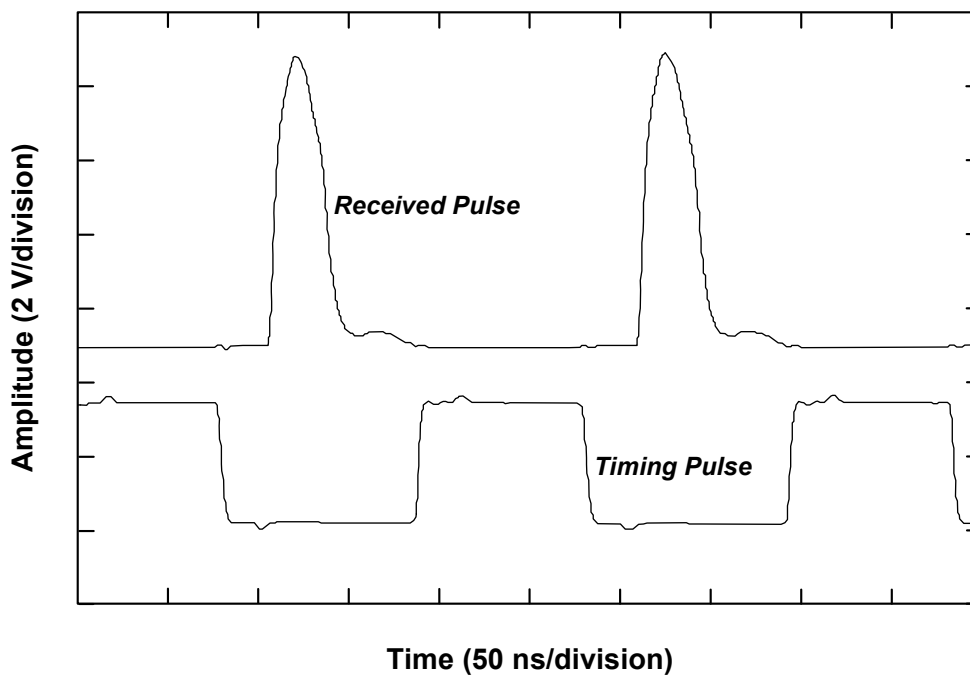


Fig. 56. Detected waveform of the received signal can be compared with the waveform of the timing signal in order to measure target range.

A plot illustrating a received pulse waveform and timing reference signal is shown in Fig. 56. The measurement shown in this figure uses a transmit signal at 5.8 GHz to range a target located 4.4 m away from the 3—12-GHz radar system. Ranging tests are conducted at 5.8 GHz for the 3—12-GHz array and at 14 GHz for the 8—20-GHz array. These frequencies are chosen because 5.8 GHz is a popular unlicensed frequency in the 3—12-GHz band and because 14 GHz is in the center of the 8-20 GHz band. As shown in Fig. 57, the measured and expected time delays agree very well. The average error is $\pm 0.14^\circ$ at 5.8 GHz and $\pm 0.13^\circ$ at 14 GHz, which corresponds to an average error of about ± 0.8 inches at both frequencies.

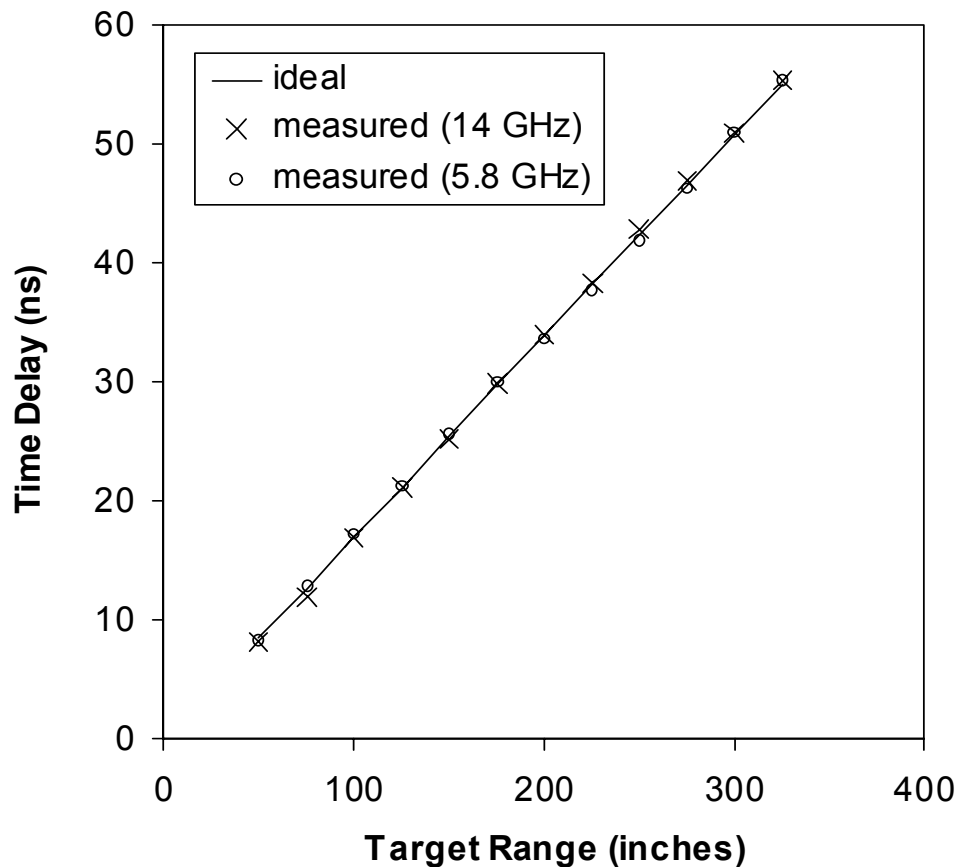
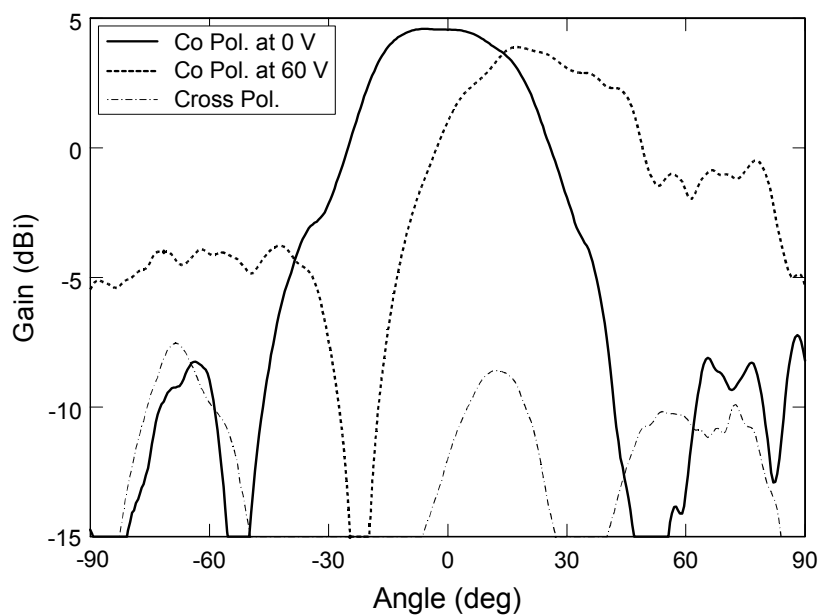


Fig. 57. Comparison between measured and ideal time delays for varying target ranges.

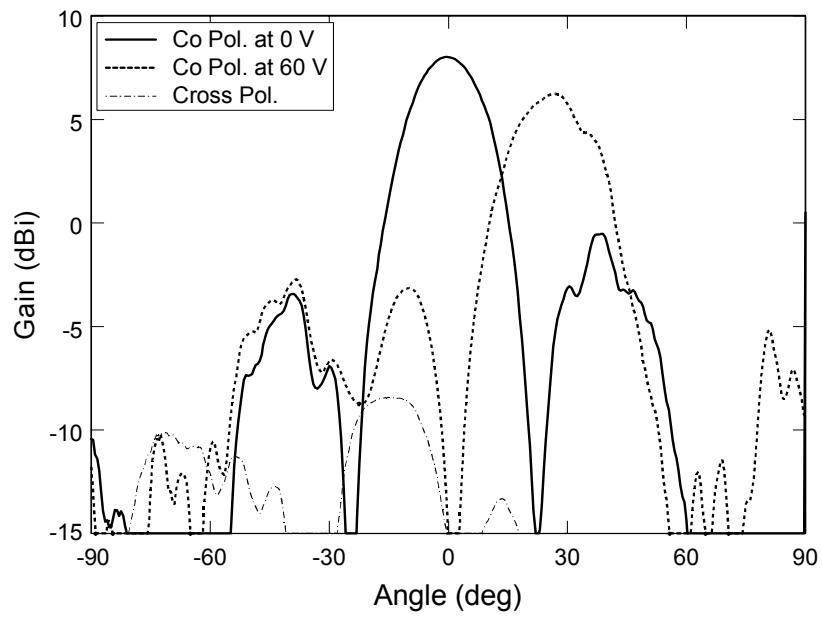
Target position can be determined by varying the beam steering angle [58]. Figs. 58 and 59 show the steered beam patterns measured from 8 to 20 GHz and from 3 to 12 GHz, respectively. Each beam is steered about 20° away from broadside in the H -plane. The maximum external bias voltage to the PET phase shifters is 60 V for both frequency ranges. Cross-polarization is less than 17 dB below the co-polarization with the mirrored array approach described in Chapter V, which reduces cross-polarization levels by more

than 20 dB at 20 GHz and 12 GHz. Imperfections in the measured patterns are due to multiple factors: the incomplete progression in the phase shifts, the phase mismatches in the connection points between the phase shifter and the antennas, the imperfect flatness of the individual antenna elements, the mutual coupling between antenna elements, and the reflection of incident energy from the circuit elements.

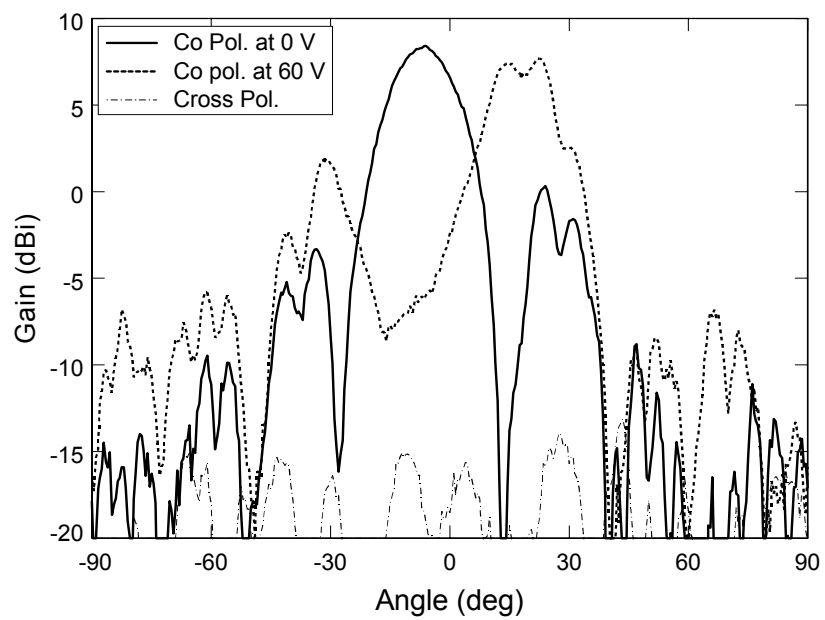


(a)

Fig. 58. Measured beam steering patterns at (a) 8 GHz. (b) 16 GHz. (c) 20 GHz.



(b)



(c)

Fig. 58. Continued.

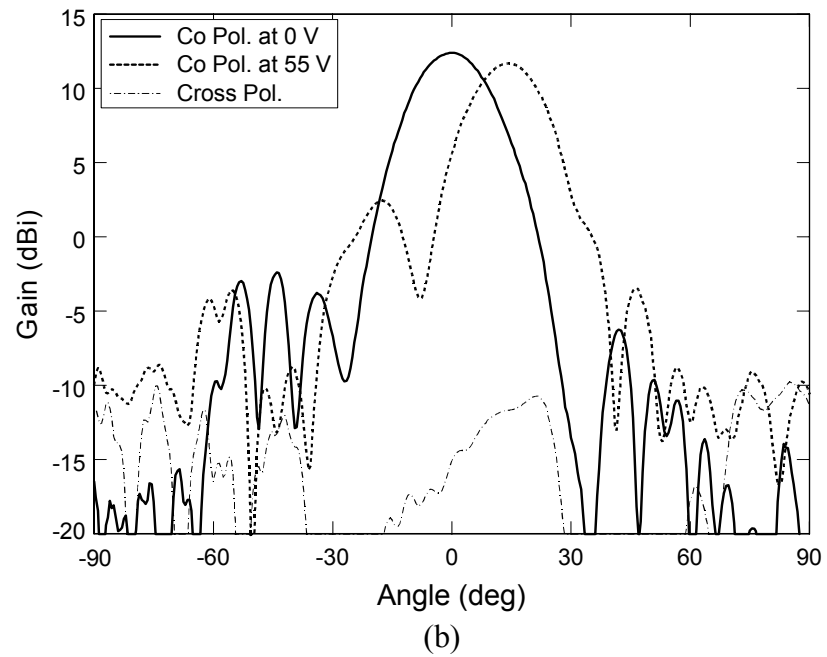
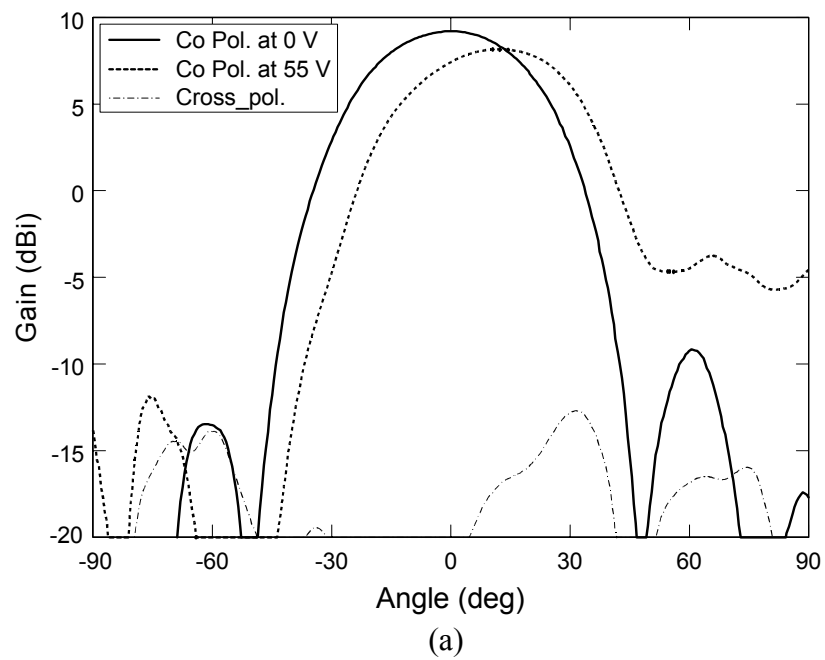


Fig. 59. Measured beam steering patterns at (a) 3 GHz. (b) 7 GHz. (c) 12 GHz.

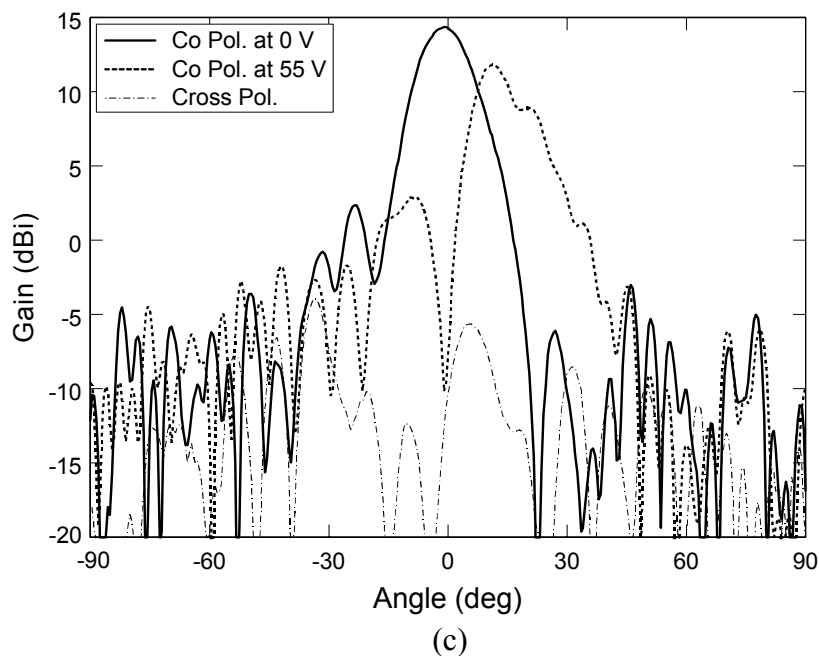


Fig. 59. Continued.

The radiation patterns, nonetheless, can be further improved by an additional optimization process and by finer fabrication tolerances.

Finally, effective isotropic radiated power (EIRP) varies approximately from 41 to 45 dBm over the 3—12-GHz range and from 35 to 38 dBm over the 8—20-GHz range.

6.5. Conclusions

Multiple radar systems can be consolidated within a single multi-function phased array radar system. This research has demonstrated an inexpensive approach for producing such a system using cross-polarization suppressed ATSA arrays, piezoelectric true-time-delay phase shifters, and decade bandwidth 1-W monolithic power amplifiers.

Two designs have been presented, one operating from 3 to 12 GHz and the other from 8 to 20 GHz. The technology is inherently scalable to larger arrays and should have wide-ranging impact on ultra-wideband multi-function radar design.

CHAPTER VII

SINGLE-FEED TRIPLE-FREQUENCY RECTANGULAR MICROSTRIP PATCH ANTENNA WITH PAIRS OF SPUR-LINES

7.1. Introduction

Recent developments in wireless communications often require antennas with compact size, low-cost and more than one operating frequencies. Due to its thin profile, light weight, low cost and easy fabrication, the microstrip patch antenna can be a good candidate for these requirements. Many dual-frequency designs of microstrip patch antennas have been published [59 - 64]. Most designs use reactively loaded elements to obtain dual-frequency operation [59, 60], while other designs use a multi-layer structure [61, 62] or multi-patches [63, 64]. But these designs require complex manufacturing procedures or larger size than that of the normal microstrip patch antenna. Compare to the dual frequency designs, not many literatures have been reported about the triple-frequency designs [65, 66]. In [65], three annular-ring slots are used instead of patch. In [66], parasitic elements are added to the slot loaded patch antenna for triple-band operation at the expense of large overall size. In this research, spur-lines are used to excite new resonant modes between TM_{10} and TM_{20} modes of the rectangular patch antenna. Two pairs of spur-lines are embedded in the non-radiating edge of the patch. The frequencies of new resonances are relatively independently tunable. Also, the antenna is fed by an inset microstrip line, which alleviates the complexity of integration

with other microwave circuit components for array systems or MMIC applications. The placements of the spur-lines have been decided considering the current distributions so that good radiation can occur at the new resonant frequencies caused by the pairs of spur lines. The physical dimensions of the spur-lines are optimized to obtain matching at the three resonant frequencies.

7.2. Antenna design

Fig. 60 (a) shows a normal rectangular microstrip patch antenna fed by an inset microstrip line at a radiating edge. The rectangular patch has dimensions of $L = 17$ mm and $W = 18$ mm and the operation frequency (f_0) of 5.8 GHz. The width of feed line (W_f) and the depth of inset from the edge (D) are 2.4 mm and 6.5 mm, respectively. The gap between the feed line and the patch (G) is 0.4 mm. The antenna patch is printed on a substrate with a relative dielectric constant, $\epsilon_r = 10.2$ and thickness, $h = 0.79$ mm. Fig. 60 (b) is the configuration of a spur-line to be embedded in the rectangular microstrip patch to excite extra resonances.

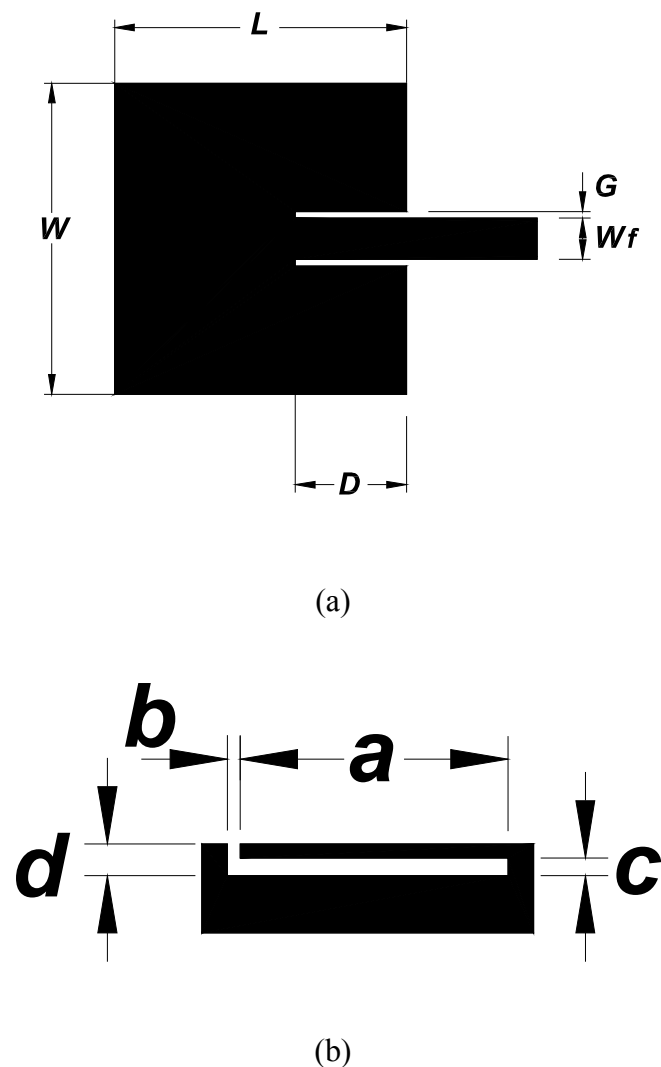
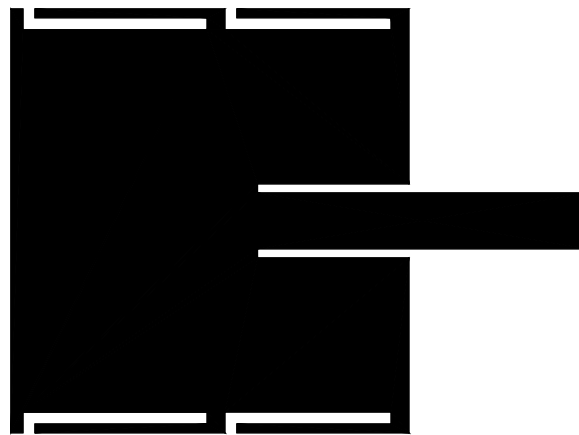


Fig. 60. (a) Inset-feed rectangular microstrip patch antenna operating at 5.8 GHz ($L = 17$ mm, $W = 18$ mm). (b) Spur-line to be embedded in the patch.

An extra resonance is achieved by embedding a pair of spur-lines in the non-radiating edges of the patch antenna [67]. In this research, one more pair of spur-lines is added for triple-frequency operation and direct inset feed is used instead of aperture-coupled feeding. The inset microstrip feeding also has an advantage of easy integration

with other circuit components. Fig. 61 shows some of possible configurations for embedding two pairs of spur-lines in the non-radiating edges of the patch.

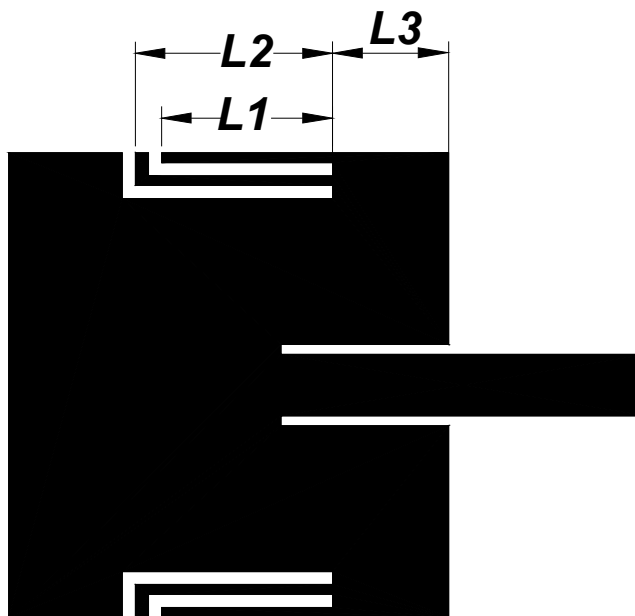


(a)



(b)

Fig. 61. Possible configurations of embedding two-pairs of spur-lines in the non-radiating edges of the rectangular patch.



(c)

Fig. 61. Continued.

But the configurations of Fig. 61 (a) and (b) have poor impedance matching and the radiation efficiency is not good at one of the extra resonant frequencies caused by embedding the spur-lines. The reason for the bad radiation efficiency can be attributed to the existence of opposite current distributions around the two displaced spur-lines. Simulation results show that the configuration of Fig. 61 (c) has good impedance matching and radiation patterns at all three resonant frequencies.

The initial dimensions of the spur-lines are obtained following the equation in [28] and then optimized using IE3D [29] to achieve good impedance matching at three resonant frequencies. After embedding the spur-lines, the simulated results show that

two extra resonances (f_1, f_2) are found at $f_1 = 6.78$ GHz and $f_2 = 7.75$ GHz and the fundamental frequency (f_0) is perturbed to 5.11 GHz. Table 10 shows the optimized physical dimensions of the spur-lines shown in Fig. 61 (c). The photo of the designed triple-frequency patch antenna is shown in Fig. 62.

TABLE 10. Physical dimensions of the spur-line shown in Fig. 61 (c). The shorter spur-lines are the pair of spur-lines located closer to the edge. The location of the spur-lines from the edge with the feed line is $L_3 = 4.5$ mm. (Unit: mm)

	Shorter spur-lines	Longer spur-lines
a	6.86 (L_1)	7.62 (L_2)
b	0.25	0.25
c	0.25	0.25
d	0.63	1.27

The frequency ratio between the fundamental (f_0) and the first extra resonant frequency (f_1) is 1.33 and the ratio between the fundamental and the second extra resonance frequency (f_2) is 1.52. These ratios can be tuned independently. Fig. 63 shows that the frequencies of the extra resonances change with variations of spur-line length.

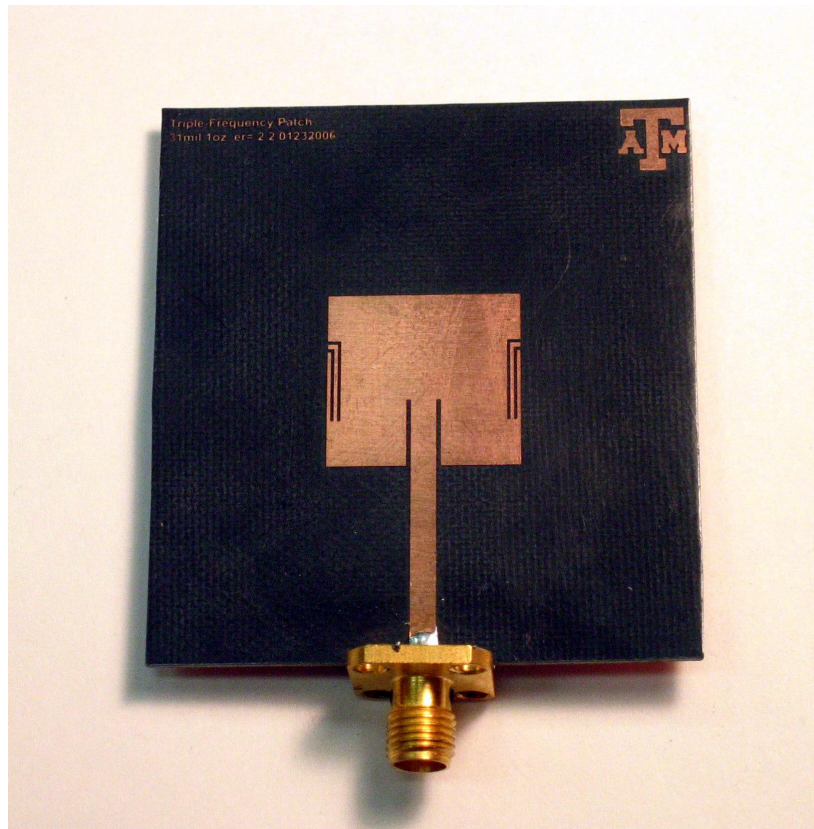
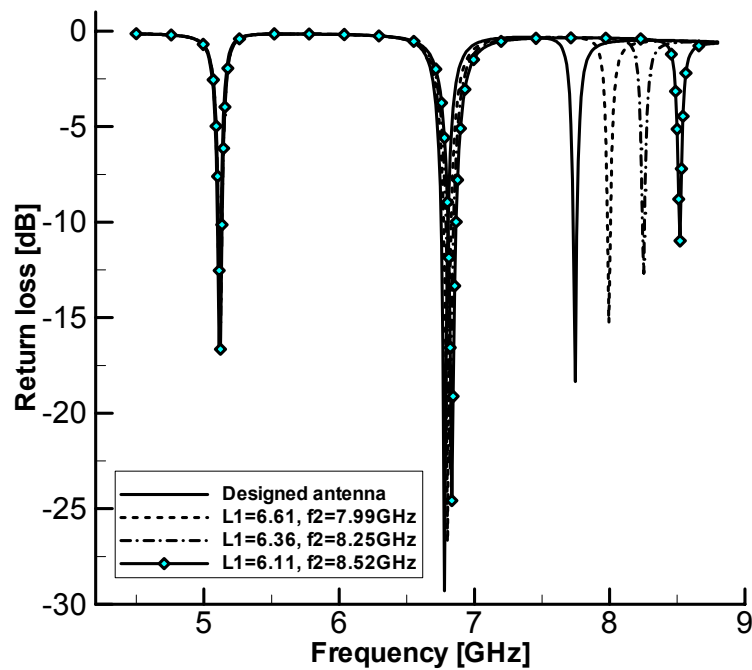
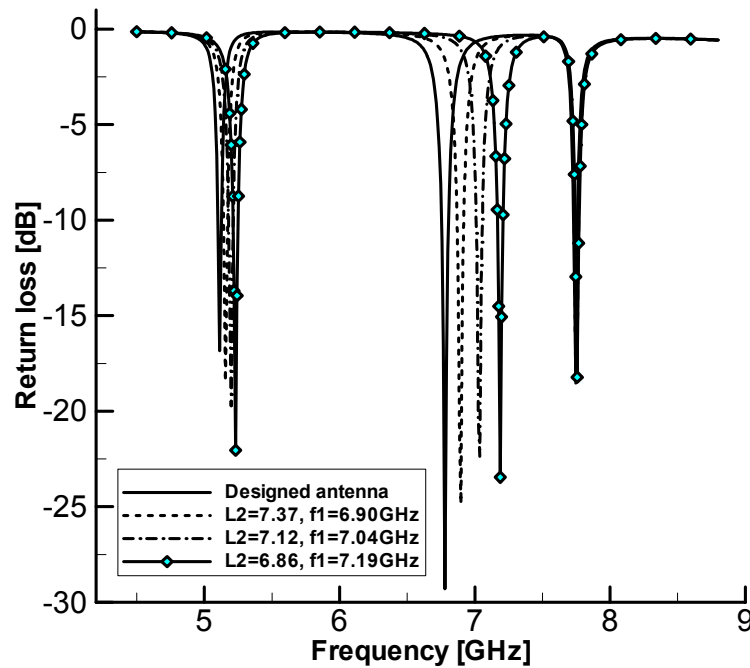


Fig. 62. Photo of the designed triple-frequency patch antenna.



(a)

Fig. 63. Tuning of the extra resonant frequencies by varying the length of spur-lines. (a) Change of the second extra resonant frequency with the variation of shorter spur-lines (L_1), (b) Change of the first extra resonant frequency with the variation of longer spur-line length (L_2). (Unit of lengths: mm)



(b)

Fig. 63. Continued.

7.3. Experimental results

The measured return loss is shown in Fig. 64 in comparison with the simulations. The measured resonant frequencies are 5.19, 6.90, and 7.89 GHz, which show good agreements with the simulation results. The measured radiation patterns for the E-plane are shown in Fig. 65. It can be seen that symmetrical radiation patterns can be achieved with a gain over 6 dBi at all three resonant frequencies. Good radiation patterns for the H-plane are also obtained in the experiments.

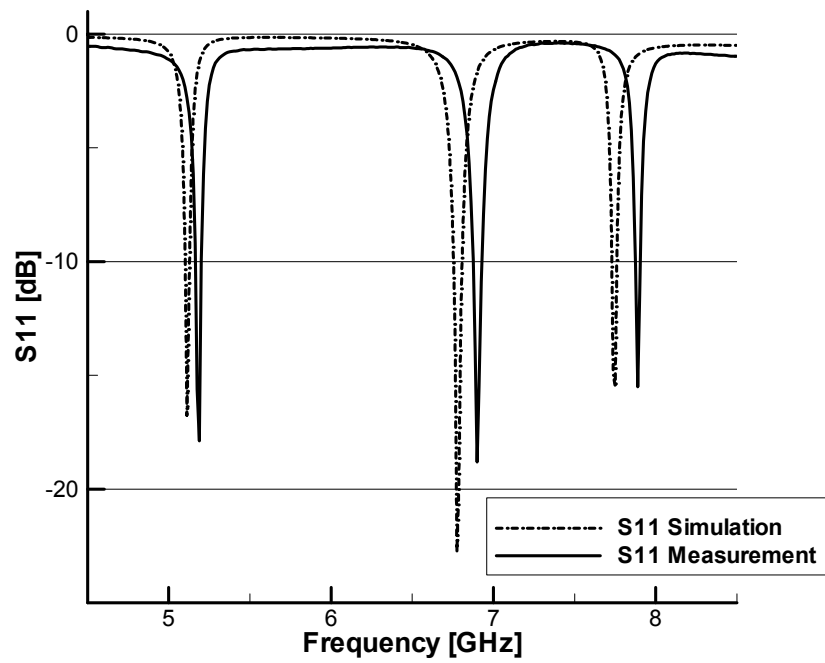
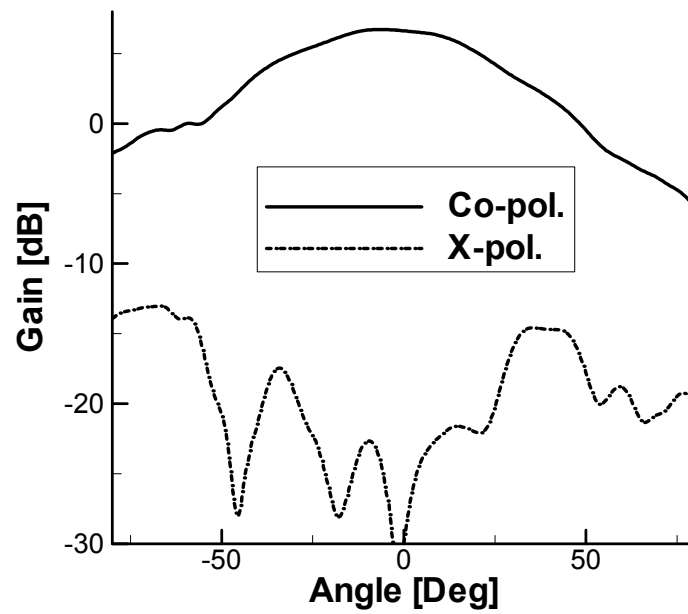
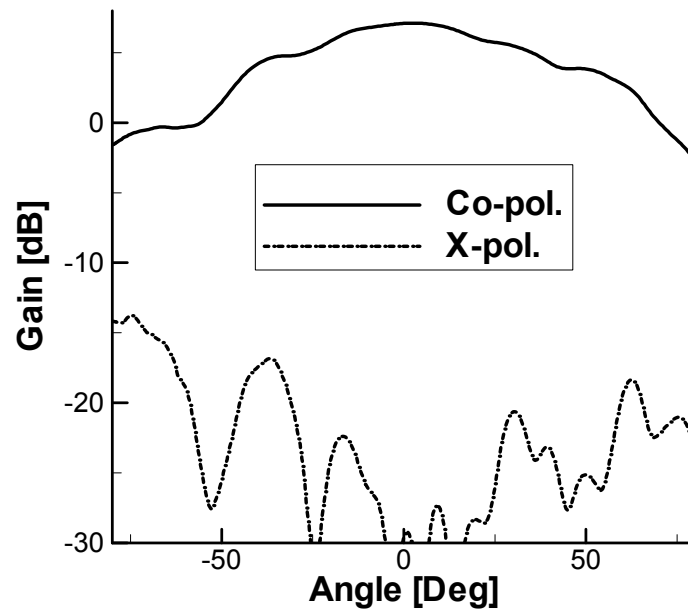


Fig. 64. Simulated and measured return losses of the designed antenna with spur-line dimensions shown in Table 10.



(a)



(b)

Fig. 65. Measured radiation patterns for the E-plane at three resonant frequencies (f_0, f_1, f_2). (a) $f_0 = 5.19$ GHz. (b) $f_1 = 6.90$ GHz. (c) $f_2 = 7.89$ GHz.

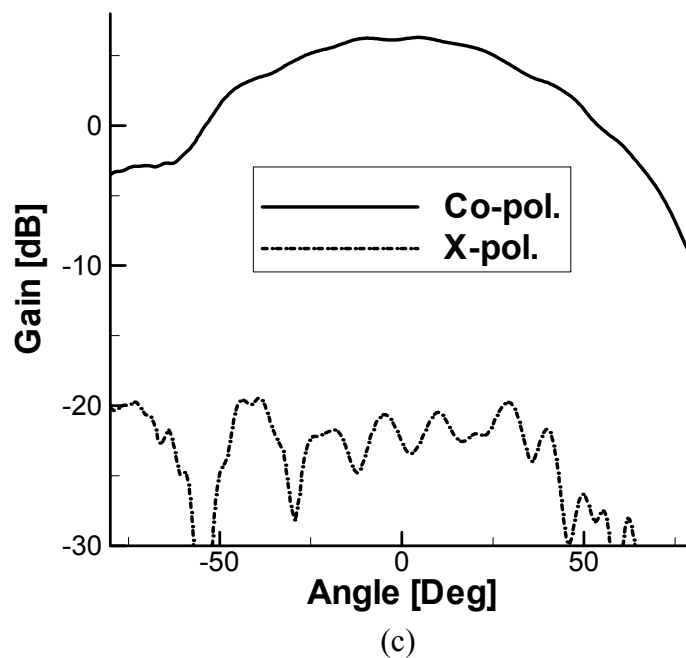


Fig. 64. Continued.

7.4. Conclusions

Two pairs of spur-lines are embedded in the non-radiating edges of the rectangular microstrip patch antenna for triple-frequency operations. The placements of the pairs of spur-lines have been optimized for good radiation efficiency and impedance matching at all three resonant frequencies. The extra resonant frequencies caused by the spur-lines can be tuned independently. Good agreements between the simulations and the measurements are obtained. The antenna is fed by an inset microstrip line for easy integration with other circuit components.

CHAPTER VIII

SUMMARY AND RECOMMENDATIONS

8.1. Summary

This dissertation has covered four main topics, which are microstrip parallel coupled-line bandpass filters with suppression of multi-spurious passbands, microstrip diplexer and multiplexer, ultra-wideband T/R module and microstrip antennas and their applications to a multi-band beam scanning antenna transceiver system and ultra-wideband phased-array radars. The microstrip bandpass filter with suppression of spurious passbands has been developed and used in the design of multiplexer. The new microstrip multiplexer with six channels ranging from 10 to 35 GHz plays an important role in designing a compact, full-duplex, ultra-wideband T/R module. This dissertation has explained the method to make MMIC amplifiers functional by assembling the MMIC amplifiers on a carrier plate with other components. The T/R module has been integrated with a phased-array of Vivaldi antennas to form a multi-band, compact, and full-duplex beam scanning antenna transceiver system. Although the transceiver system has some degradation of gain in millimeter-wave frequency range, it has shown an unprecedented operation bandwidth from 10 to 35 GHz. This research expands the bandwidth of a previously reported transceiver system by more than 10 GHz. In the followings, the topics and accomplishments covered in this dissertation are summarized chapter by chapter.

In Chapter II, two modified microstrip coupled-line bandpass filter structures for suppression of multi-spurious passbands have been presented. One structure incorporates spur-lines into the input and output resonators of the conventional microstrip parallel coupled-line bandpass filter. The other one uses small resonators placed in the vicinity of the conventional microstrip parallel coupled bandpass filter. This modified parallel coupled-line bandpass filter is used in the multiplexer described in Chapter IV. Both structures reduce the length of the filters by simple transformation of the layout of the conventional parallel coupled-line filters and suppress the spurious passbands by more than 30 dB at the second and the third harmonic frequencies.

In Chapter III, a new type of microstrip bandpass filters, which utilize the passband formed between neighboring stop bands of open-circuited stub has been introduced. Two filters have been designed at 32 and 35 GHz, respectively and connected together using T-junction to form a millimeter-wave diplexer. The measured insertion loss is 3.5 dB at 32 GHz and 3.2 dB at 35 GHz. The return loss is more than 10 dB at both 32 GHz and 35 GHz. The isolation is more than 30 dB for the two frequencies.

In Chapter IV, a six channel multiplexer composed of microstrip parallel coupled-line bandpass filters has been developed. To avoid tuning after fabrication by precise design and reduce the optimization time, both full-wave electromagnetic simulator and circuit simulator have been used in the multiplexer design and the design procedures have been described step by step. The multiplexer has 10-, 12-, 19-, 21-, 32-, and 35-GHz channels with the measured insertion losses between 2.0 and 3.2 dB. The

multiplexer developed in this chapter has been used in the ultra-wideband transceiver system.

In Chapter V, a multi-band, compact, and full-duplex beam scanning antenna transceiver system operating from 10 to 35 GHz has been discussed. The system consists of ultra-wideband Vivaldi antennas, a multi-line PET-based phase shifter, a six-channel microstrip multiplexer described in Chapter IV, and monolithic microwave integrated circuit (MMIC) amplifiers. Each component constituting the system has been described in detail. The system has been tested for its beam scanning performance and shown beam scanning capability of more than 20 degrees from broadside in the H-plane at 10, 12, 19, 21, 32, and 35 GHz.

In Chapter VI, a cost-effective implementation for extremely wideband phased array radars has been introduced. Two designs are demonstrated, one operating from 3-12 GHz and the other operating from 8-20 GHz. Ultra-wideband antipodal tapered slot antennas, a novel cross-polarization suppressed array architecture, piezoelectric true time delay phase shifters, and broadband high-power monolithic amplifiers constitute the phased array radars. The performances of detecting the target range of the designed two radars have been tested at 5.8 and 14 GHz and the measured results show the average errors of $\pm 0.14^\circ$ at 5.8 GHz and $\pm 0.13^\circ$ at 14 GHz.

In Chapter VII, a rectangular microstrip patch antenna with triple resonant frequencies has been presented as an answer to the recent demand of multi-function antenna in the wireless communication area. Two pairs of spur-lines are embedded in the non-radiating edges of the patch antenna to excite extra resonant frequencies. The

designed antenna shows good return losses at three independent resonant frequencies. The measured results show good symmetrical radiation patterns at three frequencies with gains over 6 dBi.

8.2. Recommendations for future research

Since the functionality of each component in the ultra-wideband transceiver system has been verified over its operation frequency range, the performance improvement of the system is suggested as a next step. Because the multiplexer has been printed on a soft substrate, it is very difficult to attach bonding-wires to the tips of the multiplexer. Moreover, the tips of microstrip multiplexer, which is made of copper, should be plated with gold for wire-bonding. To solve this connection problem, it is recommended to design a microstrip multiplexer on a hard substrate like alumina. By using the hard alumina substrate, which has a higher dielectric constant, the size of the multiplexer can be reduced further and the bonding machine can make connections between the MMIC assemblies and the multiplexers easily.

To improve the gain of the T/R module, it is suggested to use MMIC amplifiers with built-in DC block capacitors. Assembling all MMIC amplifiers in each communication path on a single carrier plate also increases the gain of the T/R module.

It is also suggested to design a compact, wideband, and circularly polarized antenna and then build a phased-array beam scanning antenna transceiver, which can transmit and receive circularly polarized waves.

REFERENCES

- [1] M. Guglielmi, “ Simple CAD procedure for microwave filters and multiplexer,” *IEEE Trans. Microwave Theory Tech.*, vol. 42, no. 7, pp. 1347–1352, Jul. 1994.
- [2] E. Ofli and R. Vahldieck, “A novel compact millimeter wave diplexer,” in *IEEE MTT-S Int. Microwave Symp. Dig.*, Seattle, WA, Jun. 2002. pp. 377-380.
- [3] G. Tudosie, E. Ofli, and R. Vahldieck, “Hybrid EM-simulator based optimization of microwave and millimeter wave diplexers and multiplexers,” in *IEEE MTT-S Int. Microwave Symp. Dig.*, Philadelphia, PA, Jun. 2003. pp. 1219-1222.
- [4] L. Accatino and M. Mongiardo, “Hybrid circuit-full-wave computer-aided design of a manifold multiplexers without tuning elements,” *IEEE Trans. Microwave Theory Tech.*, vol. 50, no. 9, pp. 2044–2047, Sep. 2002.
- [5] F. M. Vanin, D. Schmitt, and R. Levy, “Dimensional synthesis for wide-band waveguide filters and diplexer,” *IEEE Trans. Microwave Theory Tech.*, vol. 52, no. 11, pp. 2488–2495, Nov. 2004.
- [6] P. Blondy, A. R. Brown, D. Cros, and G. M. Rebeiz, “Low-loss micromachined filters for millimeter-wave communication systems,” *IEEE Trans. Microwave Theory Tech.*, vol. 46, no. 12, pp. 2283-2288, Dec. 1998.
- [7] A. R. Brown, and G. M. Rebeiz, “A high-performance integrated K-band diplexer,” *IEEE Trans. Microwave Theory Tech.*, vol. 47, no. 8, pp. 1477-1481, Aug. 1999.
- [8] V. K. Varadan, K. J. Vinoy and K. A. Jose, *RF MEMS and Their Applications*. Chichester, England: Wiley, 2003, p. 382
- [9] D. Rubin and D. Saul, “Millimeter wave MIC bandpass filters and multiplexers,” in *IEEE MTT-S Int. Microwave Symp. Dig.*, vol. 78, Jun, 1978. pp. 208-210.
- [10] S. C. Holme and S. J. Fiedziuszko, “A 4 GHz dielectric contiguous output

- multiplexer for satellite applications,” in *IEEE MTT-S Int. Microwave Symp. Dig.*, Atlanta, GA, Jun. 1993. pp. 443-446
- [11] R. R. Mansour, “Design of superconductive multiplexers using single-mode and dual-mode filters,” *IEEE Trans. Microwave Theory Tech.*, vol. 42, no. 7, pp. 1411-1418, Jul. 1994.
- [12] R. R. Mansour, V. Dokas, G. Thomson, W. -C. Tang, and C. M. Kudsia, “A C-band superconductive input multiplexer for communication satellites,” *IEEE Trans. Microwave Theory Tech.*, vol. 42, no. 12, pp. 2472-2479, Jul. 1994.
- [13] C. Wang and K. Chang, “Microstrip multiplexer with four channels for broadband system applications,” *Int. J. RF Microwave CAE.*, vol. 11, no. 1, pp. 48-54, Jan. 2001.
- [14] B. A. Kopp, “X-band transmit/receive module overview,” in *IEEE MTT-S Int. Microwave Symp. Dig.*, Boston, MA, Jun. 2000. pp. 705-708.
- [15] T.-Y. Yun, C. Wang, P. Zepeda, C. T. Rodenbeck, M. R. Couttant, M. -Y. Li, and K. Chang, “A 10- to 21 –GHz, low-cost, multifrequency, and full-duplex phased-array antenna system,” *IEEE Trans. Microwave Theory Tech.*, vol. 50, no. 5, pp. 641-650, May. 2002.
- [16] S. B. Cohn, “Parallel-coupled transmission-line-resonator filters,” *IRE Trans. Microwave Theory Tech.*, vol. MTT-6, pp 223-231, Apr. 1958.
- [17] A. Riddle, “High performance parallel coupled microstrip filters,” in *IEEE MTT-S Int. Microwave Symp. Dig.*, 1988, pp.427-430.
- [18] J.-T. Kuo, S.-P. Chen, and M Jiang, “Parallel-coupled microstrip filters with over-coupled end stages for suppression of spurious responses,” *IEEE Microwave Wireless Comp. Lett.*, vol. 13. no. 10, pp. 440-442, Oct. 2003.
- [19] S. L. March, “Phase velocity compensation in parallel-coupled microstrip,” in *IEEE MTT-S Int. Microwave Symp. Dig.*, 1982, pp.410-412.

- [20] I. J. Bahl, "Capacitively compensated high performance parallel coupled microstrip filters," in *IEEE MTT-S Int. Microwave Symp. Dig.*, 1989, pp.679-682.
- [21] J.-T. Kuo, W.-H. Hsu, and W.-T. Huang, "Parallel coupled microstrip filters with suppression of harmonic response," *IEEE Microwave Wireless Compon. Lett.*, vol. 12, no. 10, pp. 383-385, Oct. 2002.
- [22] B. S. Kim, J. W. Lee, and M. S. Song, "Modified microstrip filters improving the suppression performance of harmonic signals," in *IEEE MTT-S Int. Microwave Symp. Dig.*, 2003, pp.539-542.
- [23] F.-R. Yang, K.-P. Ma, Y. Qian, and T. Itoh, "A uniplanar compact photonic-bandgap (UC-PBG) structure and its applications for microwave circuits," *IEEE Trans. Microwave Theory Tech.*, vol. 47, no. 8, pp. 1509-1514, Aug. 1999.
- [24] T. Lopetegi, M. A. G. Laso, F. Falcone, F. Martin, J. Bonache, J. Garcia, L. Pérez-Cuevas, M. Sorolla, and M. Guglielmi, "Microstrip 'wiggly-line' bandpass filters with multispurious rejection," *IEEE Microwave Wireless Compon. Lett.*, vol. 14, no. 11, pp. 531-533, Nov. 2004.
- [25] P. Cheong, S.-W. Fok, and K.-W. Tam, "Miniaturized parallel coupled-line bandpass filter with spurious-response suppression," *IEEE Trans. Microwave Theory Tech.*, vol. 53, no. 5, pp. 1810-1816, May. 2005.
- [26] W.-H. Tu, and K. Chang, "Compact microstrip bandstop filter using open stub and spurline," *IEEE Microwave Wireless Compon. Lett.*, vol. 15, no. 4, pp. 268-270, Apr. 2005.
- [27] D. M. Pozar, *Microwave Engineering*, 2nd ed. New York: Wiley, 1998, Ch. 8.
- [28] R. N. Bates, "Design of microstrip spur-line band-stop filters," *IEE J. Microwav., Optics, Acoustics*, vol. 1, no. 6, pp. 209-214, nov. 1977.
- [29] IE3D, Version 11.1, Zeland Software, 48834 Kato Road, 103A, Fremont, CA 94538.

- [30] G. L. Matthaei, L. Young, and E. M. T. Jones, *Microwave Filters, Impedance – Matching Networks and Coupling Structures*. Dedham, MA: Artech House, 1980, pp. 973-999.
- [31] R. R. Romanofsky, K. B. Bhasin, G. E. Ponchak, A. N. Downey, and D. J. Connolly, “An experimental investigation of microstrip properties on soft substrates from 2 to 40 GHz,” in *IEEE MTT-S Int. Microwave Symp. Dig.*, vol. 85, Jun, 1985. pp. 675–678.
- [32] G. Henryk, “Microwave diplexer with direct coupled filters,” in *Int. Microwaves Radar Conf.*, vol. 2, 1998, pp. 620-623.
- [33] B. Strassner and K. Chang, “Wide-band low-loss high-isolation microstrip periodic-stub diplexer for multiple-frequency applications,” *IEEE Trans. Microwave Theory Tech.*, vol. 49, no. 10, pp. 1818-1820, Oct. 2001.
- [34] M. Kirschning, R. H. Jansen, and N. H. L. Koster, “Accurate model for open end effect of microstrip lines,” *Electron. Lett.*, vol. 17, no. 3, pp. 123-126, Feb. 1981.
- [35] G. I. Zysman, and A. K. Johnson, “Coupled transmission line networks in an inhomogeneous dielectric medium,” *IEEE Trans. Microwave Theory Tech.*, vol. MTT-17, no. 10, pp. 753 - 759, Oct. 1969.
- [36] J. D. Rhodes, and R. Levy, “Design of general manifold multiplexers,” *IEEE Trans. Microwave Theory Tech.*, vol. MTT-27, no. 2, pp. 111-123, Feb. 1979.
- [37] R. G. Egri, A. E. Williams, and A. E. Atia, “A contiguous-band multiplexer design,” in *IEEE MTT-S Int. Microwave Symp. Dig.*, vol. 83, May, 1983, pp. 86-88.
- [38] Microwave Office, ver 6.03, Applied Wave Research Inc., 1960 E. Grand Avenue, Suite 430, El Segundo, CA 90245.
- [39] M. Ludwig, H.-P. Feldle, and H. Ott, “A miniaturised X-band T/R module for SAR-systems based on active phased array techniques,” in *IGARSS '95. Int. Geoscience and Remote Sensing Symp.* Jul. 1995, pp. 2063-2065.

- [40] R.-S. Chu, K. M. Lee, and A. T. S. Wang, "Multiband phased-array antenna with interleaved tapered-elements and waveguide radiators," in *IEEE Antennas Propagat. Soc. Int. Symp. Dig.*, Baltimore, MD, 1996, pp. 1616-1619.
- [41] J. Ramsay, "Highlights of antenna history," *IEEE Antenna Prop. Society Newsletter*, vol. 23, pp. 7-20, Dec. 1981.
- [42] S. Wiens and K. Epstein, "Low cost deployment of auxiliary payloads," in *Proc. IEEE Aerospace Conf.*, vol. 4, pp. 329-334, Mar. 2000.
- [43] K. S. Yngvesson, D. H. Schaubert, T. L. Korzeniowski, E. L. Kollberg, T. Thungren, and J. F. Johansson, "Endfire tapered slot antennas on dielectric substrates," *IEEE Trans. Antennas Propagat.*, vol. 33, no. 12, pp 1392-1400, Dec. 1985.
- [44] E. Gazit, "Improved design of the Vivaldi antenna," *IEE Proc. Microwaves, Antennas and Propagation*, vol. 135, no. 2, pp. 89-92, Apr. 1988.
- [45] S.G. Kim and K. Chang, "Ultrawide-band transitions and new microwave components using double-sided parallel-strip lines," *IEEE Trans. Microwave Theory Tech.*, vol. 52, no. 9, pp. 2148-2152, Sep. 2004.
- [46] K. S. Yngvesson, T. L. Korzeniowski, Y.-S. Kim, E. L. Kollberg, and J. F. Johansson, "The tapered slot antenna – a new integrated element for millimeter-wave applications," *IEEE Trans. Microwave Theory Tech.*, vol. 37, pp. 365-374, Feb. 1989.
- [47] *Microwave Studio ver. 4*, CST, Darmstadt, Germany, 2003.
- [48] T.-Y. Yun and K. Chang, "Analysis and optimization of a phase shifter controlled by a piezoelectric transducer," *IEEE Trans. Microwave Theory Tech.*, vol. 50, no. 1, pp. 105-111, Jan. 2002.
- [49] S.-G. Kim and K. Chang, "A low cross-polarized antipodal vivaldi antenna array for wideband operations," in *IEEE Antennas Propagat. Soc. Int. Symp. Dig.*,

- Monterey, CA, June 2004, pp. 2269-2272.
- [50] P. F. McManmon, E. A. Watson, and M. T. Eismann, "Suggestions for low cost multifunction sensing," in *Proc. IEEE Aerospace Conf.*, Apsen, CO, March 1998, pp. 283-306.
- [51] G. J. Laughlin, E. V. Byron, and T. C. Cheston, "Very wide-band phased-array antenna," *IEEE Trans. Antennas Propag.*, vol. 20, no. 6, pp. 699-704, Nov. 1972
- [52] C. Hemmi, R. T. Dover, F. German, and A. Vespa, "Multifunction wide-band array design," *IEEE Trans. Antennas Propag.*, vol. 47, no. 3, pp. 425-431, Mar. 1999.
- [53] K. Trott, B. Cummings, R. Cavener, M. Deluca, J. Biondi, and T. Sikina, "Wideband phased array radiator," in *Proc. IEEE Int. Phased Array Systems Technology Symp.*, Boston, MA, Oct. 2003, pp. 383-386.
- [54] "Ultra-wideband transmission systems, first report and order," FCC, Washington, DC, FCC 02-48, Apr. 2002.
- [55] K. I. Jeon, J. H. Lee, S. W. Paek, D. W. Kim, W. S. Lee, C. R. Lim, H. Cha, H. Choi, and K. W. Chung, "A 5 to 27 GHz MMIC power amplifier," in *IEEE MTT-S Int. Microwave Symp. Dig.*, Boston, MA, June 2000, pp. 541-544.
- [56] J. J. Komiak, W. Kong, and K. Nichols, "High efficiency wideband 6 to 18 GHz power amplifier MMIC," in *IEEE MTT-S Int. Microwave Symp. Dig.*, Seattle, WA, Jun. 2002, pp. 905-907.
- [57] C. Wang, C. T. Rodenbeck, M. R. Coutant, and K. Chang, "A novel broadband T/R module for phased array applications in wireless communications," in *IEEE MTT-S Int. Microwave Symp. Dig.*, Seattle, WA, Jun 2002, pp. 1325-1328.
- [58] A. Hirata, T. Morimoto, and Z. Kawasaki, "DOA estimation of ultra-wideband EM waves with MUSIC and interferometry," *IEEE Antennas Wireless Propag. Lett.*, vol. 2, pp. 190-193, 2003.

- [59] R. B. Waterhouse and N. V. Shuley, "Dual frequency microstrip rectangular patches," *Electron. Lett.*, vol. 28, no. 7, pp. 606-607, Mar. 1992.
- [60] W. F. Richards, S. E. Davidson, and, S. A. Long, "Dual-band reactively loaded microstrip antenna," " *IEEE Trans. Antennas Propagat.*, vol. AP-33, no. 5, pp. 556-560, May 1985.
- [61] S. A. Long and M. D. Walton, "A dual-frequency stacked circular-disc antenna," *IEEE Trans. Antennas Propagat.*, vol. AP-27, no. 2, pp. 270-273, Mar 1979.
- [62] J. Wang, R. Fralich, C. Wu, and J. Litva, "Multifunctional aperture coupled stack patch antenna," *Electron. Lett.*, vol. 26, no. 25, pp. 2067-2068, Dec. 1990.
- [63] F. Croq and D. M. Pozar, "Multifrequency operation of microstrip antenna using aperture coupled parallel resonators," *IEEE Trans. Antennas Propagat.*, vol. 40, no. 11, pp. 1367-1374, Nov. 1992.
- [64] C. Salvador, L. Borselli, A. Falciani, and S. Maci, "Dual frequency planar antenna at S and X bands," *Electron. Lett.*, vol. 31, no. 20, pp. 1706-1707, Sep. 1995.
- [65] J.-S. Chen, "Triple-frequency annular-ring slot antennas fed by CPW and microstrip line," in *IEEE Antennas Propagat. Soc. Int. Sym. Dig.*, vol. 2, Jun. 2003, pp. 557-560.
- [66] M. Cho, I. Kim, T.-H. Seo, J-G. Yook, and H. Park, "Modified slot-loaded triple-band microstrip patch antenna," in *IEEE Antennas Propagat. Soc. Int. Sym. Dig.*, vol. 3, Jun. 2002, pp. 500-503.
- [67] H. F. Hammad, Y. M. M. Antar, and A. P. Freundorfer, "Dual band aperture coupled antenna using spur line," *Electron. Lett.*, vol. 33, no. 25. pp. 2088-2090, Dec. 1997.

VITA

Seung Pyo Hong was born in Seoul, Republic of Korea. He received a Bachelor of Science and a Master of Science degree in electronic engineering from Yonsei University in Feb. 1991 and Feb. 1993, respectively. From 1993 to 2000, he worked for LG Information and Communications as a senior research engineer developing code-division-multiple-access (CDMA) digital cellular systems and IMT-2000 systems. From 2001 to 2002, he was employed as a research assistant in the Radiation Laboratory at University of Michigan, Ann Arbor, MI, studying the effect of foliage on radar detection. After his stay at University of Michigan, he was employed as a research assistant in the Electromagnetics and Microwave Laboratory at Texas A&M University, College Station, TX under the advisement of Dr. Kai Chang. His research interests include passive and active microwave/millimeter-wave circuits, ultra-wideband T/R modules for satellite communications, and radar systems. He can be reached through Professor Kai Chang, Department of Electrical and Computer Engineering, Texas A&M University, College Station, TX 77843-3128. His permanent address is No Ryang Jin-2 Dong, Dong Jak-Ku, Seoul, Republic of Korea, 156-805.